Foundations and Trends® in Networking
Vol. 8, No. 1-2 (2013) 1–147
© 2014 M. Pierobon and I. F. Akyildiz
DOI: 10.1561/1300000033

now
the essence of knowledge

Fundamentals of Diffusion-Based Molecular Communication in Nanonetworks

Massimiliano Pierobon
Department of Computer Science & Engineering,
University of Nebraska-Lincoln
pierobon@cse.unl.edu

Ian F. Akyildiz
School of Electrical and Computer Engineering,
Georgia Institute of Technology
ian@ece.gatech.edu

Contents

1 Introduction **2**
- 1.1 Biological Nanomachines and Nanonetworks 3
- 1.2 Potential Applications of Nanonetworks Enabled by MC . . 5
- 1.3 Research Objectives and Solutions 6
- 1.4 Article Outline 7

2 Previous Work on Molecular Communication **8**
- 2.1 Molecular Communication Types 8
- 2.2 Diffusion-based Molecular Communication in Nanonetworks 10

3 Deterministic Model of a Molecular Communication Link **13**
- 3.1 Motivation and Related Work 13
- 3.2 A Basic Design of a Diffusion-based MC Link 14
- 3.3 The Emission Process 15
- 3.4 The Diffusion Process 20
- 3.5 The Reception Process 24
- 3.6 End-to-end Normalized Gain and Delay 29
- 3.7 Numerical Results 29
- 3.8 Conclusions 34

4 Stochastic Models of the Noise Sources in a MC Link **35**
- 4.1 Motivation and Related Work 35

4.2 Definition of Noise Sources in a Diffusion-based MC Link . 37
4.3 The Particle-sampling Noise 38
4.4 The Particle-counting Noise 43
4.5 The Ligand-receptor-kinetics Noise 49
4.6 Conclusions 55

5 Capacity Analysis of a Molecular Communication Link 57
5.1 Motivation and Related Work 57
5.2 Capacity Analysis through Thermodynamics 61
5.3 Capacity Analysis with Channel Memory & Molecular Noise 70
5.4 Conclusions 95

6 Interference of Multiple MC Links in a Nanonetwork 97
6.1 Motivation and Related Work 97
6.2 Intersymbol Interference and Co-Channel Interference . . . 100
6.3 Statistical-physical Model of Interference 113
6.4 Conclusions 134

7 Conclusions and Future Work 136

References 140

Abstract

Molecular communication (MC) is a promising bio-inspired paradigm for the interconnection of autonomous nanotechnology-enabled devices, or nanomachines, into nanonetworks. MC realizes the exchange of information through the transmission, propagation, and reception of molecules, and it is proposed as a feasible solution for nanonetworks. This idea is motivated by the observation of nature, where MC is successfully adopted by cells for intracellular and intercellular communication. MC-based nanonetworks have the potential to be the enabling technology for a wide range of applications, mostly in the biomedical, but also in the industrial and surveillance fields. The focus of this article is on the most fundamental type of MC, i.e., diffusion-based MC, where the propagation of information-bearing molecules between a transmitter and a receiver is realized through free diffusion in a fluid. The objectives of the research presented in this article are to analyze an MC link from the point of view of communication engineering and information theory, and to provide solutions to the modeling and design of MC-based nanonetworks. First, a deterministic model is realized to study each component, as well as the overall diffusion-based-MC link, in terms of gain and delay. Second, the noise sources affecting a diffusion-based-MC link are identified and statistically modeled. Third, upper/lower bounds to the capacity are derived to evaluate the information-theoretic performance of diffusion-based MC. Fourth, an analysis of the interference produced by multiple diffusion-based MC links in a nanonetwork is provided. This research provides fundamental results that establish a basis for the modeling, design, and realization of future MC-based nanonetworks, as novel technologies and tools are being developed.

M. Pierobon and I. F. Akyildiz. *Fundamentals of Diffusion-Based Molecular Communication in Nanonetworks.* Foundations and Trends® in Networking, vol. 8, no. 1-2, pp. 1–147, 2013.

DOI: 10.1561/1300000033.

1

Introduction

Molecular communication (MC) [2] is a bio-inspired paradigm where the exchange of information is realized through the transmission, propagation, and reception of molecules. This paradigm was first studied in biology, since it is successfully adopted in nature by cells for intracellular and intercellular communication [73]. MC is considered a promising option for communications in nanonetworks [5], which are defined as the interconnections of intelligent autonomous nanometer-scale devices, or nanomachines. Thanks to the feasibility of MC in biological environments, MC-based nanonetworks have the potential to be the enabling technology for a wide range of applications [5], mostly in the biomedical, but also in the industrial and surveillance fields. The objectives of the research presented in this article are to analyze the MC paradigm from the point of view of communication engineering and information theory, and to provide solutions to the modeling and design of MC-based nanonetworks.

1.1 Biological Nanomachines and Nanonetworks

Among the more promising research fields of today, nanotechnology is enabling the manipulation of matter at an atomic and molecular scale, from one to a hundred nanometers. One of the goals of nanotechnology is to engineer functional systems based on the unique phenomena and properties of matter at the nanoscale [32]. Currently, a great research effort is spent in the attempt to realize nanoscale machines, also called molecular machines or nanomachines, defined by E. Drexel as "mechanical devices that perform useful functions using components of nanometer-scale and defined molecular structure" [33]. More specifically, nanomachines [5, 3, 4] are expected to have the ability to sense, compute, actuate, manage their energy, and interconnect into networks, termed nanonetworks, to overcome their individual limitations and benefit from collaborative efforts.

Two main types of nanomachines can be identified within the aforementioned definition, namely, synthetic and biological. On the one hand, the synthetic nanomachines are realized either by downscaling from the current micro-scale technologies, such as microelectronics or micro-electro mechanics, or through the use of chemically synthesized nanomaterials [3]. On the other hand, the biological nanomachines are realized either by reusing biological components (e.g., DNA-based memories [52], flagellum-based actuators [18]), or by programming the behavior of biological cells from nature, such as through the genetic engineering of bacteria [41], as illustrated in 1.1.

While the engineering of fully synthetic nanomachines is still in its infancy, the research on the genetic engineering of biological cells is currently in rapid progress, thanks to the advancements made by biotechnology [16]. Several key techniques developed under the umbrella of synthetic biology have made possible today the realization of simple biological nanomachines [87]. As illustrated in Figure 1.1, through the insertion of engineered genetic code in the form of a circular DNA strand (i.e., plasmid) in a bacterium, it will be soon possible to program complete functions, including sensing, actuation, and communication, and have access to the main functionalities of the cell, such as the storage and the processing of information through DNA code, the

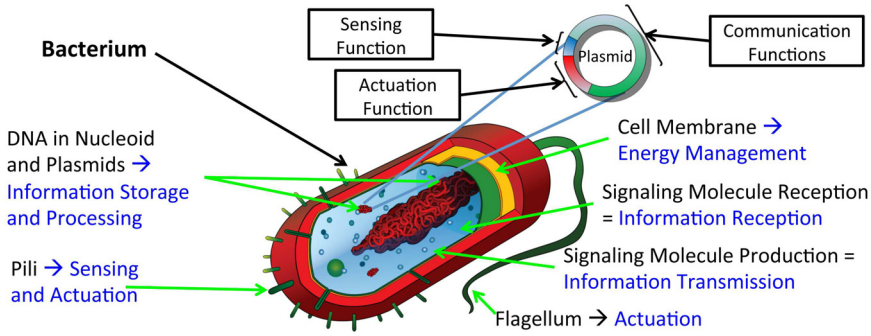

Figure 1.1: The expected functions of a biological nanomachine realized through the genetic engineering of a bacterium.

sensing and actuation through the use of the *pili* (hairlike appendages), the management of the cell energy through the cell membrane, and the transmission and reception of information through the production and the reception of signaling molecules.

The exchange of information between nanomachines, and their interconnection into nanonetworks, is key to overcome their individual limitations in size, energy and computational capabilities, and benefit from collaborative efforts. In nanonetworks, the applicability of classical communication technologies is limited by several constraints. In particular, the very restricted size of the nanomachines and the peculiarities of the environments in which they are envisioned to operate (e.g., biological scenarios) demand for novel solutions from the perspective of both the choice of the communication medium and the study of suitable communication techniques. While a possible solution to the problem of communication between synthetic nanomachines is suggested by recent studies [3] on nano-structures and on the properties of carbon nano-electronics, the imminent availability of biological nanomachines encourages to study and adopt the communication techniques naturally adopted by biological cells. In this direction, the **Molecular Communication (MC) paradigm**, inspired by the natural cell communication in biology, where message-carrying molecules are synthesized, emitted, collected, and converted to cellular responses through biochemical processes, is expected to be especially attractive

because of its inherent feasibility in a biocompatible environment [2, 5].

1.2 Potential Applications of Nanonetworks Enabled by Molecular Communication

Given the tight integration of MC within the biological environment and its feasibility at the cellular scale (nm - μm), MC is studied not only as a candidate for nanonetwork communication, but also as a possible tool for the future nanonetworks to interact with the living organisms and their biological processes. As a consequence, the number of potential applications of MC-enabled nanonetworks is very large. Amongst others, the following three main areas deserve a special attention.

Biomedical applications, such as disease control and infectious agent detection [93], smart drug delivery systems [43], and intelligent intrabody systems for monitoring glucose, sodium, and cholesterol [34, 60]. These applications are expected to greatly benefit from the use of nanomachines deployed over the body (e.g., through tattoo-like patches) or inside the body (e.g., through pills or intramuscular injection). Since MC is naturally adopted by cells, nanonetworks enabled by this paradigm are envisioned to better integrate with the intra-body biological processes and to show higher biocompatibility when compared to other possible solutions.

Industrial applications, such as the monitoring and control of microbial formations. As an example, applications based on bacterial biofilms [27], which are used to clean residual waters coming from different manufacturing processes or to treat organic waste [56], could be greatly enhanced by MC-enabled nanonetworks, since microbial organisms naturally produce and respond to molecular stimuli.

Surveillance applications will make use of biological and chemical nanosensors that have an unprecedented sensing accuracy [85, 95]. Nanonetworks composed by several MC-enabled nanosensors could serve for surveillance against biological and chemical attacks [95] by detecting toxic or infectious agents diffusing in the environment.

1.3 Research Objectives and Solutions

The focus of this article is on diffusion-based MC, where the propagation of information-bearing molecules between a transmitter and a receiver is realized through free diffusion in a fluid. This choice is motivated by a preliminary analysis, detailed in Chapter 2, which identifies the diffusion-based as the most fundamental type of MC among different options suggested in the literature. As a consequence of the differences between the diffusion-based MC paradigm and classical electromagnetic communication paradigms, the classical communication engineering models and techniques are not directly applicable for the study and the design of diffusion-based MC-enabled nanonetworks. These differences include, but are not limited to, the following:

- The process of diffusion-based molecule propagation is based on radically different phenomena with respect to the electromagnetic wave propagation in classical communication systems. While electromagnetic waves operate the propagation of energy at the speed of light, the molecule diffusion process is caused by the random walk of the molecule Brownian motion in a fluid [76, 29]. As a consequence, while an electromagnetic wave propagates in a defined direction, and with negligible delay for most of the terrestrial communication systems, molecules subject to Brownian motion propagate with a random direction and with a high delay for almost all the transmission ranges of interest.

- The biologically-inspired physical processes that can be adopted to transmit and receive information in a diffusion-based MC-enabled nanonetworks are based on different mechanisms with respect to the modulation and reception of electromagnetic radiations in classical communication systems. While in classical systems antennas transmit and receive electromagnetic radiations through moving charges in metallic conductors, in biological cell bio-signaling [73] information is transmitted through the chemical synthesis of signaling molecules, and received through chemical reactions between incoming signaling molecules and chemical receptors.

As a consequence, there is a need of to build a complete understanding of the diffusion-based MC paradigm from the ground up. The research objectives addressed in this article, and the proposed solutions, have been identified to specifically target this need, and they are summarized as follows. The first research objective is to develop of a deterministic model of diffusion-based MC link, which provides a mathematical characterization of the main physical processes involved in the transmission, propagation, and reception of molecules for the exchange of information between a transmitter and a receiver. The second research objective is to identify and stochastically model the noise sources that affect a diffusion-based MC link. The third research objective is to provide an estimate of the achievable performance of a diffusion-based MC link in terms of information capacity. The fourth research objective is to analyze the interference produced by multiple diffusion-based MC links when present at the same time in a nanonetwork.

1.4 Article Outline

The rest of this article is organized as follows. A preliminary analysis of different MC options from the literature is contained in Chapter 2, which also includes a survey of the results from previous works pertinent to the study of diffusion-based MC. The results obtained through the design and end-to-end modeling of a basic diffusion-based-MC link are presented in Chapter 3, where the contributions of each component of the system are analyzed in terms of gain and delay. In Chapter 4, the most relevant noise sources affecting a diffusion-based MC link are studied through the mathematical expression of their underlying physical processes, and modeled through the use of statistical parameters. Analytical expressions of upper and lower bounds to the information capacity of a diffusion-based MC link are derived in Chapter 5, first by using tools from thermodynamics, and then through a pure information-theoretic approach. In Chapter 6, an analysis of the interference produced by multiple diffusion-based MC links in a nanonetwork is detailed. Finally, a conclusion with the possible future avenues for this research field is provided in Chapter 7.

2

Previous Work on Molecular Communication

This chapter of the article contains a review of the literature pertinent to the research on MC and its application to nanonetworks. This review is organized as follows. In Section 2.1, different MC options from the literature are detailed on the basis of the type of adopted molecule propagation. In Section 2.2, the results from the literature focused on diffusion-based MC and its application to nanonetworks are presented and analyzed to motivate the research presented in this article.

2.1 Molecular Communication Types

Different types of MC have been studied so far, and they can be characterized on the basis of how molecules propagate through the medium [2]. Three main types of MC are identified from the literature, as shown in Figure 2.1, as the walkway-based, the advection-based, and the diffusion-based. These categories are also described on the basis of how spontaneous is the propagation of the molecules. The less spontaneous is the type of MC, the more predictable is the path followed by the molecules during their propagation, and *vice versa*.

In **walkway-based** MC, the molecules propagate through active

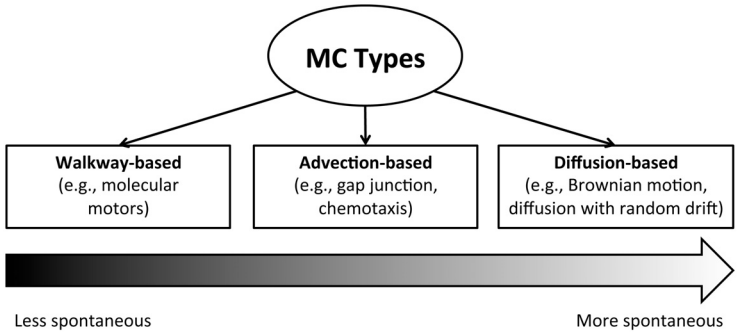

Figure 2.1: Molecular communication types.

transport by following pre-defined pathways connecting the transmitter to the receiver. The most widespread example from the literature of this type of MC is given by the use of molecular motors [69, 70]. Molecular motors [25] are protein filaments that convert chemical energy into kinetic energy, and they are at the basis of the generation of force in biology, e.g., in the muscles. In [69, 70] molecular motors filaments are studied and employed to physically interconnect nanomachines and to generate the force to propagate the information molecules from the transmitter to the receiver.

In **advection-based** MC, the molecules propagate through diffusion in a fluidic medium whose flow, and consequently the transport of the molecules, or advection, is defined and predictable. The use of gap junctions [71], which are nanofluidic pipes connecting the transmitter and the receiver, is one example of this type of MC. Advection-based MC can also be realized by using carrier entities whose motion is constrained on the average along specific paths, despite showing a random component. A good example of this flow-based MC is given by the chemotaxis-based technique in [49, 50], where flagellated bacteria released by the transmitter, and containing information encoded in DNA molecules, are guided to swim towards the receiver, which continuously releases an attractant substance.

In **diffusion-based** MC, the molecules propagate through their spontaneous diffusion in a fluidic medium [22]. Diffusion-based MC was first analyzed in [7, 92, 11], where the transmitted information

molecules cover the distance between the transmitter and the receiver by following an unbiased random walk, i.e., the Brownian motion. In diffusion-based MC, the molecules can also be affected by random advection in the fluidic medium. An example of this diffusion-based MC is given in [75], where information molecules are released in the air and are subject to a random and unpredictable component of the wind flow while they propagate.

The focus of the proposed research is on diffusion-based MC. This choice is motivated by the following arguments. First, molecule diffusion is at the basis of all the aforementioned MC options. As an example, in [70], diffusion is considered as an unavoidable propagation effect superimposed on the molecular motor transport. Moreover, in [49, 50], carrier bacteria are subject to a random walk with the same underlying rules of a biased molecule diffusion. Second, diffusion-based MC can be considered the most general and common MC option in nature, where examples are found in the calcium signaling among cells [72], the pheromonal communication among animals [24, 75], and the synaptic transmission between neurons [73]. As a consequence, the study of diffusion-based MC has the potential to benefit from the observation of nature for the design of bio-inspired and bio-compatible solutions.

2.2 Diffusion-based Molecular Communication in Nanonetworks

Different diffusion-based MC architectures for nanonetworks have been proposed and studied in the literature, and they can be classified on the basis of the technique used to encode the information in the diffusing molecules. The three most referenced architectures encode the information in either the time of molecule release, the type of each molecule, or variations in the molecule concentration.

The first type of architecture is theoretically analyzed in [55], where the authors focused on the mathematical modeling of the diffusion channel as a probabilistic contribution in the time of arrival of the molecules at the receiver, while the transmitter and the receiver have simplified ideal models. The results of simulations from [55] in terms

of achievable information rate show that, as a consequence of the high uncertainty in the propagation time, this architecture is characterized by a very low capacity.

The second type of architecture is analyzed in [70], where a piece of information is encoded in each single molecule. As a consequence, the information carried by a certain molecule is received only if that molecule reaches the receiver location. Similarly to [55], only the diffusion channel part is modeled, while the transmitter and the receiver are considered ideal. While no analytical model is provided in [70], the results of simulations reveal very low performance for this architecture if compared to other non-diffusive techniques.

The third type of architecture is treated in [92, 11, 13, 14, 36, 62, 57, 12]. In particular, a simplified receiver model of this architecture is studied in [92], where the diffusion-based channel is coupled with ideal transmitter and receiver. Simulation results in [92] show low values for the system capacity. In [11, 13], a model of a diffusion-based MC receiver is developed by using multiple chemical receptors to read the molecule concentration at the receiver location. The results of this model in terms of capacity are relatively high if compared to [92], especially when an error compensation technique is applied.

The high similarity of the third type of architecture to some biological systems [73], which are characterized by much higher performance than in the aforementioned results, encourages the investigation in this direction.

In particular, very limited research has been conducted to analyze the complete cascade of components (transmitter, channel and receiver) in diffusion-based MC link, and the complete study of its noise sources, capacity, and interference in a nanonetwork with closed-form analytical models. In [92], the analytical model of the system is reduced to the diffusion-based channel. In [11, 13, 14] the diffusion process is not captured in terms of molecule-propagation theory and, therefore, the end-to-end model reliability and accuracy are only accounted for the receiver side. In [36], the capacity of a MC system is analyzed on the basis of the effects of the diffusion-based-channel memory, but without accounting for molecular-noise sources and only for the specific case

of binary coding. Two different coding techniques are analyzed in [57] in terms of achievable rates, while the diffusion-channel models are oversimplified to a binary or a quadruple channel. Similarly, discrete-memoryless approximations are applied to the molecule-diffusion channel in [10], where the MC capacity is computed for a binary-coding scheme. In [57] the effects of intersymbol and co-channel interference are analyzed in reference to two specific modulation techniques proposed by the same authors. In [62] the intersymbol interference is characterized in a unicast MC system with binary amplitude-modulation. In [12], interference is studied for another specific modulation technique, based on the transmission order of different types of molecules.

3

Deterministic Model of a Molecular Communication Link

3.1 Motivation and Related Work

The objective of the deterministic modeling of a diffusion-based Molecular Communication (MC) link is to provide a mathematical characterization of the main physical processes involved in the transmission, propagation, and reception of molecules for the exchange of information between a transmitter and a receiver [77]. This characterization is provided in this chapter of the article in terms of transfer function and, consequently, by deriving the gain and delay parameters for each physical process, as well as for the overall end-to-end diffusion-based MC link. This characterization does not take into account noise sources that could affect the performance of a diffusion-based MC link, which will be the subject of the next chapter.

Some previous research has been conducted to address the modeling and analysis of diffusion-based MC and the according end-to-end behavior in nanonetworks. In [11, 13], a particle receiver model is developed by taking the ligand-receptor binding mechanism into account [86]. However, in both works, the diffusion process is not captured in terms of molecule propagation theory and, therefore, the end-to-end model reliability and accuracy are only accounted for the receiver side.

Moreover, an ideal digital transmitter model is used and the performance evaluation is conducted based on an ideal synchronization between the transmitter and the receiver.

In this chapter, a basic diffusion-based MC link design is provided, which aims at an interpretation of the diffusion-based MC, both in terms of molecule emission/reception and molecule propagation. In the provided diffusion-based MC link design, the desired information modulates the molecule emission at the transmitter side. This modulated signal is then propagated by the diffusion process to the receiver side. The receiver detects the concentration and generates the received signal. This diffusion-based MC link is divided into three processes: the emission process, the diffusion process and the reception process. Each process is modeled in terms of transfer function, from which the normalized gain and delay are derived. The models of the emission process and the diffusion process are built on the basis of the molecular-diffusion physics [76], while the reception-process model is interpreted by stemming from the theory of the ligand-receptor binding [86]. Finally, the end-to-end normalized gain and delay are derived for the cascade of the three processes, which provide the characterization of the complete diffusion-based MC link. Numerical results are provided to evaluate the normalized gain and delay of the diffusion-based MC link for several different values of the system frequency and the transmission range.

3.2 A Basic Design of a Diffusion-based MC Link

The end-to-end model is a characterization of a basic diffusion-based MC design in terms of transmission, propagation, and reception of molecules, as sketched in Figure 3.1.

The molecules are here called particles, since in this preliminary work their chemical properties are not taken into account. The particles are assumed as having no electrostatic charge, while their mass and shape characteristics are taken into account in the diffusion coefficient D [76, 29], introduced later in this chapter. The end-to-end model is contained in the three-dimensional space S indexed through the Cartesian axes X, Y, and Z. The space S contains a fluidic medium,

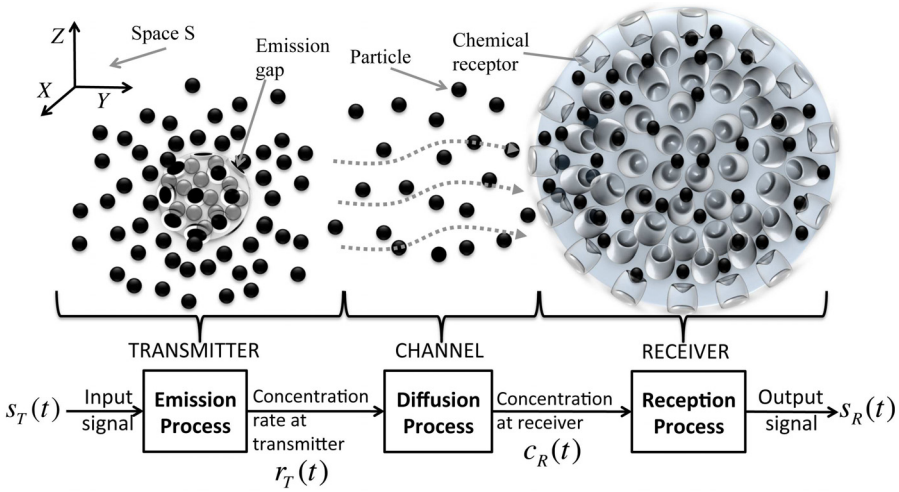

Figure 3.1: Representation of the end-to-end model.

and it is initially filled with a homogeneous concentration of particles. The emission process modulates the particle-concentration rate at the transmitter according to an input signal $s_T(t)$, function of the time t. The modulation is achieved through the release/capture of particles from/into emission gaps. The modulated-particle-concentration rate $r_T(t)$ is the output of the transmitter and the input of the channel. The channel relies on the diffusion process of the particles in the space S to propagate the signal and deliver the particle concentration $c_R(t)$ at the receiver. The receiver senses the particle concentration at its location as input, and it recovers the output signal $s_R(t)$. The reception process generates the output signal by means of chemical receptors.

3.3 The Emission Process

The task of the emission process is to modulate the particle-concentration rate $r_T(t)$ at the transmitter according to the input signal $s_T(t)$ of the end-to-end model, as shown in Figure 3.2, which is based on the following assumptions:

- The transmitter has a *spherical boundary* that divides the space in proximity of the transmitter into two areas: the inner area and

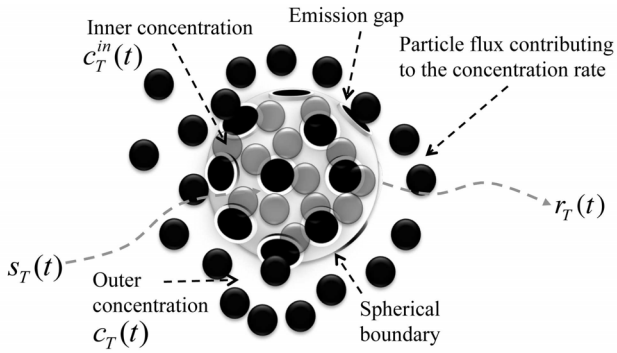

Figure 3.2: Representation of the emission process.

the outer area.

- The inner concentration $c_T^{in}(t)$ is the concentration of particles lying in the inner area, whereas the outer concentration $c_T(t)$ is the concentration of particles lying in the outer area.

- The inner area and the outer area are spatially connected by means of *emission gaps*. An emission gap is an opening in the spherical boundary which allows particles to move through due to their diffusion. The size of an emission gap allows only one particle to pass through at each time instant. Whenever a particle is traversing the emission gap, its movement has only components along the radius of the spherical boundary. As a consequence, the movement of a particle through the emission gap can only be outward (from the inner area to the outer area) or inward (from the outer area to the inner area). The emission gaps are many and homogeneously distributed on the surface of the spherical boundary. The present analysis does not depend on their precise number. We believe it will be important to discuss the impact of the number of emission gaps on the end-to-end model in our future work.

- Whenever there is a difference between the inner concentration $c_T^{in}(t)$ and the outer concentration $c_T(t)$, a movement of particles is stimulated between the inner area and the outer area through

the emission gaps.

- The movement of particles between the inner area and the outer area causes a variation in the outer concentration, whose first time derivative is the particle concentration rate at the transmitter location $r_T(t)$.

- Particles can be created/destroyed in the inner area in order to reach a desired inner concentration $c_T^{in}(t)$. The creation/destruction of particles in the inner area is supposed to be ideally perfect and instantaneous. As a consequence, we do not account for the randomness that can derive from the creation/destruction of particles. We believe that this is a reasonable approximation that allows us to analyze the contributions coming only from the emission process. Further analysis can be conducted by specifying the processes involved in the creation/destruction of particles. As an example, the creation/destruction of particles could be realized through a cascade of chemical reactions or by the emptying/filling of particle reservoirs located in the inner area.

- The transmitter is supposed to be able to adjust the inner concentration $c_T^{in}(t)$ in order to obtain a particle concentration rate $r_T(t)$ proportional to the input signal $s_T(t)$ (modulation of $r_T(t)$ according to $s_T(t)$).

This transmitter characterization is inspired by biochemistry principles related to the living cells and to the mechanism of cell biosignaling [73]. According to these principles, the spherical boundary is a simplification of the cell plasma membrane, which separates the interior of a cell from the outside environment. The emission gaps are inspired by the channels that permit the selective passage of molecules through the plasma membrane of a cell. As an example, the gated ion channels in the plasma membrane are openings that allow the passage of specific ion molecules between the interior of a cell and the outside environment and, amongst others, they serve for cell-to-cell communication purposes. As stated in [73], those ion molecules, while traversing

the gated ion channels, are driven by a force that is a sum of two terms. The first term of the force is a function of the difference between the inside and the outside concentration of the same molecules and it depends on the diffusion. The second term of the force is a function of an electrical potential and it is related to the electrostatic charge carried by the ion molecules. Since, according to our assumption, the particles in our system do not carry any electrostatic charge, when they traverse an emission gap they are driven only by the first term of the force. For this, the difference in the concentration of particles between the inner area and the outer area stimulates the driving force that permits their movement through the emission gaps either outward or inward, as explained above.

The emission process is modeled with an electrical-parallel-resistor-capacitor (RC) circuit [84]. This circuit is shown in Figure 3.3, where $I_{in}(t)$ is the input current as a function of the time t, R_e stands for the resistance value, C_e is the capacitance value and $I_{out}(t)$ is the output current, which is equal to the current $I_R(t)$ flowing through the resistance R_e.

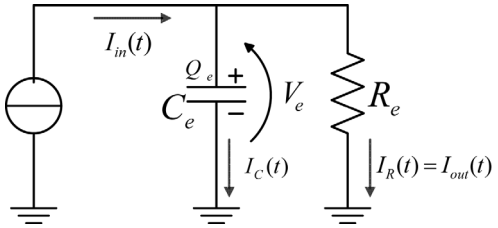

Figure 3.3: RC-circuit model of the emission process.

Within the RC-circuit model, the input signal $s_T(t)$, shown in Figure 3.2, corresponds to the input current $I_{in}(t)$. The particle-concentration gradient $\nabla c_T(t)$ at the transmitter, defined as the difference between the particle concentration inside and the particle concentration outside the transmitter, is equal to the voltage $V_e(t)$. The current $I_R(t)$ that flows through the resistance R_e is equal to the particle-concentration rate $r_T(t)$, which is the output of the transmitter. The relation between the particle concentration flux $\bar{J}(\bar{x}, t)$ and the particle-

concentration gradient $\nabla c(\bar{x}, t)$ at time t and location $\bar{x}$ is given by the Fick's first law [76, 29] as follows:

$$\bar{J}(\bar{x}, t) = -D\nabla c(\bar{x}, t) \ , \tag{3.1}$$

where D is the diffusion coefficient and it can be considered as a constant value for a specific fluidic medium.

Therefore, since $\bar{J}_T(t)$ and $\nabla c_T(t)$ are, respectively, the particle-concentration flux $\bar{J}(\bar{x}, t)$ and the opposite of the particle-concentration gradient $-\nabla c(\bar{x}, t)$ at the transmitter, and since

$$I_R(t) = \bar{J}_T(t) \ \ V_e(t) = \nabla c_T(t) \ , \tag{3.2}$$

then

$$I_R(t) = DV_e(t) \ , \tag{3.3}$$

and the constant resistance value becomes

$$R_e = \frac{1}{D} \ . \tag{3.4}$$

We relate the capacitor charging/discharging current $I_C(t)$ at time t to the difference between $s_T(t)$, equal to the input current $I_{in}(t)$, and $r_T(t)$, equal to the output current $I_R(t)$. The voltage applied to the capacitor $V_e(t)$ is equal to $\nabla c_T(t)$. The particle-concentration gradient $\nabla c_T(t)$ is the difference between the outside particle concentration $c_T(t)$ and the inside particle concentration $c_T^{in}(t)$. Therefore, the time derivative $d\nabla c_T(t)/dt$ changes according to the net flux of particles that contributes to $\nabla c_T(t)$. The net flux of particles is given by the difference between $s_T(t)$ and $r_T(t)$. This results in the following relation:

$$\frac{d\nabla c_T(t)}{dt} = s_T(t) - r_T(t) \ , \tag{3.5}$$

and, since $I_C(t) = s_T(t) - r_T(t)$ and $V_e(t) = \nabla c_T(t)$, then $I_C(t) = dV_e(t)/dt$ and, therefore, the capacitor value becomes

$$C_e = 1 \ . \tag{3.6}$$

From the electrical-circuit theory [84], the Fourier transform of the transfer function (FTTF) [30] of the RC circuit $\mathbf{H}_{RC}(f)$, equal to the FTTF $\tilde{\mathbf{A}}(f)$ of the transmitter, has the following expression:

$$\mathbf{H}_{RC}(f) = \tilde{\mathbf{A}}(f) = \frac{\tilde{\mathbf{I}}_{out}(f)}{\tilde{\mathbf{I}}_{in}(f)} = \frac{1}{1 + j2\pi f R_e C_e} \ , \tag{3.7}$$

where $\tilde{\mathbf{I}}_{in}(f)$ and $\tilde{\mathbf{I}}_{out}(f)$ are the Fourier transforms [30] of the input voltage $I_{in}(t)$ and output voltage $I_{out}(t)$, respectively.

The *normalized gain* $\Gamma_{\mathbf{A}}(f)$ of the emission process is the magnitude $|\tilde{\mathbf{A}}(f)|$ of the FTTF $\tilde{\mathbf{A}}(f)$ normalized by its maximum value $\max_f(|\tilde{\mathbf{A}}(f)|)$, which becomes 1 from (3.7), and it is expressed as

$$\Gamma_{\mathbf{A}}(f) = \frac{|\tilde{\mathbf{A}}(f)|}{\max_f(|\tilde{\mathbf{A}}(f)|)} = \frac{1}{\sqrt{(1+(2\pi f R_e C_e)^2)}} \ . \tag{3.8}$$

The *delay* $\tau_{\mathbf{A}}(f)$ of the emission process is

$$\tau_{\mathbf{A}}(f) = -\frac{d\phi_{\mathbf{A}}(f)}{df} \ , \tag{3.9}$$

where $\phi_{\mathbf{A}}(f)$ is the phase of the FTTF from (3.7), and it is expressed as

$$\phi_{\mathbf{A}}(f) = \arctan\left(\frac{\mathrm{Im}(\tilde{\mathbf{A}}(f))}{\mathrm{Re}(\tilde{\mathbf{A}}(f))}\right) = \arctan(-2\pi f R_e C_e) \ , \tag{3.10}$$

which is computed from the real part $\mathrm{Re}(\tilde{\mathbf{A}}(f))$ and the imaginary part $\mathrm{Im}(\tilde{\mathbf{A}}(f))$ of the FTTF $\tilde{\mathbf{A}}(f)$.

3.4 The Diffusion Process

The diffusion process, as shown in Figure 3.4, deals with the propagation of the particle-concentration rate $r_T(t)$ from the transmitter, located at the Cartesian coordinates $[0,0,0]$, across the space S by means of free particle-diffusion in the fluidic medium. The particle concentration $c_R(t)$ at the receiver location $[x_R, y_R, z_R]$ is considered the output of the diffusion process.

We use the particle concentration distribution flux to study the signal propagation occurring during the diffusion process. According to the Fick's first law [76, 29], the particle concentration flux $\bar{J}(\bar{x},t)$ at time instant t and location $\bar{x}$, is equal to the spatial gradient (operator ∇) of the particle concentration $c(\bar{x},t)$ occurring at time instant t and location $\bar{x}$ multiplied by the diffusion coefficient D, expressed as follows:

$$\bar{J}(\bar{x},t) = -D\nabla c(\bar{x},t) \ , \tag{3.11}$$

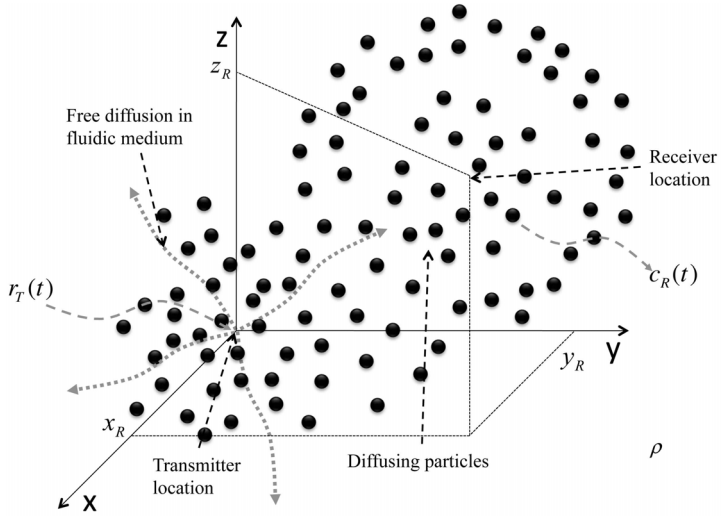

Figure 3.4: Representation of the diffusion process.

where $\nabla c(\bar{x}, t)$ is a vector containing the spatial first derivatives of $c(\bar{x}, t)$ along the three spatial dimensions.

At time t we assume to have a particle concentration rate $r(\bar{x}, t)$ at the location $\bar{x}$ in the space S and time t. The principle of mass/matter conservation allows us to formulate the Continuity Equation [26], which states that the time derivative of the particle concentration $\partial c(\bar{x}, t)/\partial t$ is equal to

$$\frac{\partial c(\bar{x}, t)}{\partial t} = -\nabla \bar{J}(\bar{x}, t) + r(\bar{x}, t) \ . \tag{3.12}$$

Substituting the Fick's first law from (3.11) into (3.12), we end up with the inhomogeneous Fick's second law of diffusion. According to this, the time derivative of the particle concentration $\partial c(\bar{x}, t)/\partial t$ at location $\bar{x}$ and the time t is equal to the Laplacian (operator ∇^2) of $c(\bar{x}, t)$ occurring at time instant t and location $\bar{x}$ multiplied by D (diffusion coefficient) plus the incoming particle concentration rate $r(\bar{x}, t)$, expressed as follows:

$$\frac{\partial c(\bar{x}, t)}{\partial t} = D\nabla^2 c(\bar{x}, t) + r(\bar{x}, t) \ , \tag{3.13}$$

where $\nabla^2 c(\bar{x}, t)$ is the sum of the spatial second derivatives of $c(\bar{x}, t)$

along the three spatial dimensions.

As pointed out in [35], the second Fick's law is in contradiction with the theory of special relativity. The solution of the second Fick's law allows particle concentration information to propagate instantaneously from one point to another point in the space S, with a so-called superluminal information propagation speed. In order to overcome this problem, it was proposed in [8] to add a new term to the Fick's second law accounting for a finite speed of propagation in the concentration information. With this additional term, we obtain the following Telegraph Equation [8]:

$$\tau_d \frac{\partial^2 c(\bar{x},t)}{\partial t^2} + \frac{\partial c(\bar{x},t)}{\partial t} = D\nabla^2 c(\bar{x},t) + r(\bar{x},t) \ , \tag{3.14}$$

where τ_d is called relaxation time and it has its origin from statistical mechanics of the electrons distribution for heat diffusion [8]. Heat diffusion stems from the same laws underlying the particle diffusion process. Therefore, despite the fact that the Telegraph Equation in (3.14) was originally formulated for the case of heat transfer, it can also be applied to the diffusion of particle concentration.

We propose to model the processing of the system input $r(\bar{x},t)|_{\bar{x}=\mathbf{0}}$ through the linear system denoted by the impulse response $g_d(\bar{x},t)$. This process is a convolution operation performed both in time t and in space $\bar{x}$, expressed as follows:

$$c(\bar{x},t)|_{\bar{x}\epsilon S} = \int_S \int_{t'=0}^{+\infty} r(\bar{x}',t') g_d(\bar{x}'-\bar{x}, t-t')\, dt'\, d\bar{x}' \ , \tag{3.15}$$

where the system input is the particle concentration rate at transmitter $r(\bar{x},t)|_{\bar{x}=\mathbf{0}}$ and the system output is the particle concentration value $c(\bar{x},t)$ at any space location $\bar{x}\epsilon S$ and at any time instant t.

Since the input particle concentration rate is a non-zero value only at the transmitter, this can be also seen as the multiplication of a Dirac delta in the space S by the particle concentration rate $r_T(t)$ at the transmitter. Therefore, the convolution operation is performed only in time, expressed as follows:

$$c(\bar{x},t)|_{\bar{x}\epsilon S} = \int_{t'=0}^{+\infty} r_T(t') g_d(\bar{x}, t-t')\, dt' \ , \tag{3.16}$$

The impulse response $g_d(\bar{x},t)$ of the system is the Green's function [9] (the propagator) of the diffusion process occurring between the transmitter and any other location $\bar{x}$ in the space S. The Green's function is in this case the diffusion process response to a particle concentration rate at the transmitter given by a Dirac delta in time ($r_T(t) = \delta(t)$). In order to compute the function $g_d(\bar{x},t)$ we study the equations governing the diffusion process and the physical conditions constraining their validity.

The Green's function $g_d(\bar{x},t)$ of the Telegraph Equation in (3.14), which is analytically equivalent to the wave equation in a lossy medium [6, 89], is the analytical solution for the concentration evolution in space and time when $r(\bar{x},t)$ is a Dirac delta function both in time t and in space S: $r(\bar{x},t) = \delta(\bar{x})\delta(t)$. It is analytically expressed as

$$g_d(\bar{x},t) = U\left(t - \|\bar{x}\|/c_d\right) e^{-\frac{t}{2\tau_d}} \frac{\cosh\left(\sqrt{t^2 - \left(|\bar{x}\|/c_d\right)^2}\right)}{\sqrt{t^2 - \left(\|\bar{x}\|/c_d\right)^2}} \ , \qquad (3.17)$$

where $\|\bar{x}\|$ is the distance from the transmitter and c_d is the wavefront speed, defined as $c_d = \pm\sqrt{D/\tau_d}$, where D is the diffusion coefficient, τ_d is the relaxation time in (3.14) and $U(.)$ is the step function.

The FTTF $\tilde{\mathbf{B}}(f)$ of the diffusion process is the Fourier transform of the Green's function $g_d(\bar{x},t)$ from (3.17), expressed as

$$\tilde{\mathbf{B}}(f) = \int_{-\infty}^{\infty} g_d(\bar{x}_R,t) e^{-j2\pi ft} dt \ , \qquad (3.18)$$

where $\bar{x}_R$ is the receiver location. The values of $\tilde{\mathbf{B}}(f)$ are computed numerically.

The *normalized gain* $\Gamma_{\mathbf{B}}(f)$ of the diffusion process is the magnitude $|\tilde{\mathbf{B}}(f)|$ of the FTTF $\tilde{\mathbf{B}}(f)$ normalized by its maximum value $\max_f(|\tilde{\mathbf{B}}(f)|)$, which is numerically computed from (3.18):

$$\Gamma_{\mathbf{B}}(f) = \frac{|\tilde{\mathbf{B}}(f)|}{\max_f(|\tilde{\mathbf{B}}(f)|)} \ . \qquad (3.19)$$

The *delay* $\tau_{\mathbf{B}}(f)$ of the diffusion process is

$$\tau_{\mathbf{B}}(f) = -\frac{d\phi_{\mathbf{B}}(f)}{df} \ , \qquad (3.20)$$

where $\phi_{\mathbf{B}}(f)$ is the phase of the FTTF $\tilde{\mathbf{B}}(f)$, as

$$\phi_{\mathbf{B}}(f) = \arctan\left(\frac{\mathrm{Im}(\tilde{\mathbf{B}}(f))}{\mathrm{Re}(\tilde{\mathbf{B}}(f))}\right) , \tag{3.21}$$

which stems from the real part $\mathrm{Re}(\tilde{\mathbf{B}}(f))$ and the imaginary part $\mathrm{Im}(\tilde{\mathbf{B}}(f))$, numerically computed from (3.18).

3.5 The Reception Process

Through the reception process, the receiver senses the particle concentration $c_R(t)$, and accordingly modulates the output signal $s_R(t)$ of the diffusion-based MC link model. The reception process, sketched in Figure 3.5, is based on the chemical theory of the ligand-receptor binding [86], and on the following assumptions:

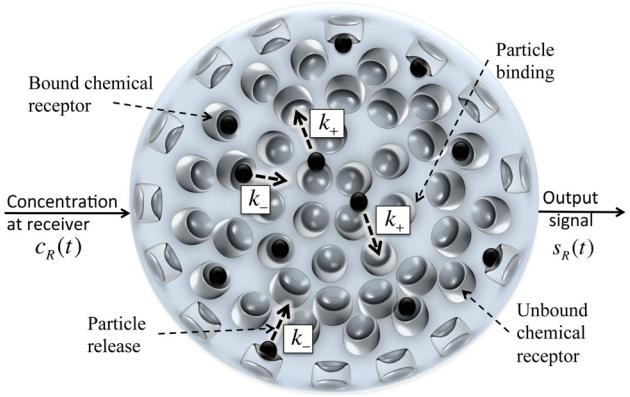

Figure 3.5: Representation of the reception process.

- The measure of the particle concentration takes place inside the *receptor space*. The receptor space has a spherical shape of radius ρ.
- The input *particle concentration* $c_R(t)$ is considered homogeneous inside the receptor space and equal to the particle concentration value at the receiver location.
- The reception is realized by means of N_R *chemical receptors*.

- The chemical receptors are assumed to homogeneously occupy the volume of the receptor space.
- Each chemical receptor, at the same time instant t, is exposed to the same particle concentration $c_R(t)$.
- The chemical receptors, when exposed to the particle concentration $c_R(t)$, can remain in their state, namely, *bound* or *unbound*, or they can change their state by undergoing two possible chemical reactions: the *particle binding* reaction if the receptor was previously unbound, or the *particle release* reaction if the chemical receptor was previously bound to a particle.
- The particle binding occurs with a rate k_+, while the particle release occurs with the rate k_-.

When a particle concentration $c_R(t)$ is present at time t inside the reception space, the chemical receptors change their states accordingly. The trend is to reach a ratio between the number of bound chemical receptors over the not-bound chemical receptors proportional to $c_R(t)$ itself. The concentration of chemical receptors inside the receptor space is the number of chemical receptors N_R divided by the reception space size ρ. Therefore, we define $\hat{s}_R(t)$ as the desired of the number of bound chemical receptors over the number of not-bound chemical receptors inside the receptor space with the following expression: $\hat{s}_R(t) = \rho/N_R\, c_R(t)$.

We define $n_c(t)$ as the number of bound chemical receptors (complexes) inside the emission space at time t. The time differential in the number of complexes $dn_c(t)dt$ inside the reception space is equal to the number of receptors N_R multiplied by the time differential of the system output signal $ds_R(t)dt$:

$$dn_c(t)dt = N_R\, ds_R(t)dt \tag{3.22}$$

The reception process described above is inspired by cellular systems from biology. According to these systems, the chemical receptors are models of the transmembrane receptors [73] embedded in the plasma membrane of living cells and involved in the signal transduction

process. In this section of the report, we do not model the location of the chemical receptors as if they were on the plasma membrane, but we place them homogeneously in the receptor space. This allows us to simplify the treatment related to the chemical changes which ultimately lead to the signal transduction. The signal transduction in bio-signaling involves the conversion of a chemical change (e.g., the change in concentration of the chemical components in the surrounding environment) into information. From this point of view, the molecules of the biochemical components are modeled by the particles and the biological surrounding environment is the receptor space.

The reception process is modeled through a series-resistor-capacitor (RC) circuit [84]. This circuit is shown in Figure 3.6, where $V_{in}(t)$ is the input voltage, function of the time t, R_r^{ch} is the resistance value of the resistor that is active during the capacitance-charging phase, R_r^{dis} is the resistance value of the resistor that is active during the capacitance-discharging phase, C_r is the capacitance value, and $I_{out}(t)$ is the output current, equal to the current $I_r(t)$ that is charging or discharging the capacitance. In the following, it is assumed that $R_r^{ch} \simeq R_r^{dis}$. Under this assumption, the diodes can be removed, and a single resistor R_r is considered.

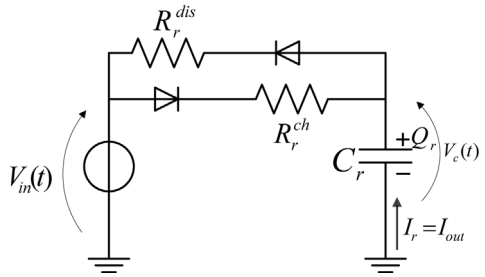

Figure 3.6: RC-circuit model of the reception process

From the electrical circuit theory [84], the Fourier transform of the transfer function (FTTF) [30] of the RC circuit $\mathbf{H}_{RC}(f)$ between the

input voltage $V_{in}(t)$ and the output current $I_{out}(t)$ is

$$\mathbf{H}_{RC}(f) = \frac{\tilde{\mathbf{I}}_{out}(f)}{\tilde{\mathbf{V}}_{in}(f)} = \frac{j2\pi f C_r}{1 + j2\pi f R_r C_r} \ , \tag{3.23}$$

where $\tilde{\mathbf{V}}_{in}(f)$ and $\tilde{\mathbf{I}}_{out}(f)$ are the Fourier transforms [30] of the input voltage $V_{in}(t)$ and output current $I_{out}(t)$, respectively.

In this scheme, we identify the desired ratio $\hat{s}_R(t)$ of the number of bound chemical receptors over the number of not-bound chemical receptors inside the receptor space with the input voltage $V_{in}(t)$ of the RC circuit. The system output signal $s_R(t)$ is equal to the output current I_{out}. The number n_c of bound chemical receptors inside the receptor space is considered as the charge Q_r stored in the capacitor at time t. The time differential $dQ_r(t)dt$ of the charge stored in the capacitor is equal to the capacitor value C_r multiplied by the time differential $dV_c(t)dt$ of the output voltage, expressed as follows:

$$dQ_r(t)dt = C_r \, dV_c(t)dt \ . \tag{3.24}$$

The similarity of (3.22) and (3.24) implies that N_R is the total number of chemical receptors inside the receptor space can be considered equal to the capacitor value C_r, expressed as

$$C_r = N_R \ . \tag{3.25}$$

A number of bound chemical receptors inside the reception space generates a proportional ratio between bound chemical receptors and not-bound chemical receptors as in an ideal capacitor, the stored charge $Q_r(t)$ generates a proportional voltage $V_c(t)$. The proportionality constants are N_R and C_r, respectively.

The rates of increase and decrease in the number of bound chemical receptors $V_c(t)$ are related to the rate constant k_+ of binding reaction and the rate constant k_- of release reaction, respectively. We assume that the probability of a chemical receptor to build/break a complex and to capture/release a particle is affected by the ratio $V_c(t)$ between the bound chemical receptors and not-bound chemical receptors itself. When $V_c(t)$ increases, the probability of capturing a particle decreases. When $V_c(t)$ decreases, the release rate decreases. We assume to have a

linear relation, which leads to the following expression:

$$\frac{dn_c}{dt} = (V_{in}(t) - V_c(t))k \; . \tag{3.26}$$

When $V_{in}(t) > V_c(t)$, then $k = k_+$, whereas, when $V_{in}(t) < V_c(t)$, then $k = -k_-$.

We relate the number of complexes n_c to the capacitor charge $Q_r(t)$ stored in the capacitor. $dn_c(t)/dt$ is therefore related to the capacitor charge current $I_r(t)$ at time t, equal to $dQ_r(t)/dt$, expressed as follows:

$$I_r(t) = \frac{(V_{in}(t) - V_c(t))}{R_r} \;\Rightarrow\; R_r = \frac{1}{k} \; , \tag{3.27}$$

where we assume that $k = k_- \simeq k_+$

From the electrical-circuit theory [84], the FTTF $\tilde{\mathbf{C}}(f)$ of the transmitter can be expressed as function of the FTTF of the RC circuit as follows:

$$\tilde{\mathbf{C}}(f) = \frac{\rho}{N_R}\mathbf{H}_{RC}(f) = \frac{j2\pi f C_r \rho}{N_R(1 + j2\pi f R_r C_r)} \; , \tag{3.28}$$

where $\tilde{\mathbf{I}}_{in}(f)$ and $\tilde{\mathbf{I}}_{out}(f)$ are the Fourier transforms [30] of the input voltage $I_{in}(t)$ and output voltage $I_{out}(t)$, respectively.

The *normalized gain* $\Gamma_{\mathbf{C}}(f)$ of the reception process is the magnitude $|\tilde{\mathbf{C}}(f)|$ of the FTTF $\tilde{\mathbf{C}}(f)$ normalized by its maximum value $\max_f(|\tilde{\mathbf{C}}(f)|)$, which becomes $\rho/(N_R\, R_r)$ from (3.28). This normalized gain has the following expression:

$$\Gamma_{\mathbf{C}}(f) = \frac{|\tilde{\mathbf{C}}(f)|}{\max_f(|\tilde{\mathbf{C}}(f)|)} = \frac{2\pi f R_r C_r}{\sqrt{(1 + (2\pi f R_r C_r)^2)}} \; . \tag{3.29}$$

The *delay* $\tau_{\mathbf{C}}(f)$ of the reception process is computed similarly to (3.9), where the phase of the FTTF of (3.28) is applied in place of the phase $\phi_{\mathbf{A}}(f)$, expressed as

$$\phi_{\mathbf{C}}(f) = \arctan\left(\frac{\mathrm{Im}(\tilde{\mathbf{C}}(f))}{\mathrm{Re}(\tilde{\mathbf{C}}(f))}\right) = \arctan\left(\frac{1}{2\pi f R_r C_r}\right) \; , \tag{3.30}$$

which is computed from the real part $\mathrm{Re}(\tilde{\mathbf{C}}(f))$ and the imaginary part $\mathrm{Im}(\tilde{\mathbf{C}}(f))$ of the FTTF $\tilde{\mathbf{C}}(f)$.

3.6 End-to-end Normalized Gain and Delay

The end-to-end *normalized gain* $\Gamma_{\mathbf{T}}(f)$ is computed by multiplying the normalized-gain contributions coming from the three processes, expressed as

$$\Gamma_{\mathbf{T}}(f) = \Gamma_{\mathbf{A}}(f) \cdot \Gamma_{\mathbf{B}}(f) \cdot \Gamma_{\mathbf{C}}(f) \ , \tag{3.31}$$

where $\Gamma_{\mathbf{A}}(f)$ is obtained from (3.8), (3.4) and (3.6); $\Gamma_{\mathbf{B}}(f)$ is numerically computed from (3.18) and (3.17); $\Gamma_{\mathbf{C}}(f)$ is obtained from (3.29), (3.27) and (3.25). The end-to-end *delay* $\tau_{\mathbf{T}}(f)$ is obtained by summation of the delay contributions coming from the three processes, expressed as

$$\tau_{\mathbf{T}}(f) = \tau_{\mathbf{A}}(f) + \tau_{\mathbf{B}}(f) + \tau_{\mathbf{C}}(f) \ , \tag{3.32}$$

where $\tau_{\mathbf{A}}(f)$ is obtained from (3.9), (3.10), (3.4) and (3.6); $\tau_{\mathbf{B}}(f)$ is numerically computed from (3.18) and (3.17); $\tau_{\mathbf{C}}(f)$ is obtained from (3.9), (3.30), (3.27) and (3.25).

3.7 Numerical Results

In this section, we show the numerical results in terms of *normalized gain and delay for each process*, as well as for the *overall end-to-end model*. The frequency spectrum considered in these results ranges from 0 Hz to 1 kHz. Although we believe that there is no biological justification for taking into account this frequency range, we are expecting to study networks of new devices which will be able to exploit the MC end-to-end model by using various modulation techniques, even the ones not used by biological entities. For this, we believe that the results in this frequency range could help the future development of nano-scale communication systems. We do not consider a wider frequency range since the results up to 1 kHz already show clearly the trend of the end-to-end model attenuation and delay as functions of the frequency.

The normalized gain $\Gamma_{\mathbf{A}}(f)$ for the emission process $\mathbf{A}$, shown in Figure 3.7, is computed from (3.8), (3.4) and (3.6), for a frequency spectrum from 0 Hz to 1 kHz and a diffusion coefficient $D \sim 10^{-6} m^2 sec^{-1}$ of

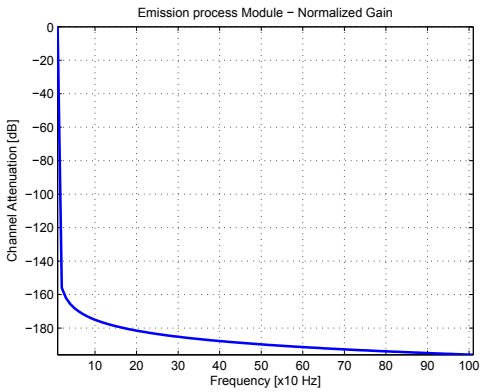

Figure 3.7: The normalized gain for the emission process A.

calcium molecules diffusing in a biological environment (cellular cytoplasm, [31]). The normalized gain $\Gamma_{\mathbf{A}}(f)$ shows a non-linear behavior with respect to the frequency, as expected from an RC circuit. The curves for the normalized gain in Figure 3.7 show the maximum value 1 (0 dB) at the frequency 0Hz and they monotonically decrease as the frequency increases and approaches 1 Hz. This phenomenon can be explained considering that if the frequency of the end-to-end model input signal $s_T(t)$ increases, the resulting modulated particle concentration rate $r_T(t)$ decreases in its magnitude. This is due to the fact that the particle mobility in the diffusion process between the inside and the outside of the transmitter is constrained by the diffusion coefficient. The higher is the diffusion coefficient, the faster is the diffusion process given a value for the particle concentration gradient between the inside and the outside of the transmitter.

The delay $\tau_{\mathbf{A}}(f)$ for the emission process $\mathbf{A}$, obtained from (3.9), (3.10), (3.4) and (3.6), shows a constant zero value in the frequency range from 0 Hz to 1 kHz and, for this reason, we omitted its plot here. Consequently, the transmitter does not distort any input signal having a bandwidth contained in the analyzed frequency range.

The normalized gain $\Gamma_{\mathbf{B}}(f)$ for the diffusion process $\mathbf{B}$, shown in Figure 3.8, is numerically computed from (3.19), (3.18) and (3.17) for a transmitter-receiver distance from 0 μm to 50 μm and a frequency spec-

trum from 0 Hz to 1 kHz. The diffusion coefficient is the one of calcium molecules diffusing in a biological environment (cellular cytoplasm, [31]) $D \sim 10^{-6}$ m^{2}sec^{-1}. The relaxation time τ_d from (3.14) is set approximatively to the relaxation time computed for water molecules: $\tau_d \sim 10^{-9}$ sec. The normalized gain $\Gamma_{\mathbf{B}}(f)$ shows a non-linear behavior both with respect to the distance d and the frequency f. The maximum value of the normalized gain (0 dB) is at the transmitter location (distance = 0) and for the frequency $f = 0$. As the frequency increases, the normalized gain decreases monotonically. The behavior with respect to the distance from the transmitter is monotonically decreasing.

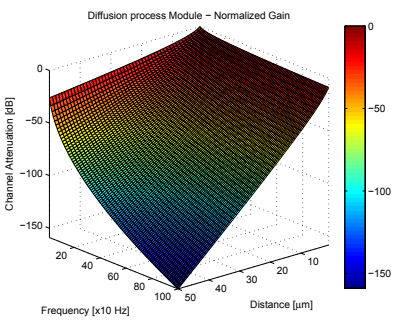

Figure 3.8: The normalized gain for the diffusion process B.

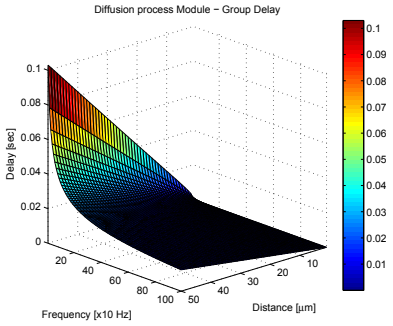

Figure 3.9: The group delay for the diffusion process B.

The delay $\tau_{\mathbf{B}}(f)$ for the diffusion process $\mathbf{B}$, shown in Figure 3.9, is numerically computed from (3.20), (3.21), (3.18) and (3.17). The delay $\tau_{\mathbf{B}}(f)$ is shown both with respect to the distance and the frequency. For low frequency values, the delay is non-linear with respect to the distance from the transmitter. Therefore, the particle diffusion process B has a dispersive behavior in the frequency range from 0 Hz to 1 kHz and, consequently, the signal propagating through the molecular diffusion process can be distorted.

The normalized gain $\Gamma_{\mathbf{C}}(f)$ for the reception process $\mathbf{C}$, shown in Figure 3.10, is obtained from (3.29), (3.27) and (3.25), for a variable number of receptors N_R from 20 to 100, a frequency spectrum from 0 Hz to 1 MHz, rate constants $k_+ = k_- = 10^8$ M^{-1}sec^{-1} (see [68]), and $\rho = 10$ μm. The reception process normalized gain shows a non-

linear behavior with respect to the frequency, as expected from an RC circuit. Each different curve is related to a different value in the number of receptors N_R. All the curves show the maximum value 1 at the frequency 0 Hz. The normalized gain monotonically increases as the frequency increases. This phenomenon can be explained considering that if the frequency of the particle concentration $c_R(t)$ increases, the resulting output signal $s_R(t)$ increases its magnitude. This is due to the fact that the particle receptors are constrained by the rate of release and binding in the sensing of the particle concentration $c_R(t)$. The curves related to lower values of N_R show lower values of normalized gain throughout the frequency spectrum range. A higher number of receptors N_R requires a higher number of molecules released or captured in order to reach a desired ratio of bound receptor to non bound receptors. The number of receptors N_R is also related to the precision of the particle concentration measurement. Then the higher is the number N_R of receptors inside the receptor space S_r, the smaller is the minimum concentration variation $dc_r(t)$ sensed by the reception process and translated into a variation in the system output signal $s_R(t)$.

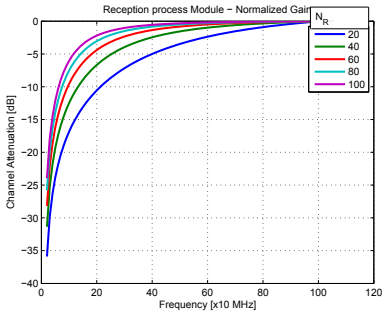

Figure 3.10: The normalized gain for the reception process C.

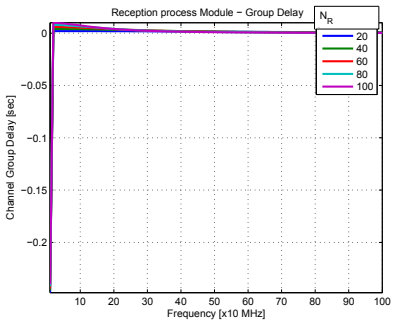

Figure 3.11: The group delay for the reception process C.

The delay $\tau_{\mathbf{C}}(f)$ for the reception process $\mathbf{C}$, shown in Figure 3.11, is obtained from (3.30), (3.27) and (3.25). The delay $\tau_{\mathbf{C}}(f)$ curves are shown in Figure 3.11 with the same input parameters as before. For every curve, the delay has a non-linear behavior with respect to frequency. This means that the shape of the system output signal $s_R(t)$

is distorted with respect to the particle concentration $c_R(t)$. This behavior is enhanced for higher values in the number N_R of receptors.

The normalized gain $\Gamma_{\mathbf{T}}(f)$ for the end-to-end model T, shown in Figure 3.12, is computed from (3.31) for a transmitter-receiver distance from 0 μm to 50 μm. The number of receptors is assumed to be $N_R = 10$, since it corresponds to the lowest normalized gain for the reception process, while maintaining a reasonable number of receptors at the receiver. The end-to-end normalized gain shows a non-linear behavior with respect to the frequency. Each different curve is related to a different value of the transmitter-receiver distance. All the curves show the maximum value 1 at the frequency 0Hz. The normalized gain monotonically decreases as the frequency increases. If the frequency of the end-to-end model input signal $s_T(t)$ increases, the resulting output signal $s_R(t)$ decreases its magnitude. The curves related to higher values of the transmitter-receiver distance show lower values of normalized gain throughout the frequency spectrum range.

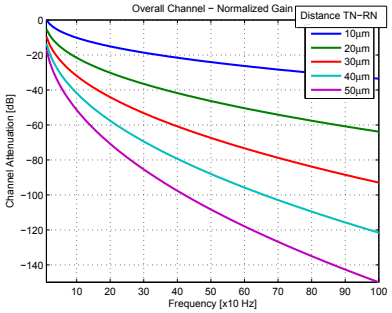

Figure 3.12: The normalized gain for the reception process T.

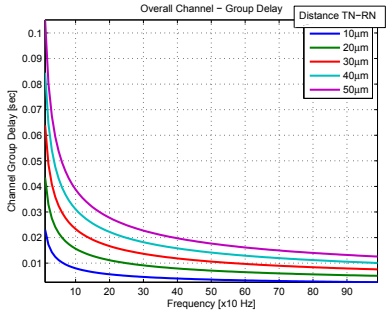

Figure 3.13: The group delay for the end-to-end model T.

The delay $\tau_{\mathbf{T}}(f)$ for the end-to-end model T, shown in Figure 3.13, is computed from (3.32). The delay $\tau_{\mathbf{T}}(f)$ curves are shown in Figure 3.13, one for each value of the transmitter-receiver distance. For every curve, each frequency is delayed by a different time. Consequently, the shape of the system output signal $s_R(t)$ is distorted with respect to the end-to-end model input signal $s_T(t)$. This behavior is enhanced for higher values of the transmitter-receiver distance.

3.8 Conclusions

In this chapter of the article, a deterministic model for a diffusion-based MC link is proposed. For this, a basic diffusion-based MC link design is provided, which aims at an interpretation of the diffusion-based MC, both in terms of molecule emission/reception and molecule propagation. In the provided diffusion-based MC link design, the deterministic model is studied as the composition of three subsequent processes, namely, the particle emission, the particle diffusion, and the particle reception. The normalized gain and delay are computed as functions of the frequency and the transmission range for the three physical processes, as well as for the overall end-to-end model. Numerical results are provided to evaluate the normalized gain and delay of the diffusion-based MC link for several different values of the signal frequency and the transmission range.

Typical communication engineering paradigms can be applied to this model in order to study the end-to-end behavior in terms of noise, capacity and throughput. Moreover, in light of the results, several classical modulation schemes could be studied when information is sent over this diffusion-based MC link. However, this analysis does not account for stochastic phenomena present in the aforementioned processes that can act as noise on the information signal. In the next chapter, the models for the three processes are further refined by providing an analysis of the noise sources affecting the diffusion-based MC.

4

Stochastic Models of the Noise Sources in a Molecular Communication Link

4.1 Motivation and Related Work

The proper study and characterization of the noise is one of the main challenges in the information theoretic analysis of diffusion-based Molecular Communication (MC). The noise in a communication system is defined as an unwanted and unavoidable random component that affects the information-bearing signal [94]. The modeling of the noise sources is fundamental to design the components of a communication system, and increase the probability of correct exchange of information between the transmitted and the receiver. From the point of view of communication engineering, the most useful characterization the noise sources is achieved, whenever possible, through a stochastic modeling, where the generated noise signal is interpreted as the output of random processes with known statistical parameters. The objective of this chapter of the article is to identify the most relevant noise sources affecting a diffusion-based MC link, and provide stochastic models with a proven physical validity.

Most of the contributions from the literature to the noise analysis for diffusion-based MC are mainly based on the results of simulations, and do not provide stochastic models for the noise sources in terms

of random processes. As an example, in [92] the results of simulations show a noise for the diffusion-based MC which follows a non-Gaussian statistics, although the analytical model for this statistics is not investigated. In [70] the noise effects on the diffusion-based MC are resulting only from simulation and there is no analytical model of diffusion-based noise and no stochastic study of its underlying physical phenomena. Moreover, in [70] there is no specific analysis of the noise sources which affect the reception side of a diffusion-based MC link. In [14], the diffusion-based MC reception noise is analyzed in terms of probability of having erroneous digital reception, under the assumption of a binary squared pulse code modulation signal. As a consequence, the work in [14] addresses the noise analysis for a diffusion-based MC link having specific characteristics in terms of modulation scheme and type of transmitted messages.

Contributions from the biochemistry literature provide descriptions of some physical processes underlying the noise sources in diffusion-based MC link. Seminal works in biochemistry, such as [20], analyzed how free space diffusion of molecules impairs the proper measurement of the molecule concentration. A more recent contribution to the physical analysis of molecule diffusion and reception in biochemical signaling can be found in [23]. However, these contributions tend to focus on the explanation of natural phenomena, and do not provide suitable models for MC engineering. The work in [83] stems, on the contrary, from the simulation of a biological signal transduction mechanism and its associated noise using tools from communication engineering. However, the analysis of the system is limited to a numerical evaluation of the simulation results using communication engineering parameters (e.g., the Signal to Noise Ratio, SNR). No stochastic models are provided in [83] for the noise sources, but the results are coming from numerical simulations. In [61], the authors develop only a preliminary information theoretic model applied to the study of intracellular communication with the diffusion of calcium ions.

In this chapter of the article, three noise sources affecting a diffusion-based MC link are identified, namely, the sampling noise, the counting noise [78], and the ligand-receptor-binding noise [80], and they

are related to the transmitter, the signal propagation in the channel, and the receiver, respectively. These noise sources are modeled in a twofold fashion: the physical model provides a mathematical analysis of the physical processes which generate the noise, while the stochastic model aims at capturing those physical processes through statistical parameters. The physical model contains all the physical variables which contribute to the generation of the noise. The stochastic model summarizes the noise generation using random processes and their associated parameters. Sets of noise data realizations are generated through simulation of the physical model. These sets of noise data are then used to test the stochastic model ability to capture the behavior of the physical processes which generate the noise.

4.2 Definition of the Noise Sources in a Diffusion-based MC Link

Three noise sources, which affect the diffusion-based MC link defined in Chapter 3, are identified and studied in this section, namely, the particle-sampling noise, the particle-counting noise, and the ligand-receptor-kinetics noise. In the following, each noise source is defined with reference to the block scheme in Figure 4.1.

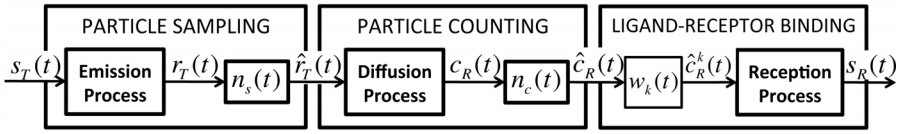

Figure 4.1: Block scheme of the diffusion-based MC link that includes the noise sources.

The particle-sampling noise is related to the emission process at the transmitter, and it is expressed as $n_s(t)$. This noise generates an unwanted perturbation on the output of the emission process $r_T(t)$, which results in $\hat{r}_T(t)$, as shown in Figure 4.1. The particle-sampling noise occurs when the particle-concentration rate is being modulated through the emission of the particles. During this emission, since particles are discrete, the particle-concentration rate $r_T(t)$ is sampled by the

particles themselves, resulting in the noisy particle-concentration rate $\hat{r}_T(t)$. Further details on the analysis of this type of noise are provided in Section 4.3.

The particle-counting noise is related to the signal propagation during the diffusion process, and it is expressed as $n_c(t)$. This noise generates an unwanted perturbation on the output of the diffusion process $c_R(t)$, which results in $\hat{c}_R(t)$, as shown in Figure 4.1. The particle-counting noise occurs when the particle concentration value is being measured at the receiver location, and it is due to the randomness in the particle motion and to the discreteness of the particles. The particle concentration $c_R(t)$ at the receiver location is computed by counting the number of particles present inside the receptor space. Fluctuations and imprecisions in counting the particles impair the proper computation of the concentration $c_R(t)$. As a result, the actual computed concentration $\hat{c}_R(t)$ differs from $c_R(t)$. The analysis of this type of noise is provided in Section 4.4.

The ligand-receptor-kinetics noise affects the molecular receiver as a consequence of random fluctuations in the ligand-receptor-binding process. As a consequence of this noise contribution, denoted by $w_k(t)$, the particle concentration $\hat{c}_R(t)$ is subject to an unwanted perturbation, resulting in $\hat{c}_R^k(t)$. This perturbation propagates to the output signal $\hat{s}_R^k(t)$ after the reception process, as shown in Figure 4.1. Further details on the analysis of this type of noise are provided in Section 4.5.

In the following, the analysis of each noise source, which results in both a *physical model* and a *stochastic model*, is detailed. With the former the mathematical expression of the physical process underlying the noise source is obtained, while with the latter the noise source behavior is modeled through the use of statistical parameters.

4.3 The Particle-sampling Noise

The model of the emission process provided in Chapter 3 does not take into account the discrete nature of the particles. In this section, an additional assumption is considered for the particle-emission process:

- The particle flux through the emission gaps in the spherical

boundary is composed of discrete particles.

As a result, the relation between the input signal $s_T(t)$ and the resulting particle-concentration rate, denoted by $\hat{r}_T(t)$, is no longer a continuous function as in Chapter 3. During the emission process, as shown in Figure 3.2, single particles flowing through the emission gaps contribute to the concentration rate $\hat{r}_T(t)$ with a value k_n at discrete time instants $t_n = t_1, t_2, \ldots$. These time instants are not equally spaced, as a consequence of the random nature of the particle motion through the emission gaps. Therefore, the resulting particle-concentration rate $\hat{r}_T(t)$ assumes values equal to k_n at randomly-spaced time instants t_n, and it is zero for any other time instant. This particle-concentration rate is expressed as follows:

$$\hat{r}_T(t) = \sum_{n \epsilon \mathbb{N}} \frac{k_n}{t_n - t_{n-1}} \delta(t - t_n) \ , \tag{4.1}$$

where $\delta(.)$ is a Dirac delta function.

The Physical Model The physical model of the particle-sampling noise is represented by the block scheme shown in Figure 4.2. The signal $s_T(t)$ is the input of the emission-process block, whose output is the particle-concentration rate $r_T(t)$. The physical model of the particle-sampling noise $n_s(t)$ takes as input the particle-concentration rate $r_T(t)$ that the emission process would produce in output in the absence of noise. The particle-sampling noise $n_s(t)$ is composed of a decision block and a non-uniform sampler, which have as input the transmitter kinetic state $\bar{S}_T(t)$, and a divisor. The output of the particle-sampling noise $n_s(t)$ is the particle-concentration rate $\hat{r}_T(t)$ affected by noise.

The **transmitter kinetic state** $\bar{S}_T(t)$, as shown in Figure 4.3, is a set composed by the location $\bar{x}_p(t)$ and the velocity $\bar{v}_p(t)$ of each particle p at time t present in the surrounding of the transmitter spherical boundary, expressed as

$$\bar{S}_T(t) = \{\bar{x}_p(t), \bar{v}_p(t) | \ \ p = 1, ..., P(t)\} \ , \tag{4.2}$$

where $P(t)$ is the number of particles in the system, and it is a function of the particle-concentration rate $r_T(t)$, output of the emission-process block, as shown in Figure 4.2.

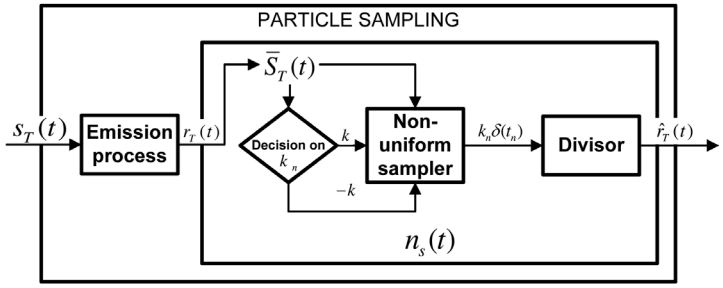

Figure 4.2: Block scheme of the physical model for the particle-sampling noise.

The **decision** block, shown in Figure 4.2, assigns the value of k_n according to the transmitter kinetic state $\bar{S}_T(t)$. This output k_n is assigned a positive k value or a negative $-k$ value according to whether there is an event in the kinetic state $\bar{S}_T(t)$ of a particle flowing through an emission gap. The output k_n is assigned a positive k if the particle is going outside the spherical boundary, and a negative $-k$ if the particle is coming inside the spherical boundary. The value of k equals a contribution of one particle to the concentration at the transmitter location.

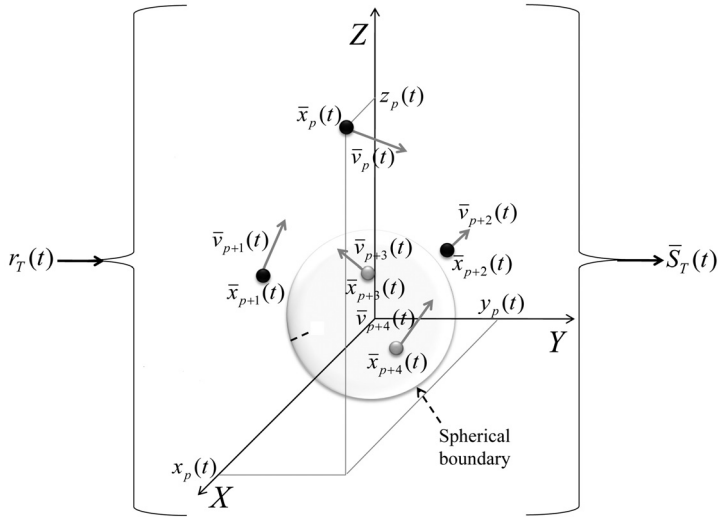

Figure 4.3: Graphical sketch of the transmitter kinetic state $\bar{S}_T(t)$ at time t.

The **non-uniform-sampler** block, shown in Figure 4.2, samples at time instants t_n, which are functions of the transmitter kinetic state $\bar{S}_T(t)$. If, at time instant t_n, there is an event in the kinetic state $\bar{S}_T(t_n)$ of a particle flowing through an emission gap, the non-uniform-sampler block produces a Dirac impulse at t_n, with amplitude equal to the current value of k_n, which is the output of the decision block.

The **divisor** block, shown in Figure 4.2, divides the output of the non-uniform sampler by the time interval between the previous sample at t_{n-1} and the current sample at t_n.

Since it is not possible to always have the knowledge of the kinetic state of the system $\bar{S}_T(t)$ because of the huge amount of information and the randomness in the particle motion, the value of $\hat{r}_T(t)$ cannot be analytically computed as function of $r_T(t)$ from the physical model of the particle-sampling noise. Using the physical model provided here, only numerically simulations of the behavior of the particle-sampling noise $n_s(t)$ can be performed. A sinusoidal particle-concentration rate $r_T(t)$ as the input, and the corresponding noisy particle-concentration rate $\hat{r}_T(t)$ as the output of a simulation of the physical model are shown in Figure 4.4 and Figure 4.5, respectively, where the radius of the transmitter spherical boundary is $\rho = 1\mu m$, and the diffusion coefficient is $D \sim 10^{-6} cm^2 sec^{-1}$ [31].

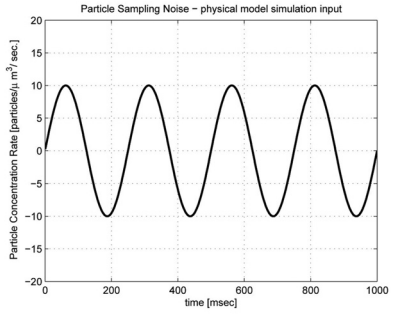

Figure 4.4: The particle sampling noise physical model simulation input.

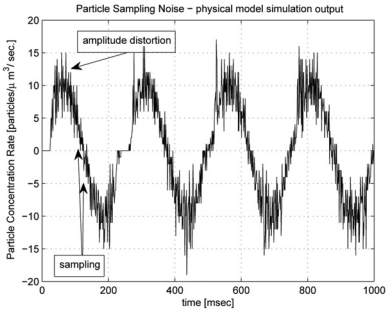

Figure 4.5: The particle sampling noise physical model simulation output.

The Stochastic Model The particle-sampling noise can also have another formulation, through statistical parameters, that is suitable when theoretical studies require an analytical expression of the noise. In this formulation, the particle-sampling noise $n_s(t)$ is generated by a random process $\tilde{n}_s(t)$, whose contribution corresponds to the difference between the particle-concentration rate $\hat{r}_T(t)$ affected by noise and the particle-concentration rate $r_T(t)$ expected in the absence of noise, expressed as follows:

$$\tilde{n}_s(t) = \hat{r}_T(t) - r_T(t) \ . \tag{4.3}$$

In Figure 4.6, the main block scheme of the stochastic model for the particle-sampling noise is shown. The random process $\tilde{n}_s(t)$, as it is proved in the following, depends on the value of the particle-concentration rate $r_T(t)$, output from the emission-process block, which receives the signal $s_T(t)$ as input. The sum of the random process $\tilde{n}_s(t)$ and the particle-concentration rate $r_T(t)$ is the particle-concentration rate $\hat{r}_T(t)$ affected by the particle-sampling noise.

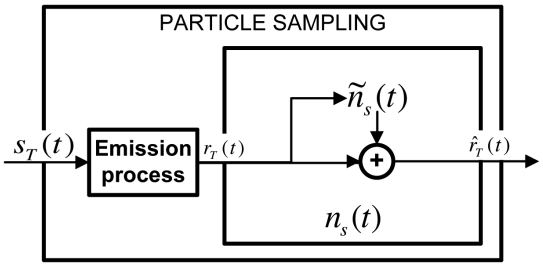

Figure 4.6: Block scheme of the stochastic model for the particle-sampling noise .

When the emission process is subject to the particle-sampling noise, the particle-concentration rate at the transmitter location $\hat{r}_T(t_n)$ corresponds to the finite-time difference of the particle concentration $\hat{c}_T(t)$ at the transmitter, which is step wise and, therefore, not derivable, and it is expressed as

$$\hat{r}_T(t_n) = \frac{\hat{c}_T(t_n) - \hat{c}_T(t_{n-1})}{t_n - t_{n-1}} \ . \tag{4.4}$$

Through an analysis of the stochastic processes underlying the emission process, the particle concentration $\hat{c}_T(t)$ at the transmitter is proved

to be a double non-homogeneous Poisson counting process, whose rate of occurrence corresponds to the expected particle-concentration rate $r_T(t)$. This process is expressed as follows:

$$\hat{c}_T(t) \sim \begin{cases} Poiss(r_T(t)) & r_T(t) > 0 \\ -Poiss(-r_T(t)) & r_T(t) < 0 \end{cases} . \tag{4.5}$$

As a consequence, the particle-concentration rate $\hat{r}_T(t)$ is the finite-time difference of a double non-homogeneous Poisson counting process. Therefore, the random process $\tilde{n}_s(t)$, defined in (4.3), is white [74] and its mean-squared value $\langle \tilde{n}_s^2(t) \rangle$ is equal to the expected particle-concentration rate $r_T(t)$, expressed as

$$\langle \tilde{n}_s^2(t) \rangle = r_T(t) . \tag{4.6}$$

The root-mean-squared (RMS) value of the perturbation $\mathrm{RMS}(\tilde{n}_s(t))$ on the expected particle-concentration rate $r_T(t)$ is equal to the square root of the expected particle-concentration rate $r_T(t)$, expressed as

$$\mathrm{RMS}(\tilde{n}_s(t)) = \sqrt{r_T(t)} . \tag{4.7}$$

The statistical-likelihood test is applied in order to assess the stochastic-model ability to capture the behavior of the physical processes that generate the noise. For this, the likelihood, which is the probability of the noisy data coming from the physical-model simulation given the stochastic model of the particle-sampling noise, is computed and shown in Figure 4.7. These results are compared to the results obtained by using a Gaussian model in place of the stochastic model computed above, shown in Figure 4.8.

4.4 The Particle-counting Noise

The model of the diffusion process provided in Chapter 3 does not take into account the discrete nature of the particles and the randomness of their motion when the concentration $c(\bar{x}_R, t)$ inside the receptor space is measured. In the present analysis, the following assumptions are introduced:

- The receptor space contains a discrete number of particles.

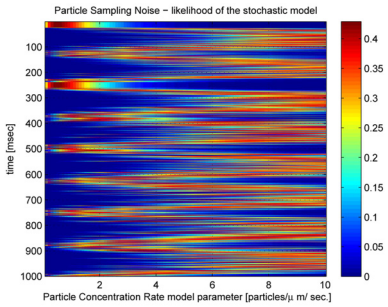
Particle Sampling Noise – likelihood of the stochastic model
time [msec]
Particle Concentration Rate model parameter [particles/μ m/ sec.]

Figure 4.7: The particle sampling stochastic model likelihood.

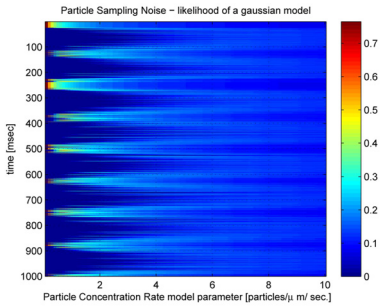
Particle Sampling Noise – likelihood of a gaussian model
time [msec]
Particle Concentration Rate model parameter [particles/μ m/ sec.]

Figure 4.8: The Gaussian model likelihood for the particle sampling noise.

- Particles may enter/leave the receptor space as a consequence of the diffusion process, even when the concentration $c(\bar{x}_R, t)$ at the receiver location is maintained at a constant value.

As a result, the measured particle concentration $\hat{c}_R(t)$ suffers from two effects. The first effect is given by the quantization of the concentration measure, which is due to the discrete number of particles inside the receptor space. The second effect is given by fluctuations in the concentration measure, which are due to single events of particles entering/leaving the receptor space.
During the reception process, particles present inside the receptor space at time instant t are counted, and their number $\hat{N}_p(t)$ is divided by the size of the receptor space $(4/3)\pi\rho^3$, expressed as

$$\hat{c}_R(t) = \frac{\hat{N}_p(t)}{(4/3)\pi\rho^3}, \quad \hat{N}_p(t)\epsilon\mathbb{N} \ , \tag{4.8}$$

where $\mathbb{N}$ denotes the set of the positive integers.

The Physical Model The physical model of the particle-counting noise is represented though the block scheme shown in Figure 4.9.

The particle-concentration rate $\hat{r}_T(t)$ is the input of the diffusion-process block, whose output is the true particle concentration $c_R(t)$. The physical model of the particle-counting noise $n_c(t)$ takes as input the true particle concentration $c_R(t)$ that the diffusion process would

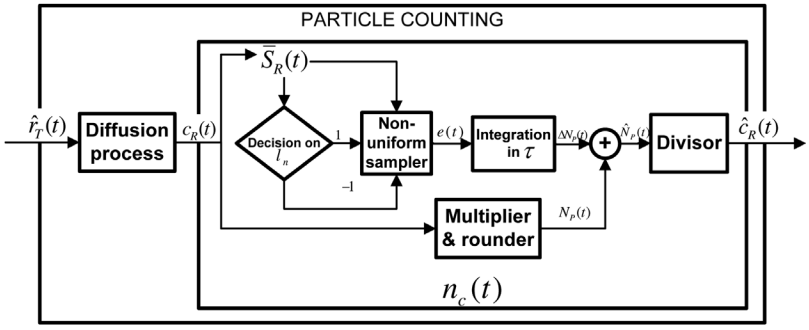

Figure 4.9: Block scheme of the physical model for the particle-counting noise.

produce in output in the absence of noise. The particle-counting noise $n_c(t)$ is composed of two branches. The upper branch has a decision block and a non-uniform sampler, which have as input the receiver kinetic state $\bar{S}_R(t)$, while the lower branch has a multiplier and rounder block, and it takes as input the true particle concentration $c_R(t)$. The two branches are then added and the result is the input of a divisor. The output of the particle-counting noise $n_c(t)$ is the particle concentration $\hat{c}_R(t)$ affected by noise.

The **receiver kinetic state** $\bar{S}_R(t)$, as shown in Figure 4.10, is a set composed by the location $\bar{x}_p(t)$ of each particle p at time t present in the surrounding of the receptor space, expressed as

$$\bar{S}_R(t) = \{\bar{x}_p(t) |\ \ p = 1, ..., P(t)\}\ \ , \tag{4.9}$$

where $P(t)$ is the number of particles in the simulation space S_S, and it is a function of the particle concentration $c_R(t)$, as shown in Figure 4.10.

The **decision** block, shown in Figure 4.9, assigns the value of l_n according to the receiver kinetic state $\bar{S}_R(t)$. This output l_n can assume either value 1 or -1 depending on whether the kinetic state $\bar{S}_R(t)$ has an event of a particle entering or leaving the receptor space.

The **non-uniform-sampler** block, shown in Figure 4.9, samples at time instants t_n, which are functions of the receiver kinetic state $\bar{S}_R(t)$. If, at time instant t_n, there is an event in the kinetic state $\bar{S}_R(t_n)$ of a particle entering or leaving the receptor space, the non-uniform-sampler block produces a Dirac impulse at t_n with amplitude equal to

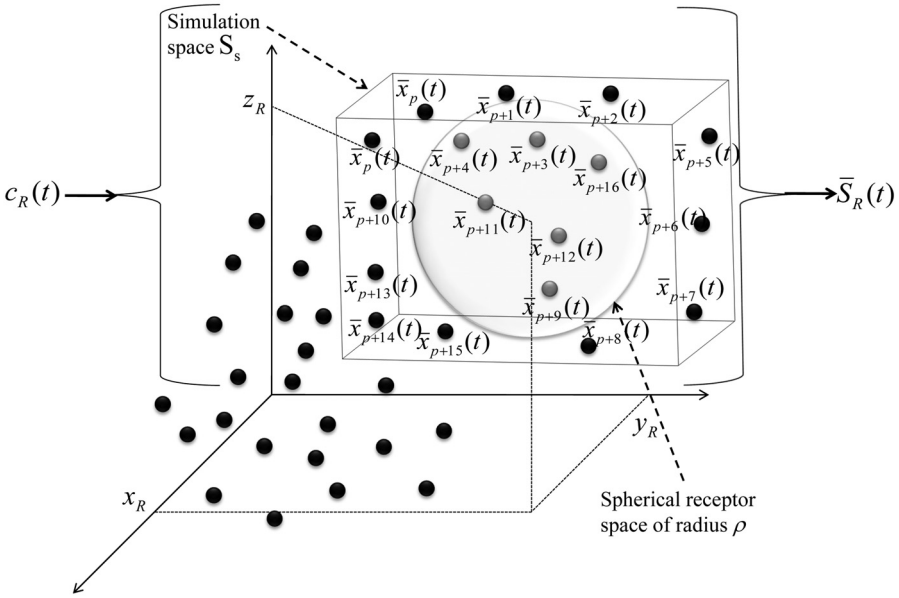

Figure 4.10: Graphical sketch of the receiver kinetic state $\bar{S}_R(t)$ at time t.

the current value of l_n, which is the output of the decision block.

The **integration** block, shown in Figure 4.9, integrates the output from the non-uniform sampler for a past time interval equal to τ, from $t - \tau$ up to time t, where τ corresponds to the time interval in which a quasi-constant particle concentration is expected. The result of the integration block is the perturbation $\Delta N_p(t)$ at time t of the number of particles inside the receptor space.

The **multiplier and rounder** block, shown in Figure 4.9, rounds the particle concentration $c_R(t)$ multiplied by the size of the receptor space $(4/3)\pi\rho^3$. Finally, the **divisor** block divides the sum of the outputs of the two branches, $\Delta N_p(t)$ and $N_p(t)$, respectively, by the size of the receptor space, which is equal to $(4/3)\pi\rho^3$.

Since it is not possible to always have knowledge of the kinetic state of the system $\bar{S}_R(t)$ because of the huge amount of information and the randomness in the particle motion, the value of $\hat{c}_R(t)$ cannot be analytically computed as function of $c_R(t)$ from the physical model of the particle-counting noise, but only numerically, as shown in Figure 4.12.

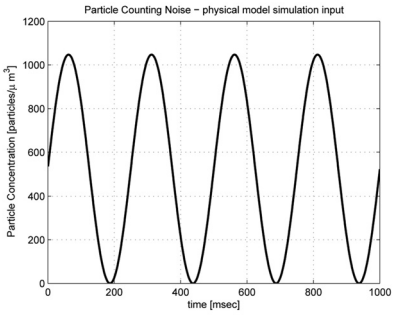

Figure 4.11: The particle counting noise physical model simulation input.

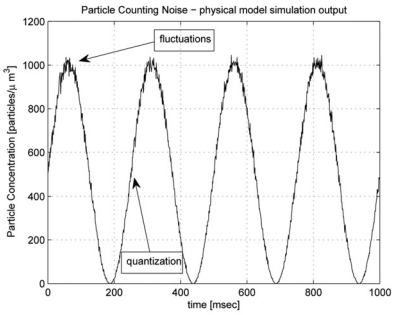

Figure 4.12: The particle counting noise physical model simulation output.

As performed for the particle-sampling noise in Section 4.3, a sinusoidal particle concentration $c_R(t)$ as the input, and the corresponding noisy particle concentration $\hat{c}_R(t)$ as the output of a simulation of the physical model are shown in Figure 4.11 and Figure 4.12, respectively, where the radius of the spherical receptor space is $\rho = 1\mu m$, and the diffusion coefficient is $D \sim 10^6 cm^2 sec^{-1}$.

The Stochastic Model The particle-counting noise, similarly to the particle-sampling noise, can also have another formulation, through statistical parameters. The particle-counting noise $n_c(t)$ is generated by a random process $\tilde{n}_c(t)$, whose contribution corresponds to the difference between the measured particle concentration $\hat{c}_R(t)$ and the particle concentration $c_R(t)$ expected in the absence of noise, expressed as follows:

$$\tilde{n}_c(t) = \hat{c}_R(t) - c_R(t) \ . \tag{4.10}$$

The main block scheme of the stochastic model for the particle-counting noise is shown in Figure 4.13. The random process $\tilde{n}_c(t)$, as it is proved in the following, depends on the value of the particle concentration at the receiver $c_R(t)$, output from the diffusion process, which receives the transmitted particle-concentration rate $r_T(t)$ as input. The sum of the random process $\tilde{n}_c(t)$ and the true particle concentration at

the receiver $c_R(t)$ is the particle concentration $\hat{c}_R(t)$ affected by the particle-counting noise.

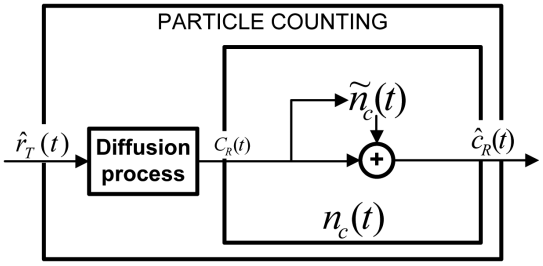

Figure 4.13: Block scheme of the stochastic model for the particle-counting noise .

As a consequence of the particle-counting noise, the measured particle concentration $\hat{c}_R(t)$ corresponds to the actual number of particles $\hat{N}_p(t)$ divided by the size of the receptor space, expressed as

$$\hat{c}_R(t) = \frac{\hat{N}_p(t)}{(4/3)\pi\rho^3} \ . \tag{4.11}$$

It is possible to prove that the actual number of particles $\hat{N}_p(t)$ inside the receptor space is a volumetric non-homogeneous Poisson counting process, whose rate of occurrence corresponds to the expected particle concentration $c_R(t)$. This process is expressed as follows:

$$\hat{N}_p(t) \sim \text{Poiss}(c_R(t)) \ . \tag{4.12}$$

As a consequence, given (4.10), the random process $\tilde{n}_c(t)$ has zero average value and the RMS value of the perturbation $\tilde{n}_c(t)$ on the actual measured particle concentration $\hat{c}_R(t)$ is

$$\text{RMS}(\tilde{n}_c(t)) = \sqrt{\frac{c_R(t)}{(4/3)\pi\rho^3}} \ . \tag{4.13}$$

It is possible to reduce the value of $\text{RMS}(\tilde{n}_c(t))$ by averaging in time several measures of the particle concentration $\hat{c}_R(t)$. It is proved that, if a quasi-constant expected concentration is assumed in a time interval τ, the final expression for the RMS of the perturbation $\text{RMS}(\tilde{n}_c(t))$

becomes as follows:

$$\mathrm{RMS}(\tilde{n}_c(t)) = \sqrt{\frac{c_R(t)}{(4/3)\pi D\rho\tau}}\ , \tag{4.14}$$

where $c_R(t)$ is the expected measured particle concentration, D is the diffusion coefficient, ρ is the radius of the receptor space, and τ is the time interval in which a quasi-constant particle concentration is expected. The validity of (4.14) is confirmed by the results from [23], where the authors obtain the same expression as in (4.14) for the RMS of the particle-counting noise by applying a different approach.

Similarly to Section 4.3, as shown in Figure 4.15, the results of the statistical-likelihood test applied to the stochastic model of the particle-counting noise are shown in Figure 4.14, while the results obtained through the use of a Gaussian model are shown in Figure 4.15.

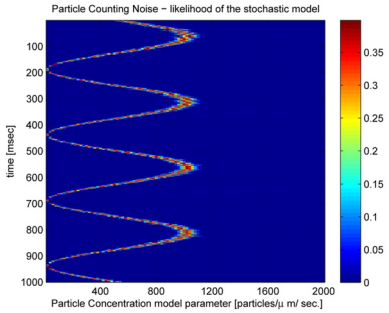

Figure 4.14: The particle counting stochastic model likelihood.

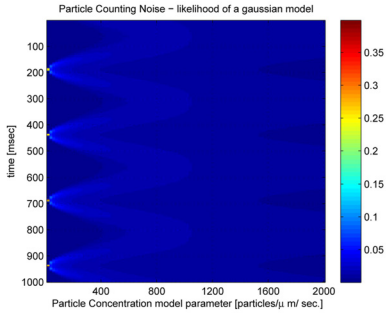

Figure 4.15: The Gaussian model likelihood for the particle counting noise.

4.5 The Ligand-receptor-kinetics Noise

The model of the reception process provided in Chapter 3 does not take into account the random fluctuations in the ligand-receptor-binding process. The following additional assumptions are here considered:

- The binding reaction occurs only if the kinetic energy of the particle colliding with an unbound receptor is higher than the activation energy.

- Whenever a binding reaction occurs, there is a subtraction of a particle from the receptor space. Whenever a release reaction occurs, there is an addition of a particle to the receptor space.

As a result, the relation between the particle concentration $c_R(t)$ and the actual output signal of the reception process, denoted by $\hat{s}_R^k(t)$, is subject to random fluctuations. As shown in Figure 3.5, particles subject to the Brownian motion inside the receptor space contribute to the number of bound chemical receptors, denoted with $\hat{n}_b(t)$, only at discrete time instants $t_n = t_1, t_2, \dots$ that correspond to collision events between the particles themselves and the unbound receptors. Each collision event contributes to $\hat{n}_b(t)$ according to the coefficient k_n, which is a function of the kinetic energy of the collided particle. The bound receptors can become unbound according to the particle release rate k_-, thus decreasing the value of $\hat{n}_b(t)$. Therefore, the ligand-receptor kinetics-equation is derived by extending the Reaction Rate Equation (RRE) from [23] in order to account for the random effect of the collisions, expressed as

$$\frac{d\hat{n}_b(t)}{dt} = \left(\sum_n k_n \delta(t - t_n)\right) - k_- \hat{n}_b(t), \;\; t_n = t_1, t_2, \dots \;, \qquad (4.15)$$

where $\hat{n}_b(t)$ is the number of bound chemical receptors, k_n is a coefficient related to the particle binding at time instant t_n, k_- is the rate of particle release, and $\delta(.)$ is a Dirac delta function. The time-first derivative in the number $\hat{n}_b(t)$ of bound chemical receptors in (4.15) can be substituted with the output signal of the reception process, denoted as $\hat{s}_R^k(t)$. The contribution of the ligand-receptor kinetics creates fluctuations in the output signal $\hat{s}_R^k(t)$ that are not present in the previous formulation of the reception process in Chapter 3.

The Physical Model The physical model of the ligand-receptor kinetics is represented though the block scheme shown in Figure 4.16. The particle concentration $c_R(t)$ is the input of the overall reception process + $w_k(t)$ block, whose output signal is $\hat{s}_R^k(t)$. The ligand-receptor-kinetics block is composed of the ligand-receptor kinetic state block, the integration block, and three multiplication blocks.

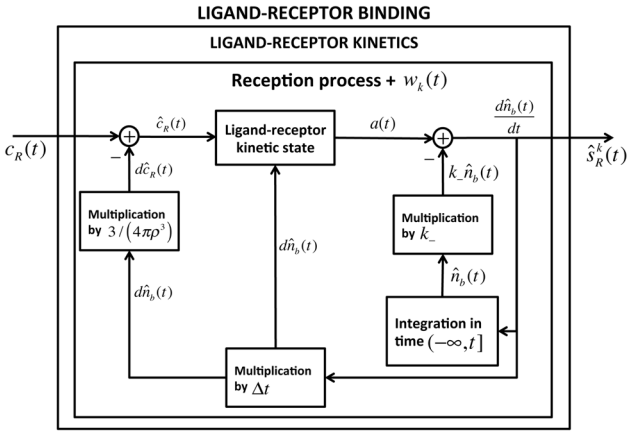

Figure 4.16: Block scheme of the physical model for the ligand-receptor kinetics.

The **ligand-receptor kinetic state** block, as shown in Figure 4.16, takes as input the concentration $\hat{c}_R(t)$ of the particles inside the receptor space, and returns the signal $a(t)$ as output. The ligand-receptor kinetic state block keeps track of the locations $\bar{x}_p(t)$ of all the particles present inside the receptor space at time t through the set $K_P(t)$, expressed as

$$K_P(t) = \{\bar{x}_p(t) |\ p = 1, ..., P(t)\}\ , \tag{4.16}$$

where $P(t)$ is the number of particles in the receptor space, and it is a function of the particle concentration $\hat{c}_R(t)$, output of the emission-process block, as shown in Figure 4.17.

The **multiplication-by-Δt** block, shown in Figure 4.16, receives as input the time-first derivative $d\hat{n}_b(t)/dt$ of the number of bound chemical receptors, and returns as output its time differential $d\hat{n}_b(t)$. The time differential $d\hat{n}_b(t)$, when positive, corresponds to the number of particles subtracted from the receptor space as a consequence of their binding to previously-unbound receptors; when negative, it corresponds to the number of particles added to the receptor space after their release from previously-bound receptors.

The **multiplication-by-3/($4\pi\rho^3$)** block, shown in Figure 4.16, receives as input the time differential $d\hat{n}_b(t)$ in the number of bound receptors, and it outputs the concentration differential $d\hat{c}_R(t)$ of bound

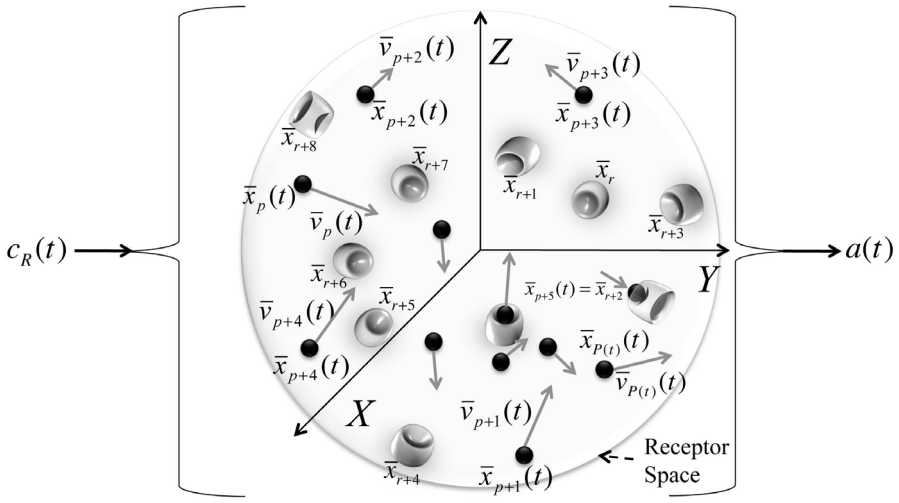

Figure 4.17: Graphical sketch of the ligand-receptor kinetic state block.

receptors. The value of $d\hat{c}_R(t)$ corresponds to the variation in the concentration of particles inside the receptor space given by the binding, or the release of particles to, or from, chemical receptors.

The **integration** block, shown in Figure 4.16, receives as input the time-first derivative $d\hat{n}_b(t)/dt$ in the number of bound chemical receptors, and gives as output the number $\hat{n}_b(t)$ of bound chemical receptors.

The **multiplication-by-k$_-$** block, shown in Figure 4.16, receives as input the number $\hat{n}_b(t)$ of bound receptors, and multiplies it by the rate k_- of release reaction. The output of the multiplication block is then subtracted from the output $a(t)$ of the ligand-receptor-kinetics block.

Since it is not possible to always have the knowledge of the ligand-receptor kinetic state because of the huge amount of information and the randomness in the particle motion, the value of $\hat{S}_R^k(t)$ cannot be analytically computed as a function of $c_R(t)$ through the ligand-receptor-kinetics model of the reception noise, but only numerically. The results of the simulations of the ligand-receptor-kinetics model, where a sinusoidal particle concentration $\hat{c}_R(t)$ is applied as input, are shown in

Figure 4.18 (left) in terms of the number $\hat{n}_b(t)$ of bound chemical receptors, and in Figure 4.18 (right) in terms of the perturbation of $\hat{n}_b(t)$ around the average value. The radius of the receptor space is $\rho = 10\mu m$, the binding reaction rate is set to $k_+ = 0.2$ $[\mu m^3/sec]$ and the release reaction rate is set to $k_- = 10$ $[1/sec]$, with reference to [86]; the number of receptors present inside the receptor space is set to $N_R = 500$, while the particle diffusion coefficient, used in the ligand-receptor kinetics, is set to $D \sim 10^{-6} cm^2 sec^{-1}$ [31]. The radii of a particle r_p and a chemical receptor r_R are set equal to $1nm$.

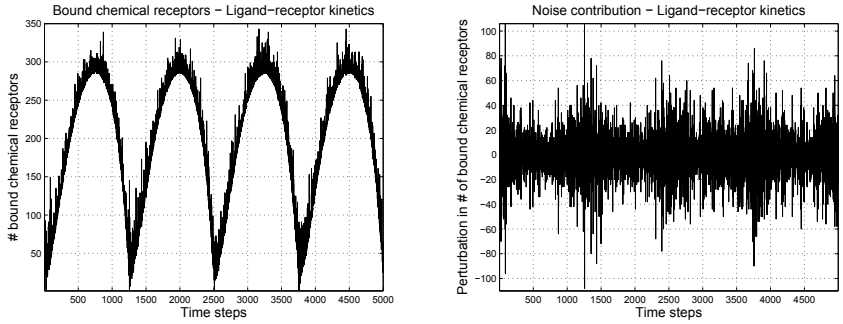
Bound chemical receptors − Ligand−receptor kinetics
bound chemical receptors
Time steps
Noise contribution − Ligand−receptor kinetics
Perturbation in # of bound chemical receptors
Time steps

Figure 4.18: The output of the first set of simulations of the physical model in terms of number of bound chemical receptors (left) and isolated noise contribution (right).

The Stochastic Model The ligand-receptor-kinetics noise can also have another formulation, through the stochastic chemical kinetics. According to this formulation, the reception noise $w_k(t)$ is generated by a random process, whose contribution corresponds to

$$w_k(t) = \hat{c}_R^k(t) - c_R(t) \ , \tag{4.17}$$

where $\hat{c}_R^k(t)$ is the actual particle concentration in input to the reception process, and $\hat{c}_R(t)$ is the expected particle concentration in input to the reception process in the absence of the reception noise. In Figure 4.19, the main block scheme of the ligand-receptor-binding process is shown, where the stochastic chemical kinetics is applied to model the reception noise. As detailed in the following, the random process $w_k(t)$

depends on the value of the particle concentration $\hat{c}_R(t)$ itself, output of the diffusion process. The sum of the random process $w_k(t)$ and the particle concentration $\hat{c}_R(t)$ is the particle concentration affected by the reception noise $\hat{c}_R^k(t)$.

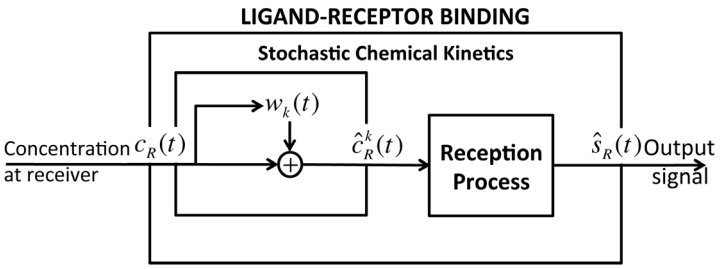

Figure 4.19: Block scheme of the stochastic chemical kinetics.

The stochastic chemical kinetics studies how the concentrations of chemical species evolve in a system as a consequence of chemical reactions. This concentration evolution is expressed through the Chemical Master Equation (CME) [48]. The CME is a stochastic differential equation that binds together the concentration of chemical species involved in chemical reactions. In the following, a particular formulation of CME, called **reversible first-order reaction**, is considered. This CME leads to a closed-form solution to the problem of the stochastic modeling of the ligand-receptor kinetics.

The reversible first-order reaction is based on the following assumptions:

- The number of particles $P(t)$ in the receptor space for any time instant t is much higher than the number N_T of chemical receptors.

As a consequence, the particle concentration $\hat{c}_R(t)$ in input to the ligand-receptor-binding process is not affected by the binding or release reactions occurring between the particles and the chemical receptors.

The solution to the problem of the stochastic modeling of the ligand-receptor kinetics can be found through a similar procedure as in [66]. The reversible first-order reaction is expressed in terms of probability generating function [74] $F(s, \tau)$. This function allows to find the

variance $Var(\hat{c}_R^k(t))$ of the perturbed particle concentration, then approximated through the formula for the variance of a function of a random variable of known variance and average [74], expressed as

$$Var(\hat{c}_R^k(t)) \approx \left[\frac{N_R k_-}{k_+(N_R - \langle \hat{n}_b(\tau)\rangle)^2}\right]^2 Var(\hat{n}_b(\tau)) \ , \tag{4.18}$$

which is valid for $\tau \in [t, t + 1/(2B_c)]$, and where N_R is the total number of chemical receptors, k_+ is the rate of the binding reaction, and k_- is the rate of the release reaction. The expressions of $\langle \hat{n}_b(\tau)\rangle$ and $Var(\hat{n}_b(\tau))$ are as follows:

$$\langle \hat{n}_b(\tau)\rangle = \frac{n_0(t)}{K}(k_1 e^{-K(\tau - t)} + k_2) \ , \tag{4.19}$$

and

$$\begin{aligned} Var(\hat{n}_b(\tau)) =& \frac{n_0(t)(\lambda e^{-K(\tau-t)} + 1)}{1+\lambda}\left(1 - \frac{\lambda e^{-K(\tau-t)} + 1}{1+\lambda}\right) \\ & \cdot \tau \in [t, t + 1/(2B_c)] \ , \end{aligned} \tag{4.20}$$

where $k_- = k_1$, $c_R(t)k_+ = k_2$, $\lambda = k_1/k_2$ and $K = k_1 + k_2$, τ is a time variable, B_c is the bandwidth of the particle concentration $\hat{c}_R(t)$, input of the stochastic model, and $n_0(t)$ is the expected number of bound receptors in the absence of noise and at chemical equilibrium.

Similarly to Section 4.3 and Section 4.4, as shown in Figure 4.20, the results of the statistical-likelihood test applied to the stochastic chemical kinetics are shown in Figure 4.20 (left), while the results obtained through the use of a Gaussian model are shown in Figure 4.20 (right).

4.6 Conclusions

In this chapter of the article, the sampling noise, the counting noise, and the ligand-receptor-binding noise are identified as the most relevant diffusion-based-noise sources affecting the diffusion-based-MC transmitter, channel, and receiver, respectively. The analysis of the noise sources results both in physical models and stochastic models. With the former we aim at the mathematical expression of the physical processes underlying the noise sources, while with the latter we model the

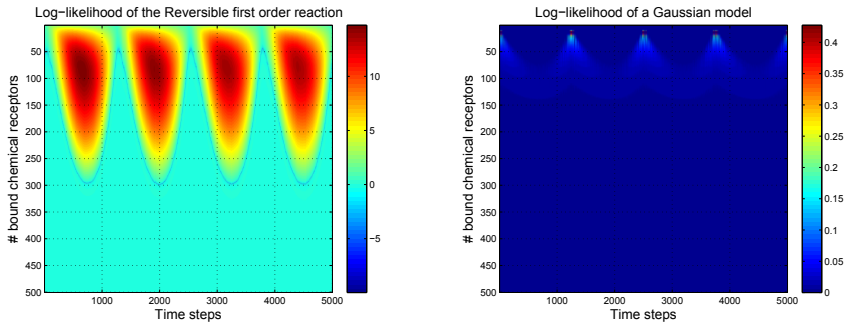
Log−likelihood of the Reversible first order reaction
bound chemical receptors
Time steps
Log−likelihood of a Gaussian model
bound chemical receptors
Time steps

Figure 4.20: The likelihoods of the stochastic models for the ligand-receptor-kinetics noise. The stochastic model of the sampling noise (left). A Gaussian model (right).

noise source behaviors through the use of statistical parameters. For all the two noise sources, the results of the physical models are summarized through block schemes, which expand the diffusion-based MC link model from Chapter 3. The stochastic models result in noise source characterization in terms of random processes, and in the analytical expression of the Root Mean Square (RMS) perturbation of the noise on the information signal. Simulations are shown to prove that the analytical formulation of the noises in terms of stochastic models is compliant with the generated noise behaviors resulting from simulations based on the physical models.

The analysis of the noise sources provided in this paper and the results in terms of mathematical modeling will serve to expand the knowledge on diffusion-based MC systems and to support further investigation on their performance in terms of link capacity and throughput. The results provided in this chapter of the article constitute an initial study on the noise sources affecting a basic design of a diffusion-based MC link, and further study is expected in the future to specialize these results in light of more specific diffusion-based MC link and network implementations.

5

Capacity Analysis of a Molecular Communication Link

5.1 Motivation and Related Work

The theoretical analysis and the modeling of the information capacity in diffusion-based MC are of primary importance to understand the performance of a diffusion-based Molecular Communication (MC) system from an information theoretic perspective. The objective of the research detailed in this chapter is to provide closed-form mathematical expressions that are valid as upper/lower bounds of the true information capacity of an MC link based on free molecule diffusion, independent from any specific coding scheme. Shannon [90] provided the famous mathematical expression of the capacity of a channel affected by additive white Gaussian noise, which has a general validity for classical electromagnetic (EM)-based communication. As detailed later in this chapter, the diffusion-based MC has two main characteristics, namely, a channel memory and a signal-dependent noise, which limit the applicability of the aforementioned classical capacity expression. The channel memory is given by the persistent effects in the channel of previous transmissions, while a signal-dependent noise is given by a correlation between the transmitted information signal and the characteristics of the noise-generating stochastic processes present in the

communication system. The impossibility of finding a closed-form analytical expression for the true capacity of such a communication system, even when affected by only one of these characteristics, is a well-known argument in information theory. As a consequence, in the attempt to provide an analytical closed-form expression that relates the performance of a diffusion-based system to physical parameters, such as the diffusion coefficient, the temperature, the transmitter-receiver distance, the bandwidth of the transmitted signal, and the average transmitted power, the results included in this chapters are based on some simplifying assumptions, mentioned in the following. These assumptions limit the validity of these expressions, which have to be considered as upper/lower bounds to the true information capacity.

Up to date, some contributions from the literature have attempted to study the information capacity in diffusion-based MC links, but often these are focused on specific modulation and coding schemes, or do not take into account the aforementioned channel memory and signal-dependent noise characteristics of the diffusion-based MC. The work in [7] addresses for the first time the capacity of MC links by emphasizing the need for its mathematical analysis, but no concrete solutions are proposed. In [11, 14], the MC capacity is computed for a specific binary coding scheme and by taking into account the molecular receiver model, but without modeling the molecule diffusion propagation. An analysis of the molecular achievable rate is conducted in [15] by assuming a single instantaneous emission of molecules from the transmitter, a deterministic diffusion channel and a detailed chemical model of the receiver, but the effects of an emission of molecules over time is not considered. In [36], the capacity of an MC link in case of binary coding is properly analyzed on the basis of the effects of the channel memory, but without accounting for molecular noise sources. The same authors complement in [37] their first work by including the contribution on the capacity of a ligand-receptor binding reception of binary coded molecular signals. Moreover, in [38] and [39], they further extend their work by considering the effects on capacity of an MC link realized through genetically engineered bacteria, where multiple bacteria act collectively as a network node. To achieve these results, the authors take into ac-

count the noise sources in the biochemical processes of molecule generation and reception, in the contexts of both binary and M-ary coding schemes. Two different coding techniques are analyzed in [57] in terms of achievable rates, while the diffusion channel models are reduced to a binary or a quadruple channel. Similarly, discrete memoryless approximations are applied to the molecule diffusion channel in [10], where the MC capacity is computed for a binary coding scheme.

In the first part of this chapter, solutions from statistical mechanics and equilibrium thermodynamics are applied to derive a preliminary upper-bound expression to the diffusion-based MC capacity [79]. This preliminary expression is derived through the simplifying assumption of having a molecular system in equilibrium, and the dynamic effects of the diffusion-based channel are not taken into account, in particular the channel memory. This derivation is based on the interpretation of a diffusion-based MC link as at the crossroad of two different disciplines, namely, information theory and statistical mechanics. While information theory [90] focuses on the quantification of the information in a communication channel, statistical mechanics [88] studies the thermodynamic behavior of systems composed of a large number of particles. While in the past years some efforts [54, 19] have been devoted to merge information theory and statistical mechanics, they were not directed towards the interpretation of a communication system. Moreover, these contributions tend to focus on the explanation of natural phenomena using information theory as a tool, and they do not provide suitable models for MC engineering. In particular, the relationship between thermodynamic entropy and information entropy is used to derive a closed-form expression of an upper bound to the true capacity in diffusion-based MC, as a function of the parameters from statistical mechanics, namely, the volume, the temperature, the number of molecules, as well as the bandwidth of the system and the thermodynamic power spent at the transmitter for releasing molecules.

In the second part of this chapter, unlike the previous contribution, a lower-bound expression of the capacity is provided by taking into account both the channel memory and the signal-dependent noise, termed molecular noise [82]. For this, we decompose the molecule dif-

fusion into two main processes: i) the Fick's diffusion, which captures solely the effects of the channel memory; ii) the particle location displacement, which isolates the molecular noise. The properties of these two processes allow to analyze them as a cascade of two separate communication systems. We compute the information capacity by assuming that the transmitter can modulate the emission of molecules in the space according to any possible time continuous input message, differently from previous contributions where the transmitter is assumed to modulate (e.g., binary coding) impulses according to discrete input messages (e.g., binary digital messages). As a consequence, this lower-bound expression to the information capacity is independent from any specific coding scheme, and it is expressed as a function of the average transmitted power, which corresponds to the thermodynamic power spent at the transmitter for molecule emission.

The information-theoretic diagram of a diffusion-based MC link is shown in Figure 5.1, and it is composed by the classical [28] cascade of information source, transmitter, channel, receiver and destination. The **Information Source** produces *messages* to be communicated to the destination. The type of message depends on the particular application in which the diffusion-based MC link is deployed. In case of intelligent drug delivery applications [44], the message can be a time sequence of ON/OFF values that trigger/stop the release of the drug molecules. In nanomachine communication [7] the message can be any function of the time carrying data such as nanomachine states [2] or sensory measurements [3]. The **Transmitter**, the **Channel**, and the **Receiver**, which are based on the molecule emission, molecule diffusion and molecule reception, respectively, are within a **Physical System**, whose underlying laws and parameters affect how these components are physically realized. The **Destination** is the recipient of the *messages* coming from the receiver. Upon reception of a message, the destination reacts according to the meaning and to the particular application.

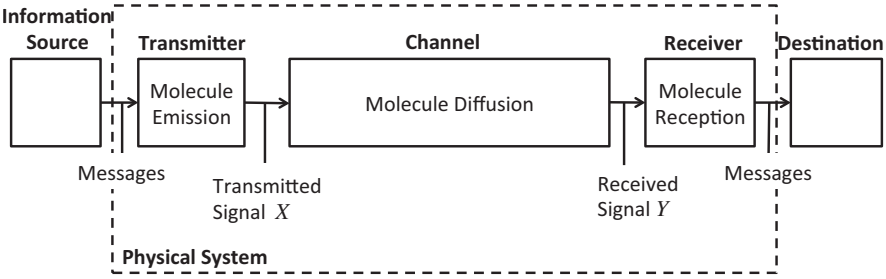

Figure 5.1: Information-theoretic diagram of a diffusion-based MC link.

5.2 Capacity Analysis through Thermodynamics

In a diffusion-based MC, the transmitter, the channel, and the receiver are functions of **physical parameters** and depend on how the diffusion-based MC link is physically realized. The physical parameters are variables that characterize a physical realization of the MC diffusion-based system. Physical parameters can be considered, e.g., the temperature or the chemical composition of the environment in which diffusion-based MC is performed. For this, we define a physical reference model that allows to identify general physical parameters in a diffusion-based MC link.

5.2.1 The Physical Reference Model

A physical reference model is defined as the most basic realization of a diffusion-based-MC system. This model stems from a simplification of the diffusion-based MC link model defined in Chapter 3, and it is described as follows. The physical reference model is contained in a spherical space S of radius r_S. The transmitter has a spherical shape of radius r_T, where $r_T << r_S$, while the receiver is considered point wise. The location of the transmitter corresponds to the center of the spherical space S, and the receiver is at a distance d from the transmitter, where $r_T < d < r_S$. Moreover, each particle is characterized by two quantities, namely, the location and the momentum. The set containing the locations and momenta of all the particles in the system is defined as the phase space Φ of the system. Given the above statements,

the particles of the physical reference model behave according to the Ideal-gas Theory [42]. Due to the simplicity of the model, the ideal gas is the most simple diffusion-based molecular system and enables us to find a closed-form expression for an upper bound to the capacity. The ideal-gas concept allows us to define the following physical parameters for the physical reference model when it is in a state of thermodynamic equilibrium [40]: the temperature T, the pressure P, the volume V, and the number of particles N_p. These physical parameters define the state of the system, and they are bound by the ideal-gas law [42]. The goal of the research work described in the following is to express the information capacity, or an upper bound to this capacity, as a function of the aforementioned physical parameters.

5.2.2 Information-theoretic Definition of Capacity

The information capacity of a communication system is expressed by the general formula from Shannon [90]. This general formula defines the information capacity as the maximum difference between the information entropy $H(x)$ of the signal x, input of the channel, and the equivocation $H_Y(x)$, expressed as

$$C = \max_{f_X(x)} \{H(x) - H_Y(x)\} \ , \tag{5.1}$$

where the maximum is found with respect to the probability-density function $f_X(x)$ in the values of the input signal x.

In the following, we study the entropy of the input signal (Section 5.2.4), the equivocation (Section 5.2.5) and the upper-bound expression of the capacity (Section 5.2.6) of a diffusion-based MC link as functions of the physical parameters such as the volume, the temperature, the number of molecules. For this, in Section 5.2.3 we investigate the similarity between two entropies that can be defined in a MC link, namely, **information entropy and thermodynamic entropy**.

5.2.3 Information-theoretic Entropy from Thermodynamic Entropy

The thermodynamic entropy is defined by Gibbs [46] as a measure of the disorder in a thermodynamic system. For the physical reference

model introduced in Section 5.2.1, the thermodynamic entropy S_r is expressed as follows:

$$S_r = -K_b \int_{\phi \epsilon \Psi} f_\Phi(\phi) \ln \left(f_\Phi(\phi) \right) \, d\phi \ , \tag{5.2}$$

where ϕ is a particular value for the phase space Φ of the system, $f_\Phi(\phi)$ is the distribution of phase-space values for a specific set of values of the physical parameters, and Ψ is the set of all the possible phase-space values.

As stated in Section 5.2.1, the physical reference model behaves in agreement with the ideal-gas theory. According to the Sackur-Tetrode equation [19], the entropy of an ideal gas in thermodynamic equilibrium has a closed-form expression as function of the physical parameters. Therefore, the entropy S_r of the physical reference model is [19]

$$S_r = N_p \, K_b \left[\ln \left(\frac{V}{N_p} \left(\frac{2\pi m K_b T}{h^2} \right)^{\frac{3}{2}} \right) + \frac{5}{2} \right] \ , \tag{5.3}$$

where N_p is the number of particles present in the system, K_b is the Boltzmann's constant [46], V and T are the volume and the absolute temperature of the system, respectively, m is the particle mass, and h is the Planck's constant [19].

The thermodynamic-entropy formula in (5.2) can be reduced to the information-theoretical-entropy formula from Shannon [90] if the Boltzmann's constant K_b is removed and the logarithm ln is set to $\log_2$. In the case of a diffusion-based-MC link, the thermodynamic entropy can be interpreted as an information-theoretical entropy, where the input-signal values correspond to the phase-space values ϕ of the physical reference model. The Boltzmann's constant K_b depends on the conventional units of the temperature, and it has meaning only in thermodynamics [46]. The logarithm ln is converted into $\log_2$ because [90] the units of the information-theoretical entropy are $[bit/sample]$ or $[bit/sec]$. Thus, the information entropy H_{ref} of the physical reference model can be expressed as

$$H_{ref} = N_p \left[\log_2 \left(\frac{V}{N_p} \left(\frac{2\pi m K_b T}{h^2} \right)^{\frac{3}{2}} \right) + \frac{5}{2} \right] \ . \tag{5.4}$$

5.2.4 The Input-signal Entropy

The input signal in the physical reference model introduced in Section 5.2.1 corresponds to the modulation of the molecular features (the local particle number and the particle type) operated by the transmitter.

A local information-theoretical entropy can be defined for the transmitter when it modulates the molecular features. This local entropy depends on the molecular features and it can be computed from (5.4). The local entropy H_T at the transmitter is a function of the set M of all possible particle types, the number N_m for each particle type m from the set M, the absolute temperature T of the system, and the transmitter volume V_T, expressed as

$$H_T = \sum_{m \epsilon M} N_m \left[\log_2 \left(\frac{V_T}{N_m} \left(\frac{2\pi m K_b T}{h^2} \right)^{\frac{3}{2}} \right) + \frac{5}{2} \right] , \qquad (5.5)$$

where the transmitter volume V_T is equal to $(4/3)\pi r_T^3$. According to the Gibbs' theorem [46], the expression in (5.5) is the sum of all the contributions coming from the application of (5.4) to each particle type at the transmitter, where these contributions are considered independent.

The total entropy H_{ref}^{mod} of the physical reference model when the transmitter is modulating the particle features can be written as the sum of H_T from (5.5) and H_{ref} from (5.4), expressed as

$$H_{ref}^{mod} = H_T + H_{ref} . \qquad (5.6)$$

While the transmitter modulates, it inserts information in the system. This information, according to the Second Law of Thermodynamics [42], eventually will fade out when the physical reference model will reach a new state of thermodynamic equilibrium, which is characterized by a higher entropy H_{ref}^{new}, expressed as follows:

$$H_{ref}^{new} = N_{tot} \left[\log_2 \left(\frac{V}{N_{tot}} \left(\frac{2\pi m K_b T}{h^2} \right)^{\frac{3}{2}} \right) + \frac{5}{2} \right] , \qquad (5.7)$$

where $N_{tot} = N_p + \sum_{m \epsilon M} N_m$ is the total number of particles in the system, and N_p is the number of particles before modulation. In order to

quantify the input-signal entropy, the total entropy H_{ref}^{mod} is subtracted from the entropy H_{ref}^{new}, expressed as

$$H(x) = H_{ref}^{new} - H_{ref}^{mod} \ , \tag{5.8}$$

where $H(x)$ is the input-signal entropy in $[bit/sample]$.

If a bandwidth W is considered for the system, $2W$ samples per second can be transmitted without equivocation. According to [90], the input-signal entropy in $[bit/sec]$ becomes

$$H'(x, W) = 2W \left(H_{ref}^{new} - H_{ref}^{mod} \right) \ . \tag{5.9}$$

5.2.5 The Equivocation

The received signal in the physical reference model introduced in Section 5.2.1 corresponds to the reading of the changes in the molecular features operated by the receiver.

The propagation of the signal from the transmitter to the receiver affects the value of the local entropy at the receiver. The variation in the local entropy H_R at the receiver at instant t and distance d corresponds to the variation in the entropy of a spherical surface $H_R^{sph}(d, t)$ at instant t and distance d, divided by the spherical surface area $4\pi d^2$, and expressed as

$$H_R(d, t) = \frac{H_R^{sph}(d, t)}{4\pi d^2} \ . \tag{5.10}$$

The variation in the entropy of the spherical surface can be computed from (5.4) by applying a number of particles N_{eq}^m and a volume V_{eq}. The variation in the entropy $H_R^{sph}(d, t)$ of the spherical surface is

$$H_R^{sph}(d, t) = \sum_{m \epsilon M} N_{eq}^m \left[\log_2 \left(\frac{V_{eq}}{N_{eq}^m(d, t)} \left(\frac{2\pi m K_b T}{h^2} \right)^{\frac{3}{2}} \right) + \frac{5}{2} \right] \ . \tag{5.11}$$

The equivalent number of particles $N_{eq}^m(d, t)$ of the ideal gas corresponds to the number of particles that diffuse from the transmitter to the receiver located at a distance d, expressed as the number N_m of transmitted particles of type m multiplied by the probability for each particle of shifting by a distance d at a time instant t. According to the

Brownian motion [40], the equivalent number of particles $N_{eq}^{m}(d,t)$ is expressed as follows:

$$N_{eq}^{m}(d,t) = N_m \frac{1}{\sqrt{4\pi Dt}} e^{-\frac{d^2}{4Dt}} \ . \tag{5.12}$$

The value of the equivalent number of particles $N_{eq}^{m}(d,t)$ divided by the equivalent volume V_{eq} is equal to the inverse of the concentration of type-m particles at the spherical surface at instant t and distance d, and it is expressed as

$$\frac{N_{eq}^{m}(d,t)}{V_{eq}} = \frac{N_m}{V_T} \frac{1}{\sqrt{4\pi Dt}} e^{-\frac{d^2}{4D\Delta t}} = \frac{N_{eq}^{m}(d,t)}{V_T} \ . \tag{5.13}$$

The equivocation formula in [90] corresponds to the increase in the entropy of the signal as it propagates in the channel, and it depends on the number of particles that reach the receiver location at a certain time t. The equivocation $H_Y(x)$ is expressed as follows:

$$H_Y(x) = H_R(d,t) - \frac{H_T}{V_T} \ , \tag{5.14}$$

where $\frac{H_T}{V_T}$ is the entropy of the transmitted signal per unit volume, and $H_R(d,t)$ is the entropy of the received signal from (5.10).

If a bandwidth W is considered for the system, up to $2W$ samples per second can be received without equivocation. This is valid only under the hypothesis of not having influences between the diffusion of two different samples. In practice, this is not physically realistic since particles diffusing after the transmission of a sample will inevitably be present in the system at the time of transmission of the consecutive sample. Since taking into account this latter effect would complicate more the treatment concerning the equivocation and since the equivocation will result in a higher value, in this section of the article we rely on the assumption of not having influences between consecutive samples. **This assumption will result in an overestimation of the capacity (upper bound to the true capacity)**. The variation in the entropy $H_{R,W}^{sph}$ of a spherical surface with bandwidth W at distance d is computed as

$$H_{R,W}^{sph} = \sum_{m \epsilon M} N_{eq,W}^{m} \left[\log_2 \left(\frac{V_{eq}}{N_{eq,W}^{m}} \left(\frac{2\pi m K_b T}{h^2} \right)^{\frac{3}{2}} \right) + \frac{5}{2} \right] \ , \tag{5.15}$$

where $N^m_{eq,W}$ is equal to the number of particles that diffuse from the transmitter to the receiver, which is located at a distance d, and for a bandwidth W, under the hypothesis of not having influences between the diffusion of two different samples. This hypothesis will result in an overestimation of the capacity, and in the computation of an upper-bound expression. The expression of $N^m_{eq,W}$ is as follows:

$$N^m_{eq,W} = N_m \sqrt{\frac{2W}{4\pi D}} e^{-\frac{2Wd^2}{4D}} \ . \tag{5.16}$$

As a consequence, the variation in the local entropy at the receiver $H_R(W)$ with bandwidth W and distance d is

$$H_R(W) = \frac{H^{sph}_{R,W}}{4\pi d^2} \ . \tag{5.17}$$

The equivocation formula in $[bit/sec]$ becomes

$$H_Y(x,W) = 2W \left(H_R(W) - \frac{H_T}{V_T} \right) \ , \tag{5.18}$$

where $H_R(W)$ is computed through (5.17), H_T through (5.5), and V_T is defined in Section (5.2.4).

5.2.6 The Capacity

The information-theoretical capacity of the diffusion-based-MC link, given the physical reference model detailed in Section 5.2.1, is expressed by the formula in (5.1), where the input-signal entropy $H(x)$ is given by (5.8), and the equivocation is given by (5.14). The final expression of the capacity, which is an upper bound to the real capacity, as explained after (5.15), and with reference to (5.7), (5.6), (5.10) and (5.5), becomes

$$C = \max_{f_X(x)} \left\{ H^{new}_{ref} - H^{mod}_{ref} - \left(H_R - \frac{H_T}{V_T} \right) \right\} \ . \tag{5.19}$$

If a bandwidth W is considered for the system, the information-theoretical capacity $C(W)$ of the diffusion-based-MC link is expressed as a function of W by the formula in (5.1), where the input-signal entropy $H(x,W)$ is given by (5.9), and the equivocation $H_Y(x,W)$ is

given by (5.18). Therefore, the information-theoretical capacity $C(W)$, with reference to (5.7), (5.6), (5.17) and (5.5), is expressed as

$$C(W) = \max_{f_X(x)} 2W \left\{ H_{ref}^{new} - H_{ref}^{mod} - \left(H_R(W) - \frac{H_T}{V_T} \right) \right\} \ . \qquad (5.20)$$

A closed-form expression for the upper bound to the capacity of the diffusion-based-MC link is given by the input-signal probability-density function $f_X(x)$ that maximizes (5.1). Such a value for $f_X(x)$ can be found by setting a constraint on the total transmitted power, which is here identified with the enthalpy power of the transmitter $P_{\mathcal{H}}$, expressed as

$$P_{\mathcal{H}} = 2\mathcal{H}W \ , \qquad (5.21)$$

where $\mathcal{H}$ is the transmitter enthalpy, and W is the bandwidth.

Theorem 5.1. The **transmitter enthalpy** is defined as the energy necessary to insert N particles in the system, and to heat these particles up to a temperature T when the system has the pressure P and the volume V [42].

In MC, the transmitter enthalpy can be computed as

$$\mathcal{H} = PV + \frac{3}{2} K_b T \sum_{m \epsilon M} N_m \ , \qquad (5.22)$$

where P and V are the pressure and the volume of the physical reference model, respectively, M is the set of all the possible particle types that the transmitter can emit, N_m is the number of particles of type m, K_b is the Boltzmann's constant, and T is the absolute temperature of the system.

The entropy H_{ref}^{mod} from (5.6) can be written as function of the transmitter power by expressing N_m as a function of $P_{\mathcal{H}}^m$

$$N_m^P = \frac{P_{\mathcal{H}}^m - 2WPV}{3WK_bT} \ , \qquad (5.23)$$

where $P_{\mathcal{H}}^m$ is the fraction of the power assigned to each particle type m, and P and V are the pressure and the volume of the physical reference model, respectively. The maximum of the input-signal entropy $H(x, W)$ corresponds to the distribution of the power that results in

the minimum H_T^{min} of H_T from (5.5), which is the even distribution of the power $P_{\mathcal{H}}^m$ among all the M types of particles that the transmitter can send. This power distribution is expressed as

$$P_{\mathcal{H}}^m = \frac{P_{\mathcal{H}}}{M} \rightarrow H_T = H_T^{min} \ . \tag{5.24}$$

The equivocation $H_Y(x)$ as function of the enthalpy power of the transmitter is computed through (5.18), where both H_T and $H_R(W)$ can be expressed as function of the fraction of the power $P_{\mathcal{H}}^m$ assigned to each particle type m. The optimal distribution of power in (5.24) minimizes $\frac{H_T}{V_T}$. This power distribution minimizes also $H_{R,W}^{sph}$ and, consequently, also $H_R(W)$ from (5.17). It is possible to logically assume that, if d is sufficiently large, the entropy $\frac{H_T}{V_T}$ is negligible with respect to the contribution of $H_R(W)$. This assumption is expressed as

$$H_R(W) >> \frac{H_T}{V_T} \ . \tag{5.25}$$

Therefore, the minimum of the equivocation $H_Y(x)$ corresponds roughly to the minimum of $H_R(W)$, denoted as $H_R^{min}(W)$, given by the even power distribution in (5.24).

A closed-form expression of the upper bound to the capacity of the diffusion-based-MC link is

$$C(W) = 2W \left[H_{ref}^{new} - H_{ref}^{mod,min} - \left(H_R^{min}(W) - \frac{H_T^{min}}{V_T} \right) \right] \ , \tag{5.26}$$

with reference to (5.7), (5.6), (5.17), (5.5), evaluated with (5.24). The transmitter volume V_T is defined in Section (5.2.4), and $H_{ref}^{mod,min}$ is equal to (5.6), where H_T is substituted with H_T^{min}. The results shown in Figure 5.2 are computed for a total transmitter enthalpy power $P_{\mathcal{H}} = 1\mu$W (arbitrary value), a radius of the space $r_S = 1$cm, a radius of the transmitter $r_T = 1\mu$m, a particle mass $m = 1.66053878283x10^{-27}$kg (standard atomic mass unit [65]), a number of particles N_p set to one mole [42] $6.0221417930x10^{23}$, and a number of possible particle types is $M = 5$. The diffusion coefficient D is set [77] to $10^{-9}[\mathrm{m}^2/sec]$ for a temperature of 25 °C as a reference.

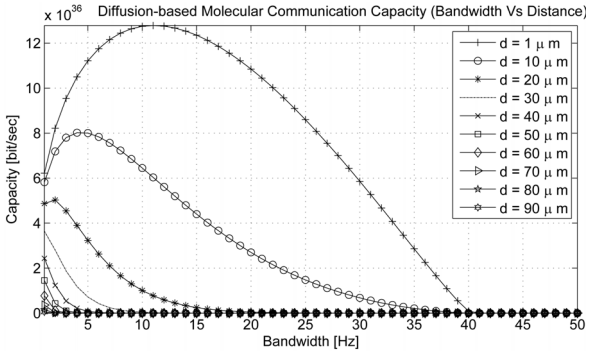
x 10^36
Diffusion-based Molecular Communication Capacity (Bandwidth Vs Distance)
Capacity [bit/sec]
Bandwidth [Hz]
d = 1 μ m
d = 10 μ m
d = 20 μ m
d = 30 μ m
d = 40 μ m
d = 50 μ m
d = 60 μ m
d = 70 μ m
d = 80 μ m
d = 90 μ m

Figure 5.2: Capacity in relation to the bandwidth and for different values of the distance d.

5.3 Capacity Analysis with Channel Memory and Molecular Noise

Differently from the previous section, the **Physical System** considered in this section of the article is sketched in Figure 5.3 and it is based on the following considerations:

- The diffusion-based MC channel is in a three-dimensional space indexed by the three axes $\mathrm{X}, \mathrm{Y}, \mathrm{Z}$ and it has infinite extent in all three dimensions. This space is filled with a fluidic medium having viscosity μ. The fluidic medium does not have flow currents or turbulence, therefore the propagation of the molecules between the transmitter and the receiver is solely realized by the Brownian motion.

- All the molecules in the system, which are emitted by the transmitter, are indistinguishable and equivalent to spherical *particles* of radius r and mass m, where $r << d$, d being the distance between the transmitter and the receiver in the diffusion-based MC link. As a consequence, from now on we will refer to particles when talking about molecules in the physical system.

- The transmitter is considered point-wise (size equal to zero) and at location $\mathbf{T} = (T_{\mathrm{X}}, T_{\mathrm{Y}}, T_{\mathrm{Z}})$ in the three-dimensional space.

- Once emitted from the transmitter, every particle moves independently from the others and according to its Brownian motion in the fluidic medium. The Brownian motion of a molecule is referred to as the random motion of the particles suspended in a fluid and its formulation according to the Langevin equation [59] states that the location $p_i^n(t)$ of the particle n at time t along any i of the three dimensional axes $\mathrm{X}, \mathrm{Y}, \mathrm{Z}$ obeys the following stochastic differential equation:

$$m\frac{\partial^2 p_i^n(t)}{\partial t^2} = -6\pi\mu r\frac{\partial p_i^n(t)}{\partial t} + f_i(t)\,, \quad i \in \{\mathrm{X}, \mathrm{Y}, \mathrm{Z}\}\,, \tag{5.27}$$

  where m is the particle mass, $\partial^2(.)/\partial t^2$ and $\partial(.)/\partial t$ are the second and first time derivative operators, respectively, μ is the viscosity of the fluid, r the radius of the particle and $f_i(t)$ is a random process whose probability density function is Gaussian and has correlation function $< f_i(t)f_j(t') >$ given by

$$< f_i(t)f_j(t') >= 12\pi\mu r k_B T\delta_{i,j}\delta(t-t') \quad i,j \in \{\mathrm{X}, \mathrm{Y}, \mathrm{Z}\}\,, \tag{5.28}$$

  where $< . >$ is the average operator, k_B is the Boltzmann constant, T is the absolute temperature of the fluid, considered homogeneous throughout the space, and $\delta_{i,j}$ is equal to 1 if $i = j$ and zero otherwise; $\delta(t-t')$ is the Dirac delta function.

- The receiver detects a signal which is proportional to the concentration of the incoming particles. The receiver location is at a distance d from the transmitter.

In the following, the components included in the physical system are described in light of the aforementioned considerations.

The **Transmitter** processes the messages from the information source and produces a signal suitable for the transmission over the channel. The *transmitted signal*, denoted by X [1], is here defined as the

[1] For the information capacity analysis of this communication system, the transmitted signal X is considered as a band-limited random process whose value at every time instant t is a realization of the random variable $n_T(t)$. As a consequence, the entropy of X is found by decomposing X into a band-limited ensemble of functions, as detailed in Section 5.3.3.

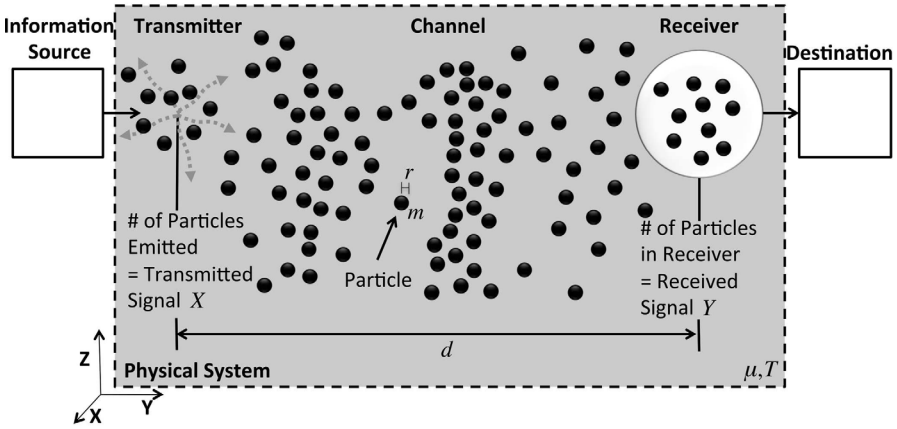

Figure 5.3: Sketch of the physical realization of the diffusion-based molecular communication system.

number of particles $n_T(t)$ emitted into the space as a function of the time t, expressed as

$$X := n_T(t)\,,\ t > 0\,. \tag{5.29}$$

At the time t of emission of a particle, denoted by $\bar{n}$, its location $\mathbf{p}^{\bar{n}}(t) = (p_{\mathrm{X}}^{\bar{n}}(t), p_{\mathrm{Y}}^{\bar{n}}(t), p_{\mathrm{Z}}^{\bar{n}}(t))$ corresponds to the location of the transmitter $\mathbf{T} = (T_{\mathrm{X}}, T_{\mathrm{Y}}, T_{\mathrm{Z}})$, expressed as

$$\mathbf{p}^{\bar{n}}(t) = \mathbf{T}\,,\ \bar{n} = \int_0^t n_T(\tau)d\tau\,,\ t > 0\,, \tag{5.30}$$

where $\mathbf{T}$ is the vector of the three-dimensional coordinates $(T_{\mathrm{X}}, T_{\mathrm{Y}}, T_{\mathrm{Z}})$ of the transmitter. $\bar{n}$ is here an index assigned to each particle on the basis of the order in which they are emitted. This index serves only for the mathematical formulation of their propagation through the Langevin equation in (5.27), while, as mentioned above, particles are identical and indistinguishable in the physical system.

The **Channel** propagates the signal from the transmitter to the receiver by means of molecule diffusion, which is the result of the collective translation by Brownian motion of many particles from an area in which they are more dense to an area of lower density. This results in the propagation of the particles emitted by the transmitter throughout the three-dimensional space. This propagation can be expressed

as the translation of the three-dimensional coordinates from the location $\mathbf{T}$ of the transmitter to a location $\mathbf{p}^n(t)$ at time t computed by applying (5.27) to each particle n from the set $\mathcal{N}_T(t)$, as

$$\mathbf{T} \rightarrow \mathbf{p}^n(t), \forall n \in \mathcal{N}_T(t)\,, \tag{5.31}$$

where $\mathcal{N}_T(t)$ is the set containing all the indexes of the particles emitted by the transmitter from time 0 to time t:

$$\mathcal{N}_T(t) = \left\{ \int_0^{t'} n_T(\tau) d\tau \middle| \, 0 < t' < t \right\}. \tag{5.32}$$

The **Receiver** reconstructs the messages (sent by the transmitter) from the *received signal* Y, which is proportional to the concentration of incoming particles. In this section of the article, we assume an ideal receiver where the received signal Y is defined as the time-varying number of particles that are present inside a spherical volume V_R centered at the receiver location and with radius $R_{V_R} << d$, where d is the distance between the transmitter and the receiver. This choice makes the results of this section of the article independent from any specific techniques for the reception (e.g., the chemical ligand-binding reception detailed in Section 3.5). As a consequence, the received signal Y is expressed as the number of particles emitted by the transmitter from time instant 0 to time instant t whose location $\mathbf{p}^n(t)$ is inside the volume V_R, as

$$Y := \#\left\{ n \in \mathcal{N}_T(t) : \mathbf{p}^n(t) \in V_R \right\}\,,\ t > 0\,, \tag{5.33}$$

where $\#\{.\}$ stands for the cardinality (number of elements) of the set enclosed in the brackets.

5.3.1 Information Capacity of a Diffusion-based MC link

The **capacity** C of a communication system in $[bit/sec]$ is defined as the maximum rate of transmission between the information source and the destination, where this maximum is with respect to all possible signals produced by the transmitter [90]. This is expressed by the general formula from Shannon [28], which defines the capacity as the maximum mutual information $I(X;Y)$ between the transmitted signal X and the

received signal Y with respect to the probability density function $f_X(x)$ in all the possible values of the transmitted signal, expressed as follows:

$$C = \max_{f_X(x)} \{I(X;Y)\} \ . \tag{5.34}$$

The **mutual information** $I(X;Y)$ in $[bit/sec]$ is defined as:

$$\begin{aligned} I(X;Y) &= H(X) - H(X|Y) = H(Y) - H(Y|X) = \\ &= H(X) + H(Y) - H(X,Y) \ , \end{aligned} \tag{5.35}$$

where $H(X)$ is the entropy per second of the transmitted signal X, defined in Section 5.3.3, $H(X|Y)$ is the entropy per second of the transmitted signal X given the received signal Y, $H(Y|X)$ is the entropy per second of the received signal Y given the transmitted signal X, and $H(X,Y)$ is the joint entropy per second of the transmitted signal X and the received signal Y.

In the following, we analytically compute the mutual information of a molecular communication system, as expressed by (5.34), by considering the transmitter, the channel and the receiver, defined through (5.29), (5.31) and (5.33), when evaluating (5.35). From the physical system defined at the beginning of Section 5.3, two phenomena play an important role in the quantification of the mutual information, namely, the channel memory and the molecular noise, as we highlight in Section 5.3.2. For this, we propose to divide the computation of the mutual information into two processes, namely, the Fick's diffusion, treated in Section 5.3.3, which captures solely the effects of the channel memory, and the particle location displacement, treated in Section 5.3.4, which isolates the effects of the molecular noise.

5.3.2 The Molecule Diffusion as Fick's Diffusion and Particle Location Displacement

The Langevin equation in (5.27) is the most general expression of the molecule diffusion due to the Brownian motion. In a MC link, it impacts on the communication performance (mutual information and capacity) through the following two phenomena:

- **Channel memory**: it is the effect of the persistent presence in the three-dimensional space of the particles from the moment

they are emitted by the transmitter until infinite time. This is a consequence of the fact that in the physical system considered in this section of the article each emitted particle is subject to the Brownian motion. For this, each particle wanders randomly in the three-dimensional space without being destroyed. This is expressed through a positive probability of having any of the emitted particles at any time after the emission instant inside the receiver volume, expressed as

$$P\left(n \in \mathcal{N}_T(t) : \mathbf{p}^n(t) \in V_R\right) > 0 \;\; \forall n \,,\; t > 0 \,, \tag{5.36}$$

where $\mathcal{N}_T(t)$ is given by (5.32), $\mathbf{p}^n(t)$ is the vector with the location coordinates for the particle n at time t and V_R is the set containing all the space coordinates included in the receiver volume.

- **Molecular noise**: it is the effect of the randomness of the particle locations in the three-dimensional space, which results in random fluctuations of the received signal. This is a consequence of the random process $f_i(t)$ of the particle locations expressed in (5.27). This is expressed by considering the received signal Y as a random variable with a generic distribution F. Its expected value $E[Y]$ is the integral of the expected particle distribution, denoted by $\rho(\mathbf{p}, t)$, integrated in the receiver volume V_R, as

$$Y \sim F \,,\; E[Y] = \int_{V_R} \rho(\mathbf{p}, t) d\mathbf{p} \,,\; t > 0 \,, \tag{5.37}$$

where $\rho(\mathbf{p}, t)$ is the particle distribution at location $\mathbf{p} = (p_{\mathrm{X}}, p_{\mathrm{Y}}, p_{\mathrm{Z}})$ and time t, whose equation will be defined in the following.

In this section of the article, we propose to analyze the impact of the aforementioned phenomena on the mutual information (5.35) by separating the molecule diffusion from the Langevin equation (5.27) into two processes, namely, the **Fick's diffusion** and the **particle location displacement**, as shown in Figure 5.4. This is possible since the molecule diffusion expressed by the stochastic differential equation in (5.27) and having X (5.29) as input and Y (5.33) as output can be

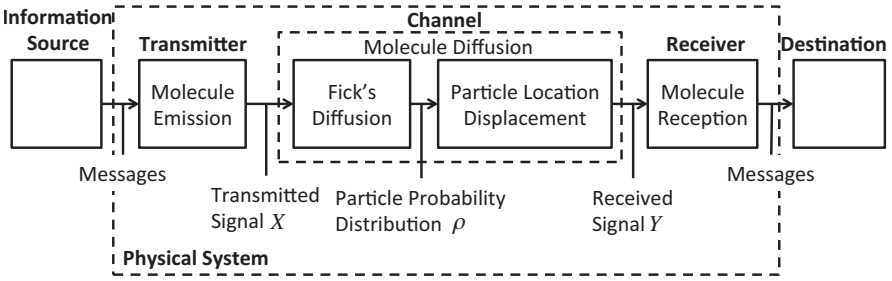

Figure 5.4: Diagram of the diffusion-based MC link with the Fick's diffusion and the particle location displacement contributions to the molecule diffusion.

equivalently expressed by the deterministic Fick's equation [29] followed by a stochastic process which results in the assignment of the particle locations in the three-dimensional space.

The Fick's equation is a parabolic partial differential equation [29] in the variable $\rho(\mathbf{p}, t)$, which is the particle distribution at location $\mathbf{p} = (p_{\mathrm{X}}, p_{\mathrm{Y}}, p_{\mathrm{Z}})$ and time t. The expression of this equation for the diffusion-based MC link accounts for the transmitter as a source of particles at location $\mathbf{T}$. This translates into an additional term, namely, $n_T(t)\delta(|\mathbf{p} - \mathbf{T}|)$, which corresponds to the number of particles $n_T(t)$ emitted into the space as a function of the time t at the location $\mathbf{T}$, where the Dirac delta $\delta(|\mathbf{p} - \mathbf{T}|)$ is non-zero. We express the Fick's equation as follows:

$$\frac{\partial \rho(\mathbf{p}, t)}{\partial t} = D\nabla^2 \rho(\mathbf{p}, t) + n_T(t)\delta(|\mathbf{p} - \mathbf{T}|)\,,\ t > 0\,, \tag{5.38}$$

where $\partial./\partial t$ is the time derivative operator of the particle distribution $\rho(\mathbf{p}, t)$, which corresponds to the expected number of particles at location $\mathbf{p}$ and time t, and ∇^2 is the Laplacian operator. D is the particle diffusion coefficient, whose expression is as follows:

$$D = \frac{K_b T}{6\pi\mu r}\,, \tag{5.39}$$

where K_b is the Boltzmann constant, T is the absolute temperature of the system, μ is the viscosity of the fluid and r is the particle radius.

The particle location displacement is expressed through the stochastic process that randomly assigns the location to each transmitted par-

ticle according to the particle distribution $\rho(\mathbf{p}, t)$ at each time instant t, as

$$\mathbf{p}^n(t) \sim \rho(\mathbf{p}, t)\,, \forall n \in \mathcal{N}_T(t)\,, \tag{5.40}$$

where $\mathcal{N}_T(t)$ is given by (5.32).

The channel memory phenomenon of the molecule diffusion introduced above is fully captured by the Fick's diffusion contribution. This is expressed by stating that the probability that the location of a particle is inside the receiver volume is never zero from the time instant of the particle emission until infinite time. This is detailed through the following relation:

$$\int_{V_R} \rho_{t'}(\mathbf{v}, t) d\mathbf{v} > 0\,,\ \forall t, t' :\ t > t' > 0\,, \tag{5.41}$$

where the integral is performed by spanning the set V_R containing all the space coordinates included in the receiver volume. $\rho_{t'}(\mathbf{v}, t)$ is the particle distribution. This is the solution of the Fick's equation in case the particles are emitted only at the time instant t'

$$\frac{\partial \rho_{t'}(\mathbf{p}, t)}{\partial t} = D\nabla^2 \rho_{t'}(\mathbf{p}, t) + n_T(t')\delta(|\mathbf{p} - \mathbf{T}|)\delta(t - t')\,,\ t > 0\,. \tag{5.42}$$

The molecular noise phenomenon is isolated into the particle location displacement contribution, since it contains the stochastic process which contributes to the Langevin equation (5.27). This is expressed by noting that the number of the particles whose location $\mathbf{p}^n(t)$ is within the receiver volume at time t is a realization of the particle location displacement, as expressed in (5.40).

The cascade of the Fick's diffusion and the particle location displacement contributions, as shown in Figure 5.4, define a Markov chain [28] in the variables X, ρ and Y following the order $X \to \rho \to Y$. This is justified by the property that X and Y are conditionally independent given ρ, which is expressed as follows:

$$f_{X,Y|\rho}(x, y) = f_{X|\rho}(x)\, f_{Y|\rho}(y)\,, \tag{5.43}$$

since ρ is function of X from (5.29) and (5.38), and the distribution of Y is a function of ρ from (5.33) and (5.40). The chain rule applied to the joint entropy of X, ρ and Y states the following [28]:

$$H(X, \rho, Y) = H(X, Y|\rho) + H(\rho) = H(X|\rho) + H(Y|\rho) + H(\rho)\,. \tag{5.44}$$

Since ρ is a deterministic function of X through the Fick's equation from (5.38), then the joint entropy per second of X, ρ and Y is equal to the joint entropy per second of X and Y:

$$H(X, \rho, Y) = H(X, Y)\,. \tag{5.45}$$

By applying (5.44) and (5.45) to the third expression in (5.35), we obtain that the mutual information $I(X;Y)$ of the transmitted signal X and the received signal Y as the sum of the mutual information of a communication system which includes only the Fick's diffusion (mutual information $I(X;\rho)$ of the transmitted signal and the particle distribution) and the mutual information of a system which includes only the particle location displacement (mutual information $I(Y;\rho)$ of the received signal and the particle distribution), respectively, with the subtraction of the entropy per second $H(\rho)$ of the particle distribution. This is expressed as follows:

$$\begin{aligned} I(X;Y) &= H(X) + H(Y) - H(X|\rho) - H(Y|\rho) - H(\rho) = \\ &= I(X;\rho) + I(Y;\rho) - H(\rho)\ , \end{aligned} \tag{5.46}$$

where we applied the first two definitions of mutual information from (5.35) to obtain the last expression.

We provide closed-form solutions to the mutual information of the Fick's diffusion and to the mutual information of the particle location displacement in Section 5.3.3 and Section 5.3.4, respectively. In Section 5.3.5 we apply (5.34) and (5.46) to the results of the previous sections to obtain a closed-form expression of a lower bound to the mutual information of the diffusion-based MC link and, ultimately, to obtain a lower bound to its capacity.

5.3.3 The Fick's Diffusion Mutual Information

The closed-form expression for the mutual information $I(X;\rho)$ in $[bit/sec]$ of the Fick's diffusion is computed by applying the following relation:

$$I(X;\rho) = H(X) - H(X|\rho)\,, \tag{5.47}$$

where $H(X)$ is the entropy per second of the transmitted signal X and $H(X|\rho)$ is the conditional entropy per second of the transmitted signal

X given the particle distribution ρ.

The entropy per second $H(X)$ of the transmitted signal is computed as the entropy measured in $[bit/symbol]$, multiplied by twice the bandwidth W, which corresponds here to the rate of the symbol transmission in $[symbol/sec]$. This results from considering the transmitted signal X defined in (5.29) as a band-limited ensemble of functions [90] within a bandwidth W. The ensemble has the following expression:

$$X = \sum_{k=0}^{\infty} n_T \left(\frac{k}{2W} \right) \frac{\sin\left[\pi(2Wt-k)\right]}{\pi(2Wt-k)}\,,\; k \in \mathbb{N}\,, \tag{5.48}$$

where the bandwidth W is here defined as the maximum frequency contained in the time-continuous signal $n_T(t)$ (5.29), which corresponds to the number of emitted particles as function of the time t. The Shannon-Hartley theorem [28] assures the equivalence of the expressions in (5.48) and (5.29), respectively. As proven in [90], we can express the entropy per second $H(X)$ of the transmitted signal X as the entropy of the ensemble per degree of freedom in $[bit/sample]$ multiplied by twice the bandwidth W in $[sample/sec]$. The entropy of the ensemble per degree of freedom corresponds to the entropy $H(\hat{n}_T)$ of a sample $n_T(k/2W)$ of the time-continuous signal $n_T(t)$, expressed as follows:

$$H(X) = 2W\, H(\hat{n}_T)\,. \tag{5.49}$$

The distribution of the stochastic process model for the sampled signal $\hat{n}_T$, which allows to compute a lower-bound expression of the capacity C through (5.34), is assigned in Section 5.3.5 as the distribution leading to the maximum possible mutual information for the MC link constrained by the average power consumption for particle emission at the transmitter.

The conditional entropy per second $H(X|\rho)$ of the transmitted signal X given the particle distribution ρ is computed as a result of the two following properties of the Fick's diffusion from (5.38):

- Its linearity, which allows to interpret the Fick's diffusion block in Figure 5.4 as a linear filter having the transmitted signal X as input and the particle distribution ρ as output. As a consequence, the formula of the entropy loss in linear filters [17] can

be applied to compute the entropy per second $H(\rho)$ of the particle distribution as the sum of the entropy per second $H(X)$ of the transmitted signal and the integral of the transfer function Fourier transform [30] of the Green's function [64] of the Fick's diffusion in the portion W of its frequency spectrum that is excited by the transmitted signal X, expressed as

$$H(\rho) = H(X) + \frac{1}{W}\int_{W} \log_2 |G_d(f)|^2 \, df \,. \tag{5.50}$$

- Its deterministic nature, since (5.38), in contrast to the expression in (5.27), does not contain any stochastic term. For this, given the transmitted signal X as the input of the Fick's diffusion, the output particle distribution ρ is completely known. As a consequence, the conditional entropy per second $H(\rho|X)$ of the particle distribution given the transmitted signal is equal to zero, expressed as

$$H(\rho|X) = 0 \,. \tag{5.51}$$

Given the aforementioned properties, the conditional entropy per second $H(X|\rho)$ of the transmitted signal X given the particle distribution ρ is computed by applying (5.50) and (5.51) to the following relation [28]:

$$H(\rho) = H(X) + H(\rho|X) - H(X|\rho) \,, \tag{5.52}$$

which results in the following expression:

$$H(X|\rho) = -\frac{1}{W}\int_{W} \log_2 |G_d(f)|^2 \, df \,, \tag{5.53}$$

where $G_d(f)$ is the transfer function Fourier transform [30] as function of the frequency f of the Green's function [64] of the Fick's diffusion, expressed by (5.38). W is the bandwidth of the transmitted signal X, which corresponds to the portion of the frequency spectrum of the transfer function $G_d(f)$ that is excited by the transmitted signal X.

The transfer function Fourier transform [30] as function of the frequency f of the Green's function [64] of the Fick's diffusion from (5.38) has the following expression:

$$G_d(f) = \frac{e^{-(1+j)\sqrt{\frac{2\pi f}{2D}}d}}{\pi D d} \,, \tag{5.54}$$

where d is the distance between the transmitter and the receiver and D is the diffusion coefficient expressed by (5.39). By applying (5.54) to (5.53) we obtain the closed-form expression of the conditional entropy per second $H(X|\rho)$ of the transmitted signal X given the particle distribution ρ as follows:

$$H(X|\rho) = 2\log_2(\pi D d) + \frac{4d}{3\ln 2}\sqrt{\frac{\pi W}{D}}\,. \tag{5.55}$$

The closed-form expression for the mutual information $I(X;\rho)$ of the Fick's diffusion is finally computed by subtracting the conditional entropy per second $H(X|\rho)$ of the transmitted signal X (5.55) given the particle distribution ρ from the entropy per second $H(X)$ (5.49) of the transmitted signal X. This results in the following expression:

$$I(X;\rho) = 2WH\left(\hat{n}_T\right) - 2\log_2\left(\pi D d\right) - \frac{4d}{3\ln 2}\sqrt{\frac{\pi W}{D}}\,, \tag{5.56}$$

where $H\left(\hat{n}_T\right)$ is the entropy of a time sample of $n_T(t)$.

5.3.4 The Particle Location Displacement Mutual Information

The mutual information $I(Y;\rho)$ in $[bit/sec]$ of the particle location displacement is computed from the following expression:

$$I(Y;\rho) = H(\rho) - H(\rho|Y)\,, \tag{5.57}$$

where $H(\rho)$ is the entropy per second of the particle distribution ρ and $H(\rho|Y)$ is the conditional entropy per second of the particle distribution ρ given the received signal Y.

The entropy $H(\rho)$ per second of the particle distribution ρ is computed from (5.50) by substituting the expression for the entropy per second $H(X)$ of the transmitted signal X from (5.49) and by applying (5.53) and (5.55) as the solution of the integral in (5.50). As a result, the entropy per second $H(\rho)$ of the particle distribution ρ has the following expression:

$$H(\rho) = 2WH\left(\hat{n}_T\right) - \log_2\left[(\pi D d)^2\right] - \frac{4d}{3\ln 2}\sqrt{\frac{\pi W}{D}}\,. \tag{5.58}$$

The conditional entropy per second $H(\rho|Y)$ of the particle distribution ρ given the received signal Y is computed similarly to (5.49) in Section 5.3.3. Under the assumption that the realizations of the stochastic process $\rho|Y$ are independent [74] for different time instants, and band limited within a bandwidth W, we express the entropy per second $H(\rho|Y)$ as the entropy of $H(\rho|\mathcal{Y})$ in $[bit]$, where $\mathcal{Y}$ is the received signal per time sample, multiplied by the maximum time sample rate $2W$ in $[1/sec]$ given by the Shannon-Hartley theorem [30], expressed as

$$H(\rho|Y) = 2W H(\rho|\mathcal{Y})\,. \tag{5.59}$$

The received signal $\mathcal{Y}$ per time sample is defined as

$$\mathcal{Y} = \sum_{i=1}^{1/(2W\tau_p)} y_i\,, \tag{5.60}$$

where $1/(2W\tau_p)$ is the number of independent measures of the number of particles inside the receiver volume that can be performed within a time sample, for which we consider a quasi-constant particle distribution. W is the bandwidth of the transmitted signal X. We assume independent measures when they are taken at time instants spaced by an interval τ_p, as we considered in Section 4.4. The time interval τ_p is equal to the squared linear dimension of the receiver volume R_{V_R} divided by the diffusion coefficient D, as derived in Section 4.4, expressed as

$$\tau_p = \frac{R_{V_R}^2}{D}\,. \tag{5.61}$$

The conditional entropy $H(\rho|\mathcal{Y})$ of the particle distribution ρ given the received signal $\mathcal{Y}$ per time sample is defined as

$$H(\rho|\mathcal{Y}) = \int H(\rho|\mathcal{Y}=\mathrm{y})p_{\mathcal{Y}}(\mathrm{y})d\mathrm{y} = \mathrm{E}_{\mathrm{y}}\left[H(\rho|\mathcal{Y}=\mathrm{y})\right]\,, \tag{5.62}$$

where $H(\rho|\mathcal{Y}=\mathrm{y})$ is the entropy of the particle distribution ρ given a value y for the received signal per time sample $\mathcal{Y}$, $p_{\mathcal{Y}}(\mathrm{y})$ is the probability density of the received signal $\mathcal{Y}$ per time sample and $\mathrm{E}_{\mathrm{y}}[.]$ is the average value operator with respect to the probability density of the value y.

The entropy $H(\rho|\mathcal{Y} = \mathrm{y})$ is based on the probability density $p_{\rho|\mathcal{Y}}(r|\mathrm{y})$ of the possible values y of the particle distribution ρ at the receiver given a value y for the received signal per time sample $\mathcal{Y}$ through the formula

$$H(\rho|\mathcal{Y} = \mathrm{y}) = -\int p_{\rho|\mathcal{Y}}(r|\mathrm{y}) \log_2 p_{\rho|\mathcal{Y}}(r|\mathrm{y}) dr \,. \tag{5.63}$$

With the goal of having a closed-form expression for this probability density, we use the following assumptions, with reference to our previous work on the particle counting noise in Section 4.4:

- The actual number of particles y_i inside the receiver volume for every measurement is a random process whose average value is the average particle distribution at the receiver $\bar{\rho}$ within a time sample multiplied by the size $size(V_R)$ of the receiver volume, expressed as

$$\mathrm{E}[y_i] = \bar{\rho}\, size(V_R) \,. \tag{5.64}$$

  Since the particle distribution ρ is the output of the Fick's diffusion, whose input is the stationary stochastic process of the number of the emitted particles $\hat{n}_T$ for every time sample, by applying the theory of the random processes through linear filters [74] we obtain

$$\bar{\rho} = \mathrm{E}\left[\hat{n}_T\right] G_d(f)|_{f=0} = \frac{\mathrm{E}\left[\hat{n}_T\right]}{\pi D d} \,, \tag{5.65}$$

  where $G_d(f)$ is from (5.54) and $\mathrm{E}\left[.\right]$ is the average operator.

- It is unlikely to have two particles occupying the same location in space at the same time instant. In other words, the probability of having a distance equal to zero between two particles is zero, expressed as

$$Pr\left[\|P_p(t) - P_q(t)\| = 0\right] = 0 \, p \neq q,\, p, q \in \mathcal{N}_T(t) \,, \tag{5.66}$$

  where $\mathcal{N}_T(t)$ is given by (5.32), $\|.\|$ is the Euclidian distance operator and p and q are two particles previously emitted by the transmitter, which are subject to the Brownian motion. This assumption is justified by the independence of the Brownian components in the movement of different particles in the space.

- An event concerning a particle which occupies a location in space is independent from any event of the same kind occurring at any other space location. This assumption is justified by the property of the Wiener process [29] underlying the particle Brownian motion of having independent realizations. This implies that the location of a particle is independent from the location of any other particle. As a consequence, the events concerning the location of particles in the space have the property of *memorylessness*.
- The occurrence rate of particle locations in the space is proportional to the particle distribution at the receiver location ρ.

Under these assumptions, the resulting single measurement y_i, which corresponds to the number of particles inside the receiver volume, is a volumetric Poisson counting process [74], whose rate of occurrence corresponds to the average value of the particle distribution $\bar{\rho}$ within a time sample, expressed as

$$y_i \sim \text{Poiss}(\bar{\rho})\,, \tag{5.67}$$

According to the theory of Bayesian inference [45], the estimator of the rate of occurrence $\hat{\rho}$ of a Poisson counting process given a series of measurements of the output of the process, which corresponds to a value y of the received signal per time sample $\mathcal{Y}$ defined in (5.60), follows a Gamma distribution with parameters y and $1/(2W\tau_p)$, expressed as

$$\hat{\rho} \sim \text{Gamma}(\text{y}, 1/(2W\tau_p))\,, \tag{5.68}$$

where W is the bandwidth of the transmitted signal X and τ_p is the time interval in which we consider a quasi-constant particle distribution. The probability density of the estimator $\hat{\rho}$ corresponds to the probability density $p_{\rho|\mathcal{Y}}(r|\text{y})$ of the possible values r of the particle distribution ρ at the receiver given a value y for the received signal in a time sample $\mathcal{Y}$ [45], expressed as

$$p_{\rho|\mathcal{Y}}(r|\text{y}) = r^{\text{y}-1}\frac{e^{-rW\tau_p}}{(W\tau_p)^{\text{y}}\Gamma(\text{y})}\,,\ r \geq 0,\ \text{y} > 0\,, \tag{5.69}$$

where $\Gamma(\text{y})$ is the gamma function [67], defined as follows:

$$\Gamma(\text{y}) = (\text{y}-1)!\,. \tag{5.70}$$

The entropy $H(\rho|\mathcal{Y}=\mathrm{y})$ of the particle distribution ρ given a value y for the received signal per time sample $\mathcal{Y}$ corresponds to the computation of the formula in (5.63) by using the expression of the probability density $p_{\rho|\mathcal{Y}}(r|\mathrm{y})$ from (5.69), thus obtaining the following expression [45]:

$$H(\rho|\mathcal{Y}=\mathrm{y}) = \mathrm{y} + \ln(2W\tau_p) + \ln\left(\Gamma(\mathrm{y})\right) + (1-\mathrm{y})\psi(\mathrm{y})\,, \tag{5.71}$$

where $\psi(\mathrm{y})$ is the digamma function.

For the final computation of the conditional entropy $H(\rho|\mathcal{Y})$, expressed in (5.62), we apply a formulation of the Jensen's inequality [74], which is based on the consideration that $H(\rho|\mathcal{Y}=\mathrm{y})$ is a concave function of y, since its expression in (5.71) is a sum of concave or linear components:

- The first term y is linear.
- The second term $\ln\left(\Gamma(\mathrm{y})\right)$ is concave in y since the gamma function $\Gamma(\mathrm{y})$ has the property of being log-concave [67].
- The third term $(1-\mathrm{y})\psi(\mathrm{y})$ is concave in y when the value of y is sufficiently high ($\mathrm{y} >> 1$). This can be proven from the decomposition of the digamma function as follows [21]:

$$\psi(\mathrm{y}) = \ln \mathrm{y} - \frac{1}{2\mathrm{y}} - \frac{1}{12\mathrm{y}^2} + \frac{1}{120\mathrm{y}^4} - \frac{1}{252\mathrm{y}^6} + O\left(\frac{1}{\mathrm{y}^8}\right)\,, \tag{5.72}$$

  By taking the limit of $(1-\mathrm{y})\psi(\mathrm{y})$ as $\mathrm{y}\to\infty$ we obtain

$$(1-\mathrm{y})\psi(\mathrm{y}) \to -\mathrm{y}\ln \mathrm{y}\,, \tag{5.73}$$

  which is a concave function of y.

For the aforementioned considerations, the Jensen's inequality [74] applied to (5.62) states that the average value $\mathrm{E}_{\mathrm{y}}\left[H(\rho|\mathcal{Y}=\mathrm{y})\right]$ of the entropy $H(\rho|\mathcal{Y}=\mathrm{y})$ as function of the value y for the received signal per time sample $\mathcal{Y}$ is less or equal than the entropy $H(\rho|\mathrm{E}\left[\mathcal{Y}\right])$ as function of the average value $\mathrm{E}\left[\mathcal{Y}\right]$ of the received signal per time sample $\mathcal{Y}$, as

$$H(\rho|\mathcal{Y}) = \mathrm{E}_{\mathrm{y}}\left[H(\rho|\mathcal{Y}=\mathrm{y})\right] \leq H(\rho|\mathrm{E}\left[\mathcal{Y}\right])\,, \tag{5.74}$$

As a consequence, by substituting the left hand side of (5.74) for the computation (5.62) of the conditional entropy $H(\rho|\mathcal{Y})$ of the particle distribution ρ given the received signal Y per time sample with the right hand side of (5.74), we provide a higher bound to the real value of $H(\rho|\mathcal{Y})$. This results in a higher bound to the conditional entropy $H(\rho|Y)$ of the particle distribution ρ given the received signal Y in (5.59) and, consequently, in a lower bound to the mutual information $I(\rho;Y)$ of the transmitted signal and the particle distribution in (5.57). **Since the capacity is the maximum mutual information $I(X;Y)$ between the transmitted signal X and the received signal Y, as expressed in** (5.34)**, the substitution of $I(\rho;Y)$ with its lower bound in the computation of the mutual information $I(X;Y)$ expressed in** (5.46) **results in a lower bound to the capacity C of a molecular communication system.** We consider this in agreement with the purpose of this section of the article, since it allows expressing achievable performance of a molecular communication system with a closed-form mathematical expression, even if it is an underestimate of the theoretical capacity C.

The average value $\mathrm{E}[\mathcal{Y}]$ of the received signal per time sample $\mathcal{Y}$ is given by (5.64) and (5.65). Since the distribution of particles ρ is a deterministic function of the transmitted signal X, whose average value per time sample is $\mathrm{E}[\hat{n}_T]$, the value of $\mathrm{E}[\mathcal{Y}]$ becomes

$$\mathrm{E}[\mathcal{Y}] = \sum_{i=1}^{1/(2W\tau_p)} \mathrm{E}[y_i] = \frac{1}{2W\tau_p}\bar{\rho} size(V_R) = \frac{D}{2WR_{V_R}^2}\frac{\mathrm{E}[\hat{n}_T]}{\pi Dd}\frac{4}{3}\pi R_{V_R}^3 = \\ = \frac{2}{3}\frac{\mathrm{E}[\hat{n}_T]\,R_{V_R}}{Wd}\,. \tag{5.75}$$

As stated previously, the expression for the conditional entropy $H(\rho|\mathcal{Y})$ can be approximated with the right hand side of (5.74), whose expression is found by applying the average value $\mathrm{E}[\mathcal{Y}]$ of the received signal per time sample $\mathcal{Y}$ to (5.71) as follows:

$$H(\rho|\mathcal{Y}) \cong H(\rho|\mathrm{E}[\mathcal{Y}]) = \mathrm{E}[\mathcal{Y}] + \ln(2W\tau_p) + \ln\left(\Gamma(\mathrm{E}[\mathcal{Y}])\right) + \\ + (1-\mathrm{E}[\mathcal{Y}])\psi(\mathrm{E}[\mathcal{Y}])\,. \tag{5.76}$$

The final approximated expression for the conditional entropy $H(\rho|\mathcal{Y})$

is found by substituting the expression in (5.75). This becomes

$$H(\rho|\mathcal{Y}) \cong \frac{2}{3}\frac{\mathrm{E}\left[\hat{n}_T\right] R_{V_R}}{Wd} + \ln(2W\tau_p) + \ln\left(\Gamma\left(\frac{2}{3}\frac{\mathrm{E}\left[\hat{n}_T\right] R_{V_R}}{Wd}\right)\right) + \\ + \left(1 - \frac{2}{3}\frac{\mathrm{E}\left[\hat{n}_T\right] R_{V_R}}{Wd}\right)\psi\left(\frac{2}{3}\frac{\mathrm{E}\left[\hat{n}_T\right] R_{V_R}}{Wd}\right), \tag{5.77}$$

where W is the bandwidth of the transmitted signal X, τ_p is the time interval in which we consider a quasi-constant particle distribution, $\psi(.)$ is the digamma function, D is the diffusion coefficient, d is the distance between the transmitter and the receiver, and R_{V_R} is the radius of the spherical receiver volume V_R.

The closed-form expression for the mutual information $I(Y;\rho)$ of the particle location displacement is finally computed by subtracting the conditional entropy $H(\rho|\mathcal{Y})$ of the particle distribution ρ given the received signal $\mathcal{Y}$ per time sample from (5.77) multiplied by two times the bandwidth W of the transmitted signal X from the entropy $H(\rho)$ (5.58) of the particle distribution ρ. This results in the following expression:

$$\begin{aligned} I(Y;\rho) =& 2WH\left(\hat{n}_T\right) - \log_2\left[(\pi Dd)^2\right] - \frac{4d}{3\ln 2}\sqrt{\frac{\pi W}{D}} \\ & - 2W\frac{2}{3}\frac{\mathrm{E}\left[\hat{n}_T\right] R_{V_R}}{Wd} + \\ & - 2W\ln(2W\tau_p) - 2W\ln\left(\Gamma\left(\frac{2}{3}\frac{\mathrm{E}\left[\hat{n}_T\right] R_{V_R}}{Wd}\right)\right) + \\ & - 2W\left(1 - \frac{2}{3}\frac{\mathrm{E}\left[\hat{n}_T\right] R_{V_R}}{Wd}\right)\psi\left(\frac{2}{3}\frac{\mathrm{E}\left[\hat{n}_T\right] R_{V_R}}{Wd}\right). \end{aligned} \tag{5.78}$$

5.3.5 The Capacity

The capacity of the diffusion-based MC link is computed from (5.34), by maximizing the mutual information $I(X;Y)$, expressed in Section 5.3.5 with respect to the probability density function $f_X(x)$ of the transmitted signal X. It is common in information theory [90] to compute the maximum probability density function $f_X(x)$ subject to a constraint on the average power of the transmitted signal X defined in (5.29). As explained in Section 5.3.5, the expression for this average power is here

related to the thermodynamic energy spent for the emission of particles in the MC signal transmission. Finally, in Section 5.3.5 we obtain the closed-form expression of the lower bound to the capacity.

The Mutual Information

The expression for the mutual information $I(X;Y)$ of the diffusion-based MC link is obtained by applying the expression of the mutual information $I(X;\rho)$ of the Fick's diffusion from (5.56), the mutual information $I(Y;\rho)$ of the particle location displacement from (5.78) and the entropy $H(\rho)$ of the particle distribution ρ from (5.58) to the formula in (5.46). We obtain the following expression:

$$\begin{aligned} I(X;Y) =& 2WH\left(\hat{n}_T(t)\right) - \log_2\left[(\pi D d)^2\right] - \frac{4d}{3\ln 2}\sqrt{\frac{\pi W}{D}} \\ & - 2W\frac{2}{3}\frac{\mathrm{E}\left[\hat{n}_T\right]R_{V_R}}{Wd} + \\ & - 2W\ln(W\tau_p) - 2W\ln\left(\Gamma\left(\frac{2}{3}\frac{\mathrm{E}\left[\hat{n}_T\right]R_{V_R}}{Wd}\right)\right) + \\ & - 2W\left(1 - \frac{2}{3}\frac{\mathrm{E}\left[\hat{n}_T\right]R_{V_R}}{Wd}\right)\psi\left(\frac{2}{3}\frac{\mathrm{E}\left[\hat{n}_T\right]R_{V_R}}{Wd}\right), \end{aligned} \tag{5.79}$$

where W is the bandwidth of the transmitted signal X, τ_p is the time interval in which we consider a quasi-constant particle distribution, $\psi(.)$ is the digamma function, D is the diffusion coefficient, d is the distance between the transmitter and the receiver and R_{V_R} is the radius of the spherical receiver volume V_R.

The Average Thermodynamic Power

Given the physical system considered at the beginning of Section 5.3, the average power necessary for signal transmission corresponds to the energy necessary to emit the average number $\mathrm{E}\left[\hat{n}_T\right]$ of particles per time sample, divided by the duration of a time sample. In thermodynamics, this energy is defined as enthalpy.

Theorem 5.2. The enthalpy $\mathcal{H}$ [96] is the energy necessary to emit N particles in the physical system and to heat these particles up to a

temperature T when the system has the pressure P and the volume V. The considerations detailed at the beginning of Section 5.3 of having spherical particles with radius $r << d$ independently and randomly moving in the space are in agreement with the approximation of the system as an ideal gas. According to the ideal gas theory [42], the enthalpy is expressed through the following formula:

$$\mathcal{H} = PV + \frac{3}{2} K_b T N \,, \tag{5.80}$$

where P and V are the pressure and the volume and T is the absolute temperature of the physical system, K_b is the Boltzmann constant.

When associated to the transmitter of the molecular communication system, the enthalpy is the energy necessary for communication when N particles are emitted into the space.

In this section of the article, we define the **average thermodynamic power** $\bar{P}_{\mathcal{H}}$ as the enthalpy variation $\Delta\mathcal{H}$ in a time sample divided by the time sample duration $1/2W$. As a consequence, the average thermodynamic power $\bar{P}_{\mathcal{H}}$ quantifies the energy necessary to emit $\mathrm{E}\left[\hat{n}_T\right]$ particles per time sample divided by the time sample duration $1/2W$, at a temperature T. This is given by the following expression:

$$\bar{P}_{\mathcal{H}} = \frac{\Delta\mathcal{H}}{1/2W} = \frac{3}{2} K_b T \mathrm{E}\left[\hat{n}_T\right] 2W \,, \tag{5.81}$$

where the enthalpy variation $\Delta\mathcal{H}$ is computed from (5.81) by taking into account that no variations in the pressure P and the volume V occur in the physical system, and the absolute temperature T is considered a constant parameter with respect to the time t.

As a consequence, a constraint on the average thermodynamic power $\bar{P}_{\mathcal{H}}$ spent by the transmitter corresponds to a constraint in the average number $\mathrm{E}\left[\hat{n}_T\right]$ of emitted particles according to the following expression:

$$\mathrm{E}\left[\hat{n}_T\right] = \frac{\bar{P}_{\mathcal{H}}}{3W K_b T} \,. \tag{5.82}$$

The Lower-bound Expression of the Capacity

In the expression of $I(X;Y)$ (5.79), only the term $H\left(\hat{n}_T(t)\right)$ depends on the probability density function $f_{\hat{n}_T}(n)$. Therefore, the lower-bound

expression of the capacity C is achieved (5.34) for a probability density function $f_{\hat{n}_T}(n)$ leading to the maximum entropy $H\left(\hat{n}_T(t)\right)$.

The distribution $f_{\hat{n}_T}(n)$ with the maximum possible entropy $H\left(\hat{n}_T\right)$ in the number of emitted particles per time sample constrained on its average value $\mathrm{E}\left[\hat{n}_T\right]$, as expressed in (5.82), is the Exponential distribution [28] whose rate corresponds to $\mathrm{E}\left[\hat{n}_T\right]$ as follows

$$f_{H(\hat{n}_T)}(n) = \frac{e^{-\frac{n}{\mathrm{E}[\hat{n}_T]}}}{\mathrm{E}\left[\hat{n}_T\right]}\,. \tag{5.83}$$

The entropy of the number $H(\hat{n}_T)$ of emitted particles per time sample is therefore [28]

$$H(\hat{n}_T) = 1 + \log_2 \mathrm{E}\left[\hat{n}_T\right]\,. \tag{5.84}$$

By applying (5.82) and (5.84) to the expression of the mutual information $I(X;Y)$ from (5.79), we obtain the lower-bound expression of the capacity C of the diffusion-based MC link as follows:

$$\begin{aligned} C =& 2W\left(1 + \log_2 \frac{\bar{P}_{\mathcal{H}}}{3WK_bT}\right) - 2\log_2\left(\pi D d\right) - \frac{4d}{3\ln 2}\sqrt{\frac{\pi W}{D}} + \\ & - 2W\frac{2\bar{P}_{\mathcal{H}}R_{V_R}}{9W^2dK_bT} - 2W\ln(W\tau_p) - 2W\ln\left(\Gamma\left(\frac{2\bar{P}_{\mathcal{H}}R_{V_R}}{9W^2dK_bT}\right)\right) + \\ & - 2W\left(1 - \frac{2\bar{P}_{\mathcal{H}}R_{V_R}}{9W^2dK_bT}\right)\psi\left(\frac{2\bar{P}_{\mathcal{H}}R_{V_R}}{9W^2dK_bT}\right)\,, \end{aligned} \tag{5.85}$$

where $\bar{P}_{\mathcal{H}}$ is the average thermodynamic power spent by the transmitter, K_b is the Boltzmann constant, T is the absolute temperature of the system, W is the bandwidth of the transmitted signal X, τ_p is the time interval in which we consider a quasi-constant particle distribution, $\psi(.)$ is the digamma function, D is the diffusion coefficient, d is the distance between the transmitter and the receiver and R_{V_R} is the radius of the spherical receiver volume V_R.

5.3.6 Numerical Results

In this section, we provide a numerical evaluation of the closed-form expression of the lower bound to the capacity of a diffusion-based MC obtained in Section 5.3.5. All the results are computed for a common

set of parameters, whose values are assigned as follows. The radius R_{V_R} of the receiver volume V_R, which we assume to be spherical, is set to 10 nm. The temperature T of the system is set to a standard room temperature of 25 °C and the diffusion coefficient D is set to 10^{-9} [m^2/sec], as explained in Chapter 3. The Boltzmann constant [46] is $K_b = 1.380650424x10^{-23}$ [Joule/K].

Capacity Vs Bandwidth

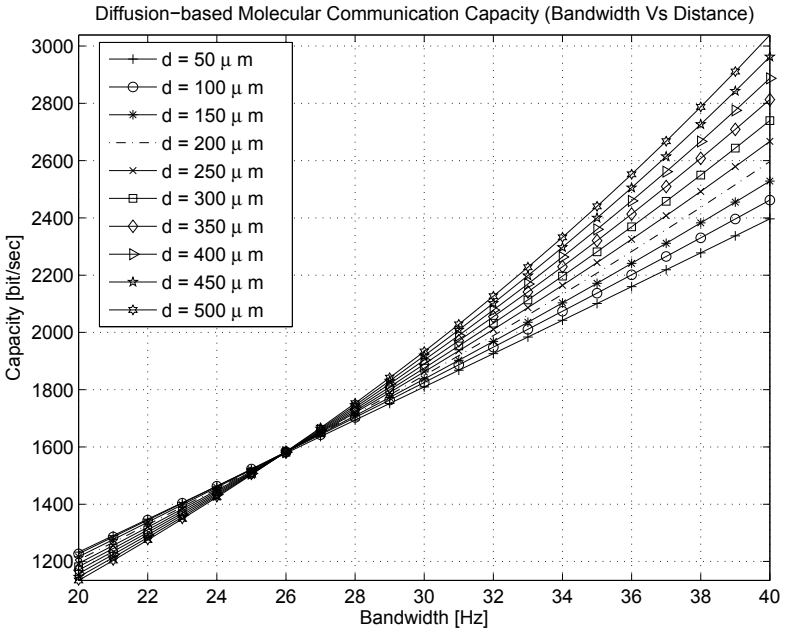

Figure 5.5: Capacity in relation to the bandwidth and for different values of the transmitter-receiver distance d.

The values of the lower bound to the capacity of a diffusion-based MC link are shown in Figure 5.5 in relation to the bandwidth W and different values of the transmitter-receiver distance d. We evaluate the capacity in [bit/sec] for a bandwidth W ranging from 20 Hz to 40 Hz and different lines refer to different distance values, from 50 μm to 500 μm. The choice of the values for the bandwidth can be justified from

a biological viewpoint, since, according to biochemical studies [73], the neurons in our brain communicate through the exchange of molecules (and their diffusion between the synapses) at a frequency of around 20 Hz for the processing of general information and around 60 Hz for the processing of visual images. We restricted our range to a maximum of 40 Hz in order to visualize better the intersection of the curves around 26 Hz. The average transmitter power $P_{\mathcal{H}}$ is set to 10^{-12} W, equivalent to 1 pW. This value should not be compared to the transmitted power values used for electrical devices, since the average transmitted power is a thermodynamic quantity. Note also that this is only a reference value, since so far we do not know how much average thermodynamic power a transmitter nanomachine will be able to provide. According to the obtained results, the capacity of a molecular communication system with the chosen parameters can achieve a value close to 3 [Kbit/sec] at a distance of 500 μm and for a bandwidth of 40 Hz. This is a theoretically achievable maximum value, which reveals the maximum potential of molecular communication. Further investigation on information coding schemes is required in order to provide achievable bit rates related to specific molecular communication implementations.

Figure 5.5 shows the trend of the MC capacity, which is monotonically increasing as the bandwidth increases from 20 Hz to 40 Hz for all the given values of the transmitter-receiver distance d. The capacity values range from 1.2 [$Kbit/sec$] to 2.4 [Kbit/sec] for a distance of 50 μm and between a few [$bits/sec$] and 3 [Kbit/sec] for a distance of 500 μm. For a bandwidth value within 20 and 26 Hz, the MC capacity values corresponding to the lowest transmitter-receiver distance d are higher than the values corresponding to other transmitter-receiver distances and, as this distance increases, the MC capacity values decrease monotonically. For a bandwidth value higher than 26 Hz, higher MC capacity values correspond to higher transmitter-receiver distances d. This behavior, which is apparently counterintuitive, can be explained as a consequence of the interactions between the channel memory and the molecular noise contributions in the second and third term of the first line and in the second, third and fourth lines of (5.85), respectively. For low bandwidth values (lower than 26 Hz), the channel mem-

ory terms tend to outperform the molecular noise terms and the MC capacity values tend to be proportional to the transmitter-received distance (higher MC capacity when lower transmitter-receiver distance). For high bandwidth values (higher than 26 Hz), the molecular noise terms outperform the channel memory terms and the MC capacity values become inversely proportional to the transmitter-receiver distance (higher MC capacity when higher transmitter-receiver distance).

Capacity Vs Distance

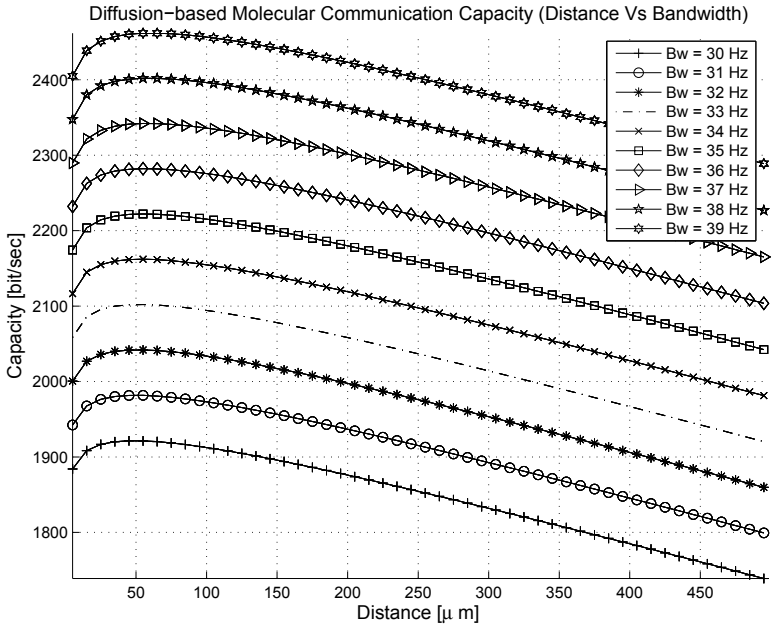

Figure 5.6: Capacity in relation to the transmitter-receiver distance and for different values of the bandwidth W.

In Figure 5.6 we show the values of the lower bound to the capacity in relation to the distance d between the transmitter and the receiver locations and different values of the bandwidth W. We evaluate the capacity in $[bit/sec]$ for a distance ranging from 1 μm to 500 μm. The different lines refer to different bandwidth W values, from 30 Hz to

39 Hz. We restricted these numerical results to this narrow bandwidth interval in order to better visualize the differences in the MC capacity for the considered values of the distance between the transmitter and the receiver. The average transmitted power $P_{\mathcal{H}}$ is set to 1 pW.

The curves in Figure 5.6 show a monotonically increasing trend of the capacity as function of the transmitter-receiver distance ranging from 1 μm to 50 μm, while they show a monotonically decreasing value for a distance ranging from 50 μm to 500 μm. The capacity values range from a value around 1.9 [Kbit/sec] and a 1.85 [$bits/sec$] for a bandwidth of 30 Hz and between 2.45 [$Kbit/sec$] and 2.3 [Kbit/sec] for a bandwidth of 39 Hz. The different behavior when the distance ranges from 1 μm to 50 μm with respect to when the distance ranges from 50 μm to 500 μm can be explained as a consequence of the interactions between the channel memory and the molecular noise contributions, similarly to Figure 5.5: as the distance increases from 1 μm to 50 μm, the contribution coming from the channel memory gets lower and the capacity values tend to increase, until reaching a distance of 50 μm, where the contribution coming from the molecular noise becomes relevant and decreases the capacity values as the distance is further increased.

Capacity and Average Transmitted Power

In Figure 5.7 we show the values of the lower bound to capacity as a function of the bandwidth W ranging from 30 Hz to 40 Hz and the average transmitted power $P_{\mathcal{H}}$. Similarly to Figure 5.6, we restricted these numerical results to this narrow bandwidth interval in order to better visualize the differences in the MC capacity for the values of the average transmitter power. Different lines refer to different average transmitted power $P_{\mathcal{H}}$ values, from 1 pW to 10 pW. The transmitter-receiver distance d is here set to 50 μm.

Figure 5.7 shows for all the curves a monotonic increasing trend as the bandwidth increases from 30 Hz to 40 Hz. The capacity values range from a value between 1.92 [$Kbit/sec$] and around 2.5 [kbits/sec] for an average transmitted power of 1 pW and between 2.05 [Kbit/sec] and 3.7 [Kbit/sec] for an average transmitted power of 10 pW. The MC capacity values are higher for higher values of the average transmitted

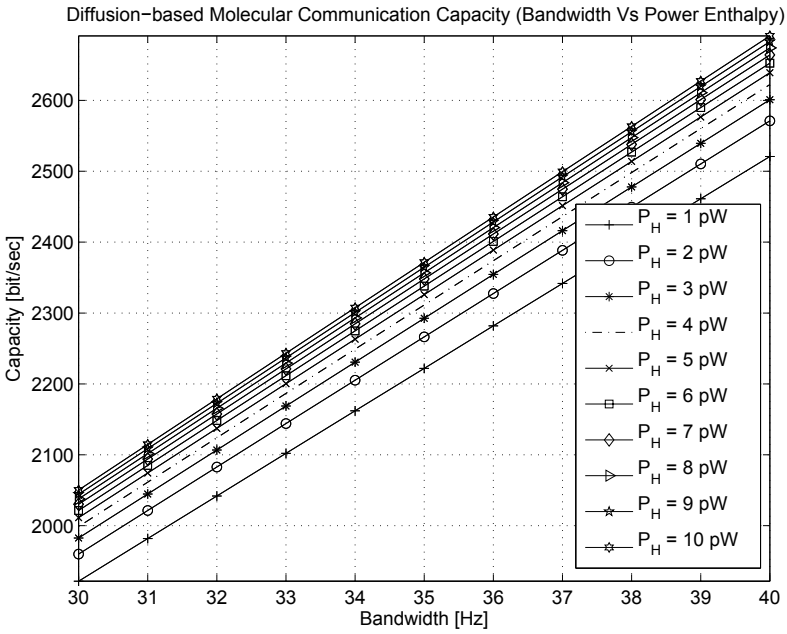

Figure 5.7: Capacity in relation to the bandwidth and for different values of the average transmitted power power $P_{\mathcal{H}}$.

power. Even if the average transmitted power is applied with constant increments of 1 pW from a value of 1 pW to 10 pW, the increment in the values of the capacity is not constant and it is higher for lower values of the average transmitted power. This behavior can be explained through the dependency of the molecular noise terms in the second, third and fourth lines of (5.85) with respect to the average transmitted power. As the average transmitted power increases, we have an increase in the first positive term in the first line of (5.85), but, at the same time, we have an increase in the aforementioned molecular noise terms.

5.4 Conclusions

In this section of the article, analytical expressions for the upper bound and lower bound to the information-theoretic capacity to the true

diffusion-based MC capacity are provided. The upper bound expression is obtained by applying solutions from statistical mechanics and equilibrium thermodynamics, and it is a function of the pressure, the volume, the temperature, the number of molecules, the bandwidth of the system, and the transmitter power. The expression of the lower bound is provided by taking into account the two main effects of the molecule diffusion channel, namely, the memory and the molecular noise. The obtained lower-bound expression of the capacity is a function of the medium diffusion coefficient, the system temperature, the distance between the transmitter and the receiver, the transmitter power, and the bandwidth of the transmitted signal.

According to the provided results, capacity values of a few [Kbit/sec] can be reached within a distance of tenth of μm between the transmitter and the receiver and for an average transmitted power around 1 pW (Note that this power value should not be compared to the transmitted power values used for electrical devices, since the transmitted power in an MC link is a thermodynamic quantity).

6

Interference of Multiple Molecular Communication Links in a Nanonetwork

6.1 Motivation and Related Work

The analysis of the interference produced at the reception of a transmitted signal, either by distortions of the signal itself or by other concurrent signals coming from different transmitters, is fundamental to design interference mitigation techniques and increase the performance of a communication systems. The focus of this chapter of the article is on the analysis of interference in diffusion-based Molecular Communication (MC)-enabled nanonetwork, where multiple transmitters access the fluid medium simultaneously and emit molecular signals directed to a single receiver.

Several different methods have been used in the engineering literature to measure the impact of the interference. In this chapter of the article, two main methods are used, namely, the InterSymbol Interference (ISI), the Co-Channel Interference (CCI). The ISI is here defined as the overlap between two consecutively received signals in molecule concentration, which were transmitted from a single molecular transmitter, while the CCI is considered here as the overlap between a received molecule concentration signal, which was transmitted by a single transmitter, and all the received molecule concentration signals

transmitted by the other concurrent transmitters. Both ISI and CCI depend greatly on the number and locations of the transmitters, how information is encoded in the signal modulation, and how the signals propagate through the channel from the moment they are transmitted until they combine at the receiver side. In most of the classical communication channels, this propagation is expressed through the so-called wave equation, while in diffusion-based MC it is expressed through the fundamentally different diffusion equation [76, 29].

Previous literature has addressed the problem of diffusion-based MC interference. In [58] the effects of the ISI and CCI are analyzed in reference to two specific modulation techniques proposed by the same authors. In [62] the ISI is characterized in a unicast MC link with binary amplitude modulation. In [12], interference is studied for another specific modulation technique, based on the transmission order of different types of molecules.

In the first part of this chapter, the ISI and the CCI are jointly analyzed for a diffusion-based MC nanonetwork having a limited number of transmitters in predetermined locations [81]. Moreover, the information transmitted in this system is encoded through the modulation of Gaussian pulses in the molecule emission rate. An in-depth analysis of the propagation of signals though a diffusion-based channel is performed by studying two main parameters, namely, the attenuation and the dispersion. For this, the diffusion equation is interpreted in terms of diffusion wave propagation, which allows to apply the wave theory to the realm of the diffusion-based MC, and to find mathematical expressions for the attenuation and the dispersion in a diffusion-based channel. From these, simple closed-form formulas for both the ISI and the CCI are derived. Two different modulation schemes, namely, the baseband modulation and the diffusion wave modulation, are considered for the release of molecules in the diffusion-based MC, and are compared in terms of interference. The obtained analytical results for both ISI and CCI are compared and validated by simulation results. This ultimately allows to assess the validity of the simple closed-form formulas for the evaluation of the interference in a diffusion-based MC system.

The objective of the second part of this chapter is to provide a statistical-physical modeling of the interference in diffusion-based MC. Our method to characterize interference differentiates from the previous literature on diffusion-based MC, since the developed statistical-physical model is independent from the transmitter number, specific transmitter locations or coding schemes. In particular, this model stems from the same general assumptions used in interference study for radio communication networks [53], namely, a spatial Poisson distribution of interfering transmitters having independent and identically distributed (i.i.d.) emissions. Moreover, the specific probability distribution used for the molecule emissions is in agreement with a chemical description of the transmitters in terms of Langevin equation [47], which models the randomness in the chemical reactions involved in the production of the molecules.

The statistical-physical modeling detailed the second part of this chapter is based on the property of the received molecular signal of being a stationary Gaussian Process (GP), which results from the molecule emission distribution and the diffusion-based molecule propagation. As a consequence, the statistical-physical modeling is operated on the received Power Spectral Density (PSD), for which it is possible to obtain an analytical expression of the log-characteristic function. The derivation of this log-characteristic function is inspired by the mathematical framework in [51], where the authors derive the log-characteristic function of the received signal in radio communication interference. The expression of the received PSD log-characteristic function ultimately leads to the estimation of the received PSD probability distribution. The received PSD probability distribution provides a complete description of the GP of the received molecular signal, which corresponds to the interference in diffusion-based molecular nanonetworks. By using the derived statistical-physical interference model, we also provide numerical results in terms of received PSD probability distribution and probability of interference for selected values of the physical parameters of the molecular nanonetwork, such as the diffusion coefficient, the transmitter density and the average power of molecule emissions, and we compare them with the outcomes of a simulation

environment.

6.2 Intersymbol Interference and Co-Channel Interference

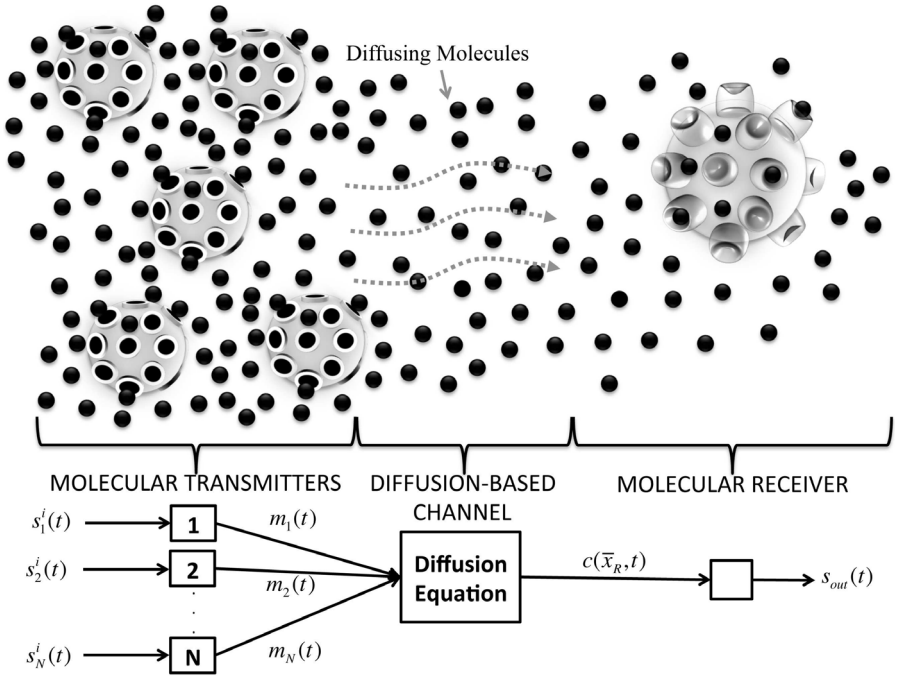

Figure 6.1: Block scheme of the diffusion-based MC nanonetwork considered in this section of the article.

The MC nanonetwork model considered in this section of the article, and shown in Figure 6.1, includes N **MOLECULAR TRANSMITTERS**. Each transmitter, denoted by n and located at $\bar{x}_n$, is responsible for the modulation of the number of molecules $m_n(t)$ emitted into the space as a function of the time t according to input information signals, denoted as $s_n^i(t)$, where $i = 1, 2, ...$ is a sequential index. We assume the emitted molecules are identical and undistinguishable between each other. Two different modulation schemes that can be adopted by the molecular transmitters are studied and compared in this section of the article from the point of view of interference, namely,

the *baseband modulation* and the *diffusion wave modulation*. For both modulation schemes, the transmitters produce a number of molecules $m_n(t)$ emitted at location $\bar{x}_n$ and time t corresponding to the amplitude modulation of an oscillation with angular frequency ω_0, expressed as

$$m_n(t) = \sum_{i=0}^{\infty} s_n^i(t) e^{j\omega_0 t} \ , \tag{6.1}$$

where $\omega_0 = 0$ in the baseband scheme and $\omega_0 > 0$ in the diffusion wave scheme.

The MC nanonetwork model includes a **DIFFUSION-BASED CHANNEL** which is based on the free diffusion of molecules between the transmitter and the receiver. Each molecular transmitter n emits a number of molecules $m_n(t)$ in this space at location $\bar{x}_n$ and time t. For this, the total number of emitted molecules $m(\bar{x}, t)$, which is the input of the molecular channel, is expressed as

$$m(\bar{x}, t) = \sum_{n=1}^{N} m_n(t) \delta(\bar{x} - \bar{x}_n) \ , \tag{6.2}$$

where $\delta(\bar{x} - \bar{x}_n)$ is a Dirac delta defined in the three dimensional space and centered at the corresponding transmitter location $\bar{x}_n$. Once emitted, every molecule moves independently from the others and according to its Brownian motion in a fluidic medium. The output of the molecular channel is the molecule concentration $c(\bar{x}, t)$ as function of the space location $\bar{x}$ and the time t, whose relation with the input $m(\bar{x}, t)$ is expressed by the **diffusion equation** [76, 29], as

$$\frac{\partial c(\bar{x}, t)}{\partial t} = D \nabla^2 c(\bar{x}, t) + m(\bar{x}, t) \ , \tag{6.3}$$

where D is the diffusion coefficient and it is considered a constant parameter within the scope of this section of the article.

The *linearity* of (6.3) gives the following results:

- Given a modulated number of emitted molecules $m_n(t)$ from a single transmitter n, the output molecule concentration $c(\bar{x}, t)$ at any location $\bar{x}$ and time t is computed through the convolution integral with the Green's function [64] $g(\bar{x}, t)$ (*linear channel*), expressed as follows:

$$c(\bar{x},t) = m(\bar{x},t) * g(\bar{x},t) = \int_0^\infty m_n(t) g(\bar{x}_n - \bar{x}, t' - t) dt' \ , \qquad (6.4)$$

where $(.*.)$ denotes the convolution integral between the two arguments. The Green's function [64] is the solution of the diffusion equation (6.3) when the input $m(\bar{x},t)$ is a Dirac delta and it is expressed as follows:

$$g(\bar{x},t) = \frac{1}{\sqrt{(4\pi D t)^3}} e^{-\frac{|\bar{x}|^2}{4Dt}} \ . \qquad (6.5)$$

- Given the modulated number of molecules $m_n(t)$ emitted simultaneously from multiple transmitters, where $n = 1, ..., N$, the output molecule concentration is the sum of the outputs of the diffusion-based channel applied independently to each single molecule concentration rate input (*additive channel*), expressed as

$$c(\bar{x},t) = \sum_{n=1}^{N} \left(m_n(t) \delta(\bar{x} - \bar{x}_n) * g(\bar{x},t) \right) \ . \qquad (6.6)$$

The MC nanonetwork model includes a single **MOLECULAR RECEIVER**, whose task is to read the incoming molecular concentration $c(\bar{x}_R,t)$ at its location $\bar{x}_R$ and to demodulate the output information signal $s_{out}(t)$. For this, the molecular receiver produces an output information signal $s_{out}(t)$ equal to the real part of the molecule concentration signal $c(\bar{x}_R,t)$ at the receiver location $\bar{x}_R$, multiplied by an oscillation with angular frequency $-\omega_0$, expressed as

$$s_{out}(t) = \Re \left\{ c(\bar{x}_R,t) e^{-j\omega_0 t} \right\} \ , \qquad (6.7)$$

where $\omega_0 = 0$ or $\omega_0 > 0$ in case the transmitter adopted the baseband or the diffusion wave modulation scheme, respectively. $\Re\{.\}$ denotes the operator which extracts the real part from the complex operand.

6.2.1 Interference Formulas

The ISI is quantified as the time integral of the product of two output information signals which derive from two input information signals sent from a transmitter n, expressed as follows:

$$ISI = \int_{-\infty}^{\infty} s^i_{n,\text{out}}(t) s^{i+1}_{n,\text{out}}(t) dt \ , \qquad (6.8)$$

where $s^i_{n,\text{out}}(t)$ is the output information signal of the MC nanonetwork when the input information signal $s^i_n(t)$ is sent by the transmitter n.

The CCI is quantified as the time integral of the product of an output information signal which is sent in a modulated number of emitted molecules by a transmitter n with all the other received output information signals which are sent as modulated number of molecules by all the other $N-1$ transmitters, expressed as follows:

$$CCI = \int_{-\infty}^{\infty} s^i_{n,\text{out}}(t) \sum_{k=1}^{N,\, k\neq n} \sum_{l=0}^{\infty} s^l_{k,\text{out}}(t)dt \ . \tag{6.9}$$

In case of *baseband modulation* scheme, the output information signal $s^i_{n,\text{out}}(t)$, which derives from the input information signal $s^i_n(t)$ sent by the transmitter n, has the following expression:

$$s^i_{n,\text{out}}(t) = s^i_n(t) * g(\bar{x}, t) \ , \tag{6.10}$$

where $(.*.)$ denotes the convolution integral between the two arguments and $g(\bar{x}, t)$ has the expression from (6.5). In case of *diffusion wave modulation* scheme the same output information signal $s^i_{n,\text{out}}(t)$ has the following expression:

$$s^i_{n,\text{out}}(t) = \Re\left\{\left[\left(s^i_n(t)e^{j\omega_0 t}\right) * g(\bar{x}, t)\right] e^{-j\omega_0 t}\right\} \ . \tag{6.11}$$

In order to evaluate the ISI through (6.8) and the CCI through (6.9), it is necessary to analyze how the shape of an information signal changes from its transmission as $s^i_n(t)$ until its reception as $s^i_{n,\text{out}}(t)$. For this, we decompose an input information signal into its frequency components $S^i_n(\omega)$ by applying the Fourier transform [30], expressed as

$$s^i_n(t) = \int_0^{\infty} S^i_n(\omega)e^{j\omega t}d\omega \ . \tag{6.12}$$

Each frequency component $S^i_n(\omega)e^{j\omega t}$, as it propagates in the diffusion-based channel defined by (6.3), is in general attenuated and it has a finite propagation velocity. As will be proved in the following section, this attenuation and velocity are functions of the angular frequency ω of the frequency component $S^i_n(\omega)$ itself. As a consequence, the output information signal $s^i_{n,\text{out}}(t)$ will be composed by the same frequency

components as the transmitted input information signal, each one attenuated by a different value and propagated with a different velocity. These two effects, identified as the **attenuation** and the **dispersion** of a signal, are at the basis of the changes in the information signal shape as it propagates through the diffusion-based channel. For this, in the following section we analyze these two parameters by using the wave theory [63].

6.2.2 Attenuation and Dispersion of Diffusion-Waves

This section deals with the analysis of the attenuation and the dispersion which affect any modulated total number of emitted molecules $m(\bar{x}, t)$ in the diffusion-based channel defined at the beginning of Section 6.2 as it propagates from the transmitter to the receiver. For this, as suggested in [63, 64], we apply the wave theory to the diffusion equation from (6.3).

According to the wave theory, given an oscillatory input $q(t)$ with angular frequency ω of the following type:

$$q(\bar{x}, t) = Q(\bar{x}, \omega)e^{j\omega t} \ , \tag{6.13}$$

the propagation of a wave defined by the following expression:

$$u(\bar{x}, t) = U(\bar{x}, \omega)e^{j\omega t} \ , \tag{6.14}$$

stems from a differential equation that can be defined in the space $\bar{x}$ and angular frequency ω as follows:

$$\nabla^2 U(\bar{x}, \omega) - k^2(\omega)U(\bar{x}, \omega) = Q(\bar{x}, t) \ , \tag{6.15}$$

where $Q(\bar{x}, t)$ and $U(\bar{x}, \omega)$ are the input and the output respectively, as function of the space $\bar{x}$ and the input angular frequency ω. $k(\omega)$ is the wavenumber, which is in general a function of ω. We have the following definitions based on $k(\omega)$:

- The attenuation of a wave $\alpha(\omega)$ is the imaginary part of the wavenumber $k(\omega)$, expressed as

  $$\alpha(\omega) = \Im\{k(\omega)\} \ , \tag{6.16}$$

  where $\Im\{.\}$ denotes the operator which extracts the imaginary part from the complex operand.

- The phase velocity v_p is equal to the angular frequency ω divided by the real part of the wavenumber $k(\omega)$ and it is defined as the propagation velocity of a point of constant phase (wavefront velocity), expressed as

$$v_p = \frac{\omega}{\Re\{k(\omega)\}} \ . \tag{6.17}$$

- The group velocity v_g is the time first derivative of the angular frequency ω with respect to the real part of the wavenumber $k(\omega)$ and it is defined as the propagation velocity of a group of waves having a narrow frequency range around ω (wave-packet velocity), expressed as

$$v_g = \frac{\partial\omega}{\partial\Re\{k(\omega)\}} \ . \tag{6.18}$$

The wave propagation expressed through (6.15) is subject to dispersion if the expressions of the phase velocity (6.17) and the group velocity (6.18) are different. The resulting propagating wave from (6.14) can be written as function of the oscillatory input $q(\bar{x},t)$, the attenuation $\alpha(\omega)$ and the phase velocity v_p as follows:

$$u(\bar{x},t) = q(\bar{x},t)e^{-\alpha(\omega)|\bar{x}|}e^{j\frac{\omega}{v_p}|\bar{x}|} \ . \tag{6.19}$$

By taking the Fourier transform [30] of the diffusion equation from (6.3) and by rearranging the terms we obtain an expression of the same type as (6.15) defined in the space $\bar{x}$ and angular frequency ω, expressed as

$$\nabla^2 C(\bar{x},\omega) - \frac{j\omega}{D}C(\bar{x},\omega) = M(\bar{x},\omega) \ , \tag{6.20}$$

where $M(\bar{x},\omega)$ and $C(\bar{x},\omega)$ are the Fourier transforms [30] of the modulated total number of emitted molecules $m(\bar{x},t)$ and the output molecule concentration signal $c(\bar{x},t)$, respectively. The similarity with the wave equation in (6.15) suggests an interpretation of the diffusion equation in terms of waves, thus identifying the so-called diffusion waves [63]. Although the diffusion waves have different properties [64]

if compared to the waves generated by the wave equation, also for the diffusion waves we can identify a wavenumber $k(\omega)$, this time equal to

$$k(\omega) = \sqrt{\frac{j\omega}{D}} = (1+j)\sqrt{\frac{\omega}{2D}} \, . \tag{6.21}$$

As a consequence, the attenuation of a diffusion wave $\alpha(\omega)$ is given by (6.16)

$$\alpha(\omega) = \sqrt{\frac{\omega}{2D}} \, . \tag{6.22}$$

The phase velocity v_p is given by applying (6.21) to (6.17)

$$v_p = \sqrt{2D\omega} \, , \tag{6.23}$$

and the group velocity v_g is computed through (6.21) and (6.18), expressed as

$$v_g = 2\sqrt{2D\omega} \, . \tag{6.24}$$

Since the phase velocity in (6.23) and the group velocity in (6.24) are different, the wave propagation in the diffusion-based channel is affected by dispersion. This is a consequence of the frequency dependency of the phase velocity and the group velocity of the diffusion waves.

The resulting propagating diffusion wave can be written as function of an oscillatory total number of emitted molecules $M(\bar{x}, \omega)e^{j\omega t}$, the attenuation $\alpha(\omega)$ and the phase velocity v_p as follows:

$$c(\bar{x}, t) = M(\bar{x}, \omega)e^{j\omega t}e^{-\sqrt{\frac{\omega}{2D}}|\bar{x}|}e^{j\sqrt{\frac{\omega}{2D}}|\bar{x}|} \, . \tag{6.25}$$

6.2.3 Interference Analysis

In this section, the i-th input information signal $s_n^i(t)$ for the transmitter n is modeled as a Gaussian-shaped pulse with standard deviation σ, which is a user-defined parameter, and it is expressed as follows:

$$s_n^i(t) = \frac{1}{\sqrt{2\pi\sigma^2}} e^{-\frac{(t-t_n-i\Delta t)^2}{2\sigma^2}} \, , \tag{6.26}$$

where $t_n + i\Delta t$ is the time instant at which the receiver n transmits the maximum of the i-th pulse. Equation (6.26) allows to simplify the following interference analysis and to find closed-form expressions for

the interference. Although these expressions depend on (6.26), this does not prevent from considering the general conclusions of this section of the article valid for any other input signal shape.

We describe the changes in the shape of the pulse sent by the transmitter n from its transmission as $s_n^i(t)$ until its reception as $s_{n,\text{out}}^i(t)$ by using two parameters, namely, the amplitude A_n at the peak maximum and the broadening factor B_n, expressed as

$$s_{n,\text{out}}^i(t) = A_n s_n^i\left(\frac{t-t_d}{B_n}\right) = A_n \frac{1}{\sqrt{2\pi\sigma^2}} e^{-\frac{(t-t_n-i\Delta t-t_d)^2}{2(B_n\sigma)^2}}, \qquad (6.27)$$

where t_d is the pulse propagation delay and its value is not relevant for the following interference analysis since we account only for the time of pulse reception. The relation in (6.27) is a first approximation of the changes in the pulse shape and it allows a simplification of the expressions of the ISI and the CCI in (6.8) and (6.9), respectively. In light of (6.27) the ISI becomes

$$ISI \simeq 2A_n^2 erfc\left(\frac{\Delta t/2}{\sqrt{2}B_n\sigma}\right)\left[1 - erfc\left(\frac{\Delta t/2}{\sqrt{2}B_n\sigma}\right)\right]. \qquad (6.28)$$

Similarly, the CCI becomes

$$CCI \simeq \sum_{k=1}^{N,k\neq n} 2A_n A_k erfc\left(\frac{|t_n-t_k|/2}{\sqrt{2}B_n\sigma}\right)\left[1 - erfc\left(\frac{|t_n-t_k|/2}{\sqrt{2}B_k\sigma}\right)\right], \qquad (6.29)$$

where t_n and t_k are the time instants of transmission of the pulses and B_n and B_k are the broadening factors for the pulses transmitted by the transmitter n and the transmitter k, respectively. $erfc(x/\sqrt{2}B_n\sigma)$ denotes the complementary error function, which corresponds to the integral of the Gaussian pulse dilated by a factor B_n between x and ∞.

By stemming from the formulas discussed in Section 6.2.1 concerning the attenuation and the dispersion of the diffusion waves, we can derive closed-form formulas for the amplitude A_n at the peak maximum and the broadening factor B_n:

- The pulse *amplitude A_n at the peak maximum* after propagation from the transmitter n located at $\bar{x}_n$ to the receiver located at

$\bar{x}_R$ is given by the double of the integral of the attenuation contribution $e^{-\sqrt{\frac{\omega}{2D}}|\bar{x}_R-\bar{x}_n|}$ of each frequency component $M(\bar{x}_n,\omega)$ of the transmitted signal, expressed as

$$A_n = 2\int_0^\infty M(\bar{x}_n,\omega)e^{-\sqrt{\frac{\omega}{2D}}|\bar{x}_R-\bar{x}_n|}d\omega \ , \tag{6.30}$$

where $M(\bar{x}_n,\omega)$ is the Fourier transform [30] of the total number of emitted molecules $m(\bar{x}_n,t)$ when only a single pulse is transmitted from (6.7), having $\omega_0 = 0$ in the case of baseband scheme and $\omega_0 > 0$ in the case of diffusion wave modulation.

- The pulse *broadening* factor B_n is computed as the squared root of the sum of 1 with the squared integral of the delay contribution $\frac{\partial}{\partial\omega}\left(\frac{1}{v_g}\right)|\bar{x}_R-\bar{x}_n|$ of each frequency component $M(\bar{x}_n,\omega)$ of the total number of emitted molecules, expressed as

$$B_n = \sqrt{1+\left(\int_0^\infty \frac{\partial}{\partial\omega}\left(\frac{1}{v_g}\right)|\bar{x}_R-\bar{x}_n|M(\bar{x}_n,\omega)d\omega\right)^2} \ , \tag{6.31}$$

where v_g is the group velocity expressed in (6.24). The first derivative of the inverse of the group velocity $1/v_g$ with respect to the angular frequency ω has the following expression:

$$\frac{\partial}{\partial\omega}\left(\frac{1}{v_g}\right) = \sqrt{\frac{1}{2D\omega^3}} \ . \tag{6.32}$$

In order to compare the ISI and CCI results for the two modulation schemes, we simplify further (6.30) and (6.31) by approximation. For the **baseband modulation** scheme, the amplitude A_n^{base} at the peak maximum becomes

$$A_n^{base} = \frac{2}{\sigma^2}e^{-\sqrt{\frac{\omega_c}{2D}}|\bar{x}_R-\bar{x}_n|} \ , \tag{6.33}$$

where ω_c is the cut-off frequency of the Gaussian pulse (6.26). The cut-off frequency is the angular frequency of the pulse spectrum component whose amplitude value is half the amplitude of the maximum. The pulse broadening factor B_n^{base} for the baseband modulation scheme can be

approximated with

$$B_n^{base} = \sqrt{1 + \left(\frac{1}{\sigma^2} \sqrt{\frac{1}{2D\omega_c^3}} |\bar{x}_R - \bar{x}_n| \right)^2} \,. \tag{6.34}$$

In case of **diffusion wave modulation** scheme, the amplitude A_n^{wave} at the peak maximum becomes

$$A_n^{wave} = \frac{2}{\sigma^2} e^{-\sqrt{\frac{\omega_0}{2D}} |\bar{x}_R - \bar{x}_n|} \,, \tag{6.35}$$

where ω_0 is the frequency of the modulating oscillation, as expressed in (6.1). The pulse broadening factor B_n^{wave} for the diffusion wave modulation scheme can be approximated with

$$B_n^{wave} = \sqrt{1 + \left(\frac{1}{\sigma^2} \sqrt{\frac{1}{2D\omega_0^3}} |\bar{x}_R - \bar{x}_n| \right)^2} \,, \tag{6.36}$$

where for both (6.35) and (6.36) we assumed to have a frequency ω_0 much higher than the the cut-off frequency ω_c of the Gaussian pulse (6.26).

The amplitude at the peak maximum for the baseband modulation scheme A_n^{base} and for the diffusion wave modulation scheme A_n^{wave}, if compared, guide to the following result:

$$A_n^{base} > A_n^{wave} \;\; \forall \omega_0 > \omega_c \,. \tag{6.37}$$

When comparing the pulse broadening in case of baseband modulation scheme B_n^{base} and in case of diffusion wave modulation scheme B_n^{wave}, we can conclude the following result:

$$B_n^{base} > B_n^{wave} \;\; \forall \omega_0 > \omega_c \,. \tag{6.38}$$

As a conclusion, for a diffusion-based channel model as defined by (6.3), the intersymbol interference $ISI_{\bar{x}_R}^{wave}$ in the case of diffusion wave modulation scheme is lower with respect to the intersymbol interference $ISI_{\bar{x}_R}^{base}$ in the case of baseband modulation scheme, expressed as

$$ISI_{wave} < ISI_{base} \;\; \forall \omega_0 > \omega_c \,. \tag{6.39}$$

In addition, we deduce that the higher is the wave modulation frequency ω_0, the lower is the value of the intersymbol interference ISI_{wave}, expressed as

$$ISI_{wave}|_{\omega_0=\omega_1} < ISI_{wave}|_{\omega_0=\omega_2} \ \ \forall \omega_1 > \omega_2 \ . \tag{6.40}$$

Similarly, we compare the co-channel interference for the two modulation schemes applied to systems having the same values for the locations $\bar{x}_n$ and the time instants t_n, which correspond to the maximum of the transmitted Gaussian pulses for all the N transmitters. We deduce also for the CCI the following result:

$$CCI_{wave} < CCI_{base} \ \ \forall \omega_0 > \omega_c \ , \tag{6.41}$$

and

$$CCI_{wave}|_{\omega_0=\omega_1} < CCI_{wave}|_{\omega_0=\omega_2} \ \ \forall \omega_1 > \omega_2 \ . \tag{6.42}$$

6.2.4 Numerical Results

In this section we simulate the system detailed at the beginning of Section 6.2 and we compare the results in terms of ISI and CCI with the simple formulas resulting from the interference analysis of Section 6.2.3, which stems from the diffusion-wave attenuation and dispersion studied in Section 6.2.2. The goal of this comparison is to prove that the simple formulas for the ISI (6.28) and for the CCI (6.29) constitute a valid approximation for the evaluation of the interference in a diffusion-based MC nanonetwork.

The simulations are based on (6.1), (6.4) and (6.7), $\omega_0 = 0$ in the baseband scheme and $\omega_0 > 0$ in the diffusion wave scheme. The diffusion coefficient D in (6.5) is set to $\sim 10^{-6} cm^2 sec^{-1}$ of calcium molecules diffusing in a biological environment (cellular cytoplasm, [31]) and the distance $\bar{x} - \bar{x}_n$ is varied from 0 to $70\mu m$.

For the evaluation of the ISI, the simulations are performed by sending two Gaussian pulses of the type in (6.26) where σ is set to $0.32sec$, Δt is set to $0.96sec$ and $i = 1, 2$. The parameter t_n is set to $4.14sec$ from the starting time of the simulation. The resulting amplitude of the received pulses as function of the time t ranging from 0 to $10sec$ and the distance $\bar{x} - \bar{x}_n$ ranging from 0 to $70\mu m$ are shown in

Figure 6.2 (upper), (left) for the baseband modulation and (right) for the diffusion wave modulation. The ISI is evaluated by applying (6.8) with the computed values of $s^1_{n,\mathrm{out}}(t)$ and $s^2_{n,\mathrm{out}}(t)$.

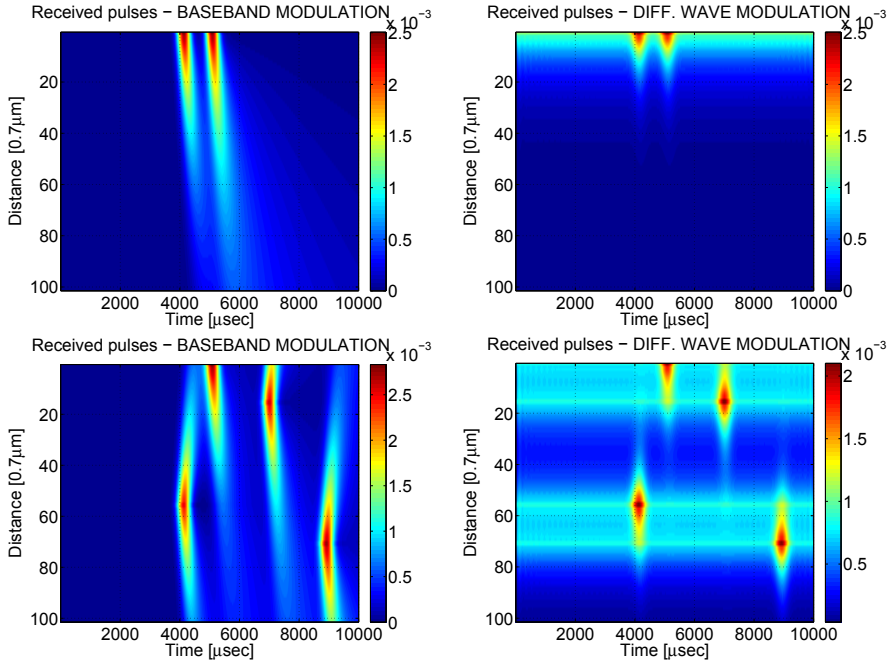
Received pulses − BASEBAND MODULATION
Received pulses − DIFF. WAVE MODULATION
Received pulses − BASEBAND MODULATION
Received pulses − DIFF. WAVE MODULATION
Distance [0.7µm]
Time [µsec]
x 10^-3

Figure 6.2: The received pulses as function of the time and the distance in the case of baseband modulation (left) and diffusion wave modulation (right) for the simulation-based for the simulation-based ISI evaluation (upper) and CCI evaluation (lower).

In Figure 6.3 (upper-right) and Figure 6.3 (lower-right) we show the results of the numerical evaluation of the formula (6.28) for the baseband modulation and the diffusion wave modulation, respectively. In case of baseband modulation, we apply (6.33) and (6.34), while for the diffusion wave modulation we used (6.35) and (6.36). The comparison of the ISI simulation results shown in Figure 6.3 (upper-left) and Figure 6.3 (lower-left) with the results of the simple formulas in Figure 6.3 (upper-right) and Figure 6.3 (lower-right) reveals strong similarities between the results of (6.8) and (6.28) in the case of baseband modulation and diffusion wave modulation and confirms the validity of

the simple formulas for the ISI developed in Section 6.2.3. Moreover, both the results in terms of ISI in the simulation and in the numerical evaluation confirm the relation in (6.39).

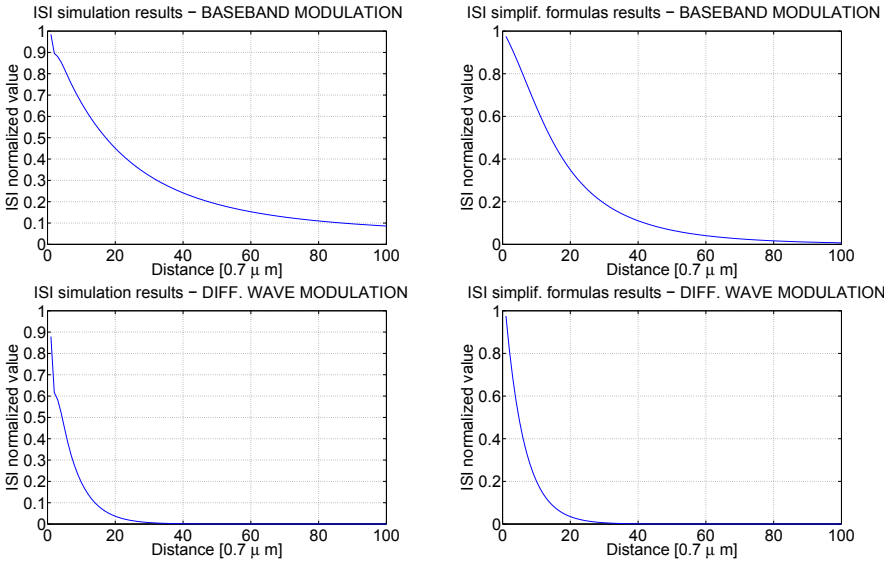
ISI simulation results − BASEBAND MODULATION
ISI simplif. formulas results − BASEBAND MODULATION
ISI simulation results − DIFF. WAVE MODULATION
ISI simplif. formulas results − DIFF. WAVE MODULATION
ISI normalized value
Distance [0.7 μ m]

Figure 6.3: The ISI values for the baseband modulation scheme (upper) and the diffusion wave modulation scheme (lower) from the simulation (left) and from the simple formulas (right).

For the evaluation of the CCI, the simulations are performed by sending a Gaussian pulse of the type in (6.26) from each one of $N = 4$ transmitters placed at distances from the second transmitter $\|\bar{x}_n - \bar{x}_2\|$ equal to $39.2\mu m$, $0\mu m$, $11.2\mu m$ and $49.7\mu m$ respectively. In (6.26) σ is set to $0.32sec$ and the index i is set to 0. We set $t_1 = 4.14sec$, $t_2 = 5.09sec$, $t_3 = 7sec$ and $t_4 = 8.9sec$. The resulting amplitude of the received pulses $s^i_{n,\text{out}}(t)$ as function of the time t ranging from 0 to $10sec$ and the distance $\bar{x}_R - \bar{x}_2$ ranging from 0 to $70\mu m$ are shown in Figure 6.2 (lower-left) and Figure 6.2 (lower-right) for the baseband modulation and the diffusion wave modulation, respectively. The CCI is evaluated through (6.9) with the values of $s^i_{n,\text{out}}(t)$.

In Figure 6.4 (upper-right) and Figure 6.4 (lower-right) we show the results of the numerical evaluation of the formula (6.29) for the

baseband modulation and the diffusion wave modulation, respectively. In case of baseband modulation, we apply (6.33) and (6.34), while for the diffusion wave modulation we used (6.35) and (6.36). The comparison of the CCI simulation results shown in Figure 6.4 (upper-left) with results of the simple formulas in Figure 6.4 (upper-right) clearly show the limit of the simple formulas to properly capture the real CCI curve as function of the distance. This is explained by the fact that the shape of the received pulse in case of baseband modulation is subject to a high value of dispersion and it is distorted with respect to the Gaussian shape assumed for the simple formula (6.29). This phenomenon is more clearly visible for the CCI computation (6.9) since its value is the result of the contributions of more than two received pulses, as in the case of the ISI (6.8). On the contrary, the results in Figure 6.4 (lower) guide to the same conclusion as mentioned above for the ISI and confirm the validity of the simple formulas for the CCI developed in Section 6.2.3. Moreover, the result from (6.41) is supported by both Figure 6.4 (upper) and Figure 6.4 (lower).

6.3 Statistical-physical Model of Interference

6.3.1 Reference Models, Assumptions, and Definitions

In this section, we describe the main reference models, assumptions, and definitions used in this paper for the statistical-physical modeling of the interference in molecular nanonetworks.

Reference Molecular Nanonetwork

In the following, we detail the main elements of the reference molecular nanonetwork considered in this paper. As sketched in Fig. 6.5, these elements are the molecular transmitters, responsible for the emission of molecular signals, the diffusion-based propagation, which broadcasts the molecular signals in the space by means of free molecule diffusion, and the molecular receiver, which senses the incoming molecular signals.

A **Molecular Transmitter**, identified by a number i and located at $\bar{x}_k$, is responsible for the emission of molecules in the space accord-

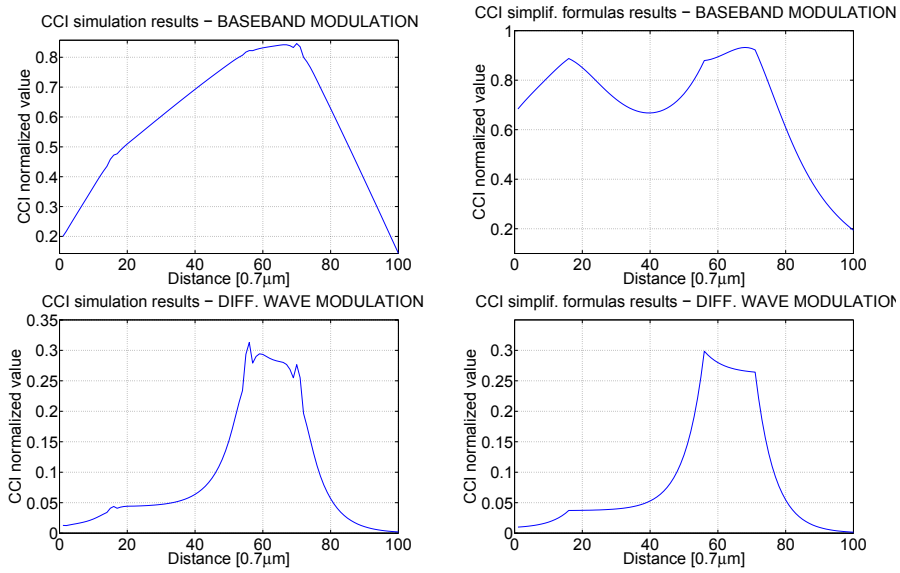
CCI simulation results − BASEBAND MODULATION
CCI simplif. formulas results − BASEBAND MODULATION
CCI simulation results − DIFF. WAVE MODULATION
CCI simplif. formulas results − DIFF. WAVE MODULATION
CCI normalized value
Distance [0.7μm]

Figure 6.4: The CCI values for the the baseband modulation scheme (upper) and the diffusion wave modulation scheme (lower) from the simulation (left) and from the simple formulas (right).

ing to a molecular signal $s_k(t)$ as function of the time t. We assume that all the transmitters emit molecules of the same species n within an equal definite volume V_T, whose size is negligible with respect to the distance between each transmitter and the receiver. Upon this emission of molecules, identified with the time derivative $dX_n(t)/dt$ in the number X_n of molecules of species n inside the volume V_T at the transmitter i, each molecular transmitter i causes a change in the molecule concentration $c(\bar{x}, t)$ at its location $\bar{x}_k$, which is expressed through the following relation:

$$\frac{\partial c(\bar{x}, t)}{\partial t} = \frac{1}{V_T} \frac{dX_n(t)}{dt} \delta(\bar{x} - \bar{x}_k) = s_k(t) \delta(\bar{x} - \bar{x}_k) \, , \tag{6.43}$$

where $\partial c(\bar{x}_k, t)/\partial t$ is the time derivative in the molecule concentration at the location $\bar{x}_k$ and time t, and $\delta(.)$ is the Dirac delta. Moreover, we assume that a transmitter is able to produce molecules, thus resulting in a positive time first derivative $dX_n(t)/dt > 0$ and a positive transmitted signal $s_k(t) > 0$, or to subtract molecules, thus resulting in a negative

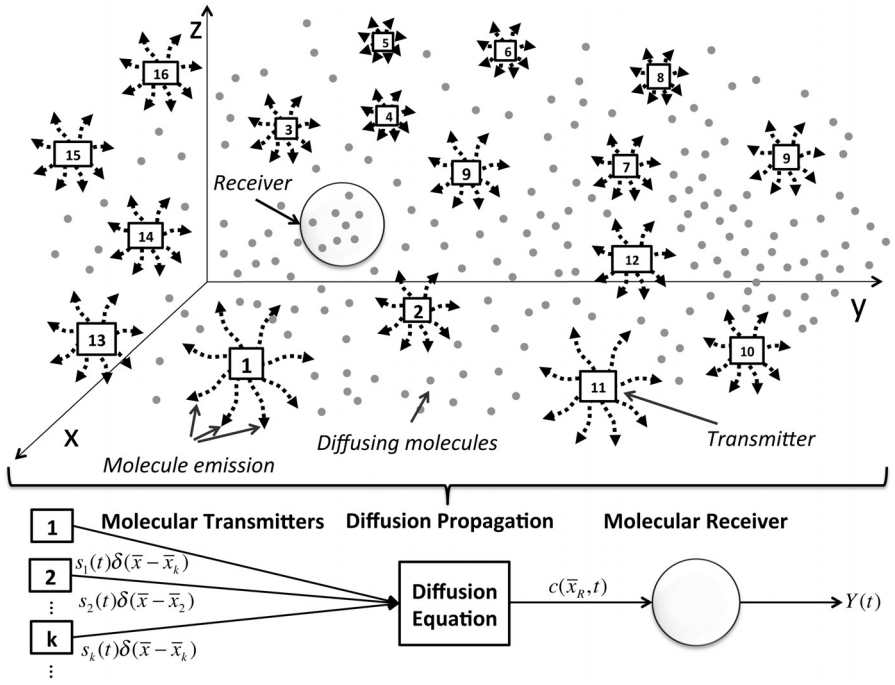

Figure 6.5: Reference diffusion-based molecular nanonetwork considered for the interference modeling.

time first derivative $dX_n(t)/dt < 0$ and in a negative transmitted signal $s_k(t) < 0$.

The **Diffusion Propagation** broadcasts the emitted molecular signal $s_k(t)$ from each transmitter location $\bar{x}_k$ to any other location $\bar{x}$ in the space. In this paper, we rely on the assumption to have a 3-dimensional space, which contains a fluidic medium and has infinite extent in all the three dimensions. Moreover, the molecules of species n are all identical and undistinguishable, and they move independently from each other according to the Brownian motion. We define the total molecule concentration in the space as $c_{base} + c(\bar{x}, t)$, where c_{base} is a component of the molecule concentration that is homogeneous in the space and constant in time, while $c(\bar{x}, t)$ is the varying component of the molecule concentration as a function of the space $\bar{x}$ and time t. We assume that the component c_{base} has a value sufficient to keep

the total molecule concentration positive throughout the space even when $c(\bar{x},t) < 0$ due to transmitters subtracting molecules from the space, $s_k(t) < 0$. The diffusion propagation is based on the following **Diffusion Equation** [76, 29] in the variable $c(\bar{x},t)$:

$$\frac{\partial c(\bar{x},t)}{\partial t} = D\nabla^2 c(\bar{x},t) \ , \tag{6.44}$$

where $\partial(.)/\partial t$ and $\nabla^2(.)$ are the time first derivative and the Laplacian operator (sum of the 3-dimensional spatial second derivatives), respectively. D is the diffusion coefficient and it is considered a constant parameter within the scope of this paper. This is in agreement with the assumption of having independent Brownian motion for every molecule in the space.

The **Molecular Receiver** senses the total incoming molecular concentration $c_{base} + c(\bar{x}_R,t)$ at its location $\bar{x}_R$ and recovers the received signal $Y(t)$ from the varying component $c(\bar{x}_R,t)$. This is expressed by the following relation:

$$Y(t) = c(\bar{x}_R,t) \ . \tag{6.45}$$

As a consequence, when no transmitter is emitting molecular signals (creating or subtracting molecules), the total molecule concentration is constant and equal to c_{base}, and the received signal $Y(t)$ is equal to zero.

Assumptions on Interferers

For our interference study, we consider multiple molecular transmitters (interferers), each one emitting a molecular signal from a different location. We apply the following assumptions:

- The molecular transmitters are assumed to be infinite in number and distributed in the 3-dimensional space according to a spatial homogeneous Poisson process whose rate is equal to the transmitter density λ, which corresponds to the average number of transmitters per unit volume. For this, the probability to find a number k of transmitters in a region V of the space is expressed as follows:

$$P(k \text{ transmitters in } V) = \frac{[\lambda V]^k e^{-\lambda V}}{k!} \ . \tag{6.46}$$

- The molecular transmitters emit independent and identically distributed (i.i.d.) molecular signals $s_k(t)$. Each $s_k(t)$ is a white Gaussian signal [74], whose values at each time instant t have zero mean and variance equal to σ^2, expressed as

$$s_k(t) \sim \mathcal{N}(0, \sigma^2) \ \forall t \,. \tag{6.47}$$

  The expression in (6.47) models the variability of the transmitter emissions according to the variance parameter σ^2, which corresponds to the average power of the molecular signals emitted by the transmitters.

The white Gaussian model for the molecular signals $s_k(t)$ expressed in (6.47) is in agreement with a chemical description of the molecule emission at the molecular transmitters. Without loss of generality, we assume that the total molecule concentration $c_{base} + c(\bar{x}_k, t)$ at each transmitter i is a function of M different chemical reactions involving N different chemical species (molecule types) within the transmitter definite volume V_T. According to the chemical Langevin equation approximation [47], the time derivative $dX_n(t)/dt$ from (6.43) in the number X_n of species-n molecules, and function of the time t, is given by the following expression:

$$\frac{dX_n(t)}{dt} = \sum_{m=1}^{M} \nu_{mn} a_m(\mathbf{X}(t)) + \sum_{m=1}^{M} \nu_{mn} \sqrt{a_m(\mathbf{X}(t))} \Gamma_m(t) \tag{6.48}$$

where $\mathbf{X}(t) = [X_1(t), X_2(t), \ldots, X_N(t)]'$ is a vector that contains the number of molecules of each reacting species, ν_{mn} corresponds to the change in the number of molecules of the chemical species n produced by the chemical reaction m, $a_m(\mathbf{X}(t))$, which is called *propensity function*, is the probability that the chemical reaction m will occur within the transmitter volume as function of the vector $\mathbf{X}(t)$, and $\Gamma_m(t)$ are i.i.d. white Gaussian signals. Under the assumption to have the chemical reactions at equilibrium within every transmitter volume, which is expressed as $\sum_{m=1}^{M} \nu_{mn} a_m(\mathbf{X}(t)) = 0$, and given (6.48), the molecular signal $s_k(t)$ in (6.43) is equal to a sum of i.i.d. white Gaussian signals as follows:

$$s_k(t) = \frac{1}{V_T} \sum_{m=1}^{M} \nu_{mn} \sqrt{a_m(\mathbf{X}(t))} \Gamma_m(t) \,. \tag{6.49}$$

As a consequence of the property of a linear combination of i.i.d. Gaussian random variables [74], $s_k(t)$, as expressed in (6.47), is a white Gaussian signal with zero mean and variance σ^2 equal to:

$$\sigma^2 = \frac{1}{V_T^2} \sum_{m=1}^{M} \nu_{mn}^2 a_m(\mathbf{X}(t)) \tag{6.50}$$

where $\mathbf{X}(t)$ is the vector that contains the number of molecules of each reacting species, ν_{mn} corresponds to the change in the number of molecules of the chemical species n produced by the chemical reaction m, and the propensity function $a_m(\mathbf{X}(t))$ is the probability that the chemical reaction m will occur within the transmitter volume as function of the vector $\mathbf{X}(t)$.

Definition of Interference

We define as interference the received signal $Y(t)$ expressed as the propagation function $f_d(.)$ of the multiple transmitted molecular signals s_k, where $k = 0, ..., \infty$, as follows:

$$Y(t) = f_d \left(\sum_{k=0}^{\infty} s_k(t) \delta(\bar{x} - \bar{x}_k) \right) , \tag{6.51}$$

where $\delta(.)$ is the Dirac delta, $f_d(.)$ is the diffusion propagation function that transforms the sum of transmitted molecular signals s_k into the incoming molecular concentration $c(\bar{x}_R, t)$ at the receiver location $\bar{x}_R$ through the diffusion equation (6.44) and, according to (6.45), into the received signal $Y(t)$.

Due to the linearity of (6.44) [76, 29], given multiple molecular signals transmitted simultaneously from multiple transmitters, the resulting varying component $c(\bar{x}, t)$ of the molecule concentration is the sum of the varying components of the molecule concentration resulting from the emission of each molecular transmitter, computed as if each transmitter were emitting alone (*additive channel*). As a consequence, we can express the received signal $Y(t)$ as the sum of the propagation functions applied separately to each transmitted molecular signal,

which results into

$$Y(t) = \sum_{k=0}^{\infty} f_d(s_k(t)\delta(\bar{x} - \bar{x}_k)) \ , \tag{6.52}$$

where the propagation function $f_d(.)$ is computed as the solution of the diffusion equation (6.44) when a single transmitter is emitting a molecular signal $s_k(t)$. For this, we consider the following expression:

$$\frac{\partial c(\bar{x}, t)}{\partial t} = D\nabla^2 c(\bar{x}, t) + s_k(t)\delta(\bar{x} - \bar{x}_k) \ . \tag{6.53}$$

The solution of (6.53) in terms of $c(\bar{x}, t)$ corresponds to the following propagation function $f_d(.)$:

$$\begin{aligned} f_d(s_k(t)\delta(\bar{x} - \bar{x}_k)) = c(\bar{x}, t) = g_d(r_k, t) * s_k(t) = \\ = \int_0^{\infty} g_d(r_k, \tau) s_k(\tau - t) d\tau \ , \end{aligned} \tag{6.54}$$

where $(.*.)$ is the convolution operator [30], and $g_d(r_k, t)$ is the Green's function of the diffusion equation [64], equal to

$$g_d(r_k, t) = \frac{e^{-\frac{{r_k}^2}{4Dt}}}{(4\pi Dt)^{3/2}} \ , \tag{6.55}$$

where r_k is the Euclidian distance between the transmitter k location and the receiver location, $r_k = \|\bar{x}_k - \bar{x}_R\|$, and D is the diffusion coefficient. As a result, we can express the received signal $Y(t)$ as

$$Y(t) = \sum_{k=0}^{\infty} g_d(r_k, t) * s_k(t) \ , \tag{6.56}$$

where $g_d(r_k, t)$ is expressed in (6.55), $(. * .)$ is the convolution operator [30], and $s_k(t)$ is the molecular signal transmitted from each transmitter k, whose distribution is given by (6.47).

6.3.2 Statistical-physical Interference Modeling

The goal of the statistical-physical interference modeling is to find a **probabilistic description of the received signal** $Y(t)$ expressed in (6.56), **as function of the transmitter density λ, the diffusion**

coefficient D, and the average power σ^2 of the molecular signals emitted by the transmitters.

In standard statistical-physical modeling of the interference for radio communication networks [53], since the propagation function corresponds to a multiplication of each transmitted signal (uncorrelated random process with zero mean value) by the radio propagation amplitude loss, independent with respect to the time variable, the received signal $Y(t)$ is an uncorrelated stochastic process with zero mean value. As a consequence, the received signal $Y(t)$ can be probabilistically described with the Probability Density Function (PDF) $P_Y(y)$ of a time sample, for which analytical expressions are usually provided in terms of log-characteristic functions [51].

Probabilistic Description of the Received Signal

In the context of diffusion-based molecular nanonetworks, as a consequence of the expression of the propagation function in (6.55) as function of the time variable t, the received signal $Y(t)$ is in general a correlated stochastic process, which cannot be described by the PDF $P_Y(y)$ of a single time sample. A probabilistic description of the received signal $Y(t)$ can be provided upon the following considerations:

- Consider a realization of the spatial homogeneous Poisson process of the transmitter locations, expressed in (6.46), which results into a set of values $R = \{r_k\}_{k=1,2,...,\infty}$ for the distances r_k between each transmitter $k = 1, 2..., \infty$ and the receiver.

- Given the previous consideration, each term of the sum in (6.56) is a convolution of a deterministic function $g_d(r_k, t)$ of the time t with a zero-mean Gaussian white random signal $s_k(t)$ with zero mean and variance equal to σ^2. The result of this convolution is a zero-mean stationary Gaussian process $y_k|r_k$ with autocorrelation function $R_{y_k|r_k}(t)$ equal to σ^2 multiplied by the correlation of $g_d(r_k, t)$ with itself [74]. This is expressed as follows:

$$\mathcal{R}_{y_k|r_k}(t) = \sigma^2 \int_0^\infty g_d(r_k, \tau) g_d(r_k, \tau + t) d\tau \ . \tag{6.57}$$

- The autocorrelation of the sum of two uncorrelated random processes is a random process whose autocorrelations is the sum of their autocorrelations [74].

As a consequence of the aforementioned considerations, the received signal $Y|R$, given a realization of the transmitter locations R, is a **zero-mean stationary Gaussian Process** (**GP**), probabilistically described as follows:

$$Y|R \sim \mathbf{GP}(0, \mathcal{R}_{Y|R}(t)) \ , \tag{6.58}$$

whose autocorrelation function $\mathcal{R}_{Y|R}(t)$ is equal to the sum for each transmitter $k = 1, 2, ..., \infty$ of the autocorrelation function $\mathcal{R}_{y_k|r_k}(t)$ in (6.57), expressed as

$$\mathcal{R}_{Y|R}(t) = \sum_{k=0}^{\infty} \mathcal{R}_{y_k|r_k}(t) \ . \tag{6.59}$$

Since $Y|R$ is a continuous time stationary random process, according to the Wiener-Khintchine theorem [74] it can be equivalently described in terms of Power Spectral Density (PSD), which corresponds to the Fourier transform [30] of the autocorrelation function $\mathcal{R}_{Y|R}(t)$. Given the expressions in (6.59) and (6.57), the PSD $\mathcal{S}_{Y|R}(\omega)$ results in the following:

$$\mathcal{S}_{Y|R}(\omega) = \sigma^2 \sum_{k=0}^{\infty} |G_d(r_k, \omega)|^2 \ , \tag{6.60}$$

where $|.|^2$ denotes the squared absolute value operator, and $G_d(r_k, \omega)$ is the Fourier transform [30] of $g_d(r_k, t)$ in (6.55), whose expression is

$$G_d(r_k, \omega) = \frac{e^{-(1+j)\sqrt{\frac{\omega}{2D}} r_k}}{\pi D r_k} \ , \tag{6.61}$$

where r_k is the Euclidian distance between the transmitter k and the receiver, and D is the diffusion coefficient.

Statistical-physical Modeling of the Received Power Spectral Density

The received PSD $\mathcal{S}_Y(\omega)$ is defined as the distribution of the power of the received signal Y over each frequency ω. Given the presence of

multiple transmitters, and the probabilistic assumptions described in Sec. 6.3.1, the received PSD $\mathcal{S}_Y(\omega)$ is a measure of the power of the interference which affects the communication system in each received frequency ω. As a consequence, we aim at the statistical-physical modeling of the received PSD $\mathcal{S}_Y(\omega)$ through the expression of its PDF $P_{\mathcal{S}_Y(\omega)}(s)$ as a function $f(.)$ of the PSD value s, the frequency ω, the transmitter density λ, the diffusion coefficient D, and the average power σ^2 of the molecular signals emitted by the transmitters. This is expressed as follows:

$$P_{\mathcal{S}_Y(\omega)}(s) = f(s, \omega, \lambda, D, \sigma^2) \ . \tag{6.62}$$

As detailed in the following, the PDF $P_{\mathcal{S}_Y(\omega)}(s)$ of the PSD $\mathcal{S}_Y(\omega)$ is computed from the PSD $\mathcal{S}_{Y|R}(\omega)$ in (6.60) by taking into account the spatial homogeneous Poisson process of the transmitter locations in (6.46).

The PDF $P_{\mathcal{S}_Y(\omega)}(s)$, as happens in standard statistical-physical modeling for the PDF $P_Y(y)$ of the interference for radio communication networks [53], does not have a closed-form mathematical expression. As a consequence, by following the standard statistical-physical modeling of the interference for radio communication networks [53], we aim at the expression of the log-characteristic function $\psi_{\mathcal{S}_Y(\omega)}(\Omega)$ of the received PSD $\mathcal{S}_Y(\omega)$, which is defined as the natural logarithm of the characteristic function $\phi_{\mathcal{S}_Y(\omega)}(\Omega)$, as

$$\psi_{\mathcal{S}_Y(\omega)}(\Omega) = \ln\left[\phi_{\mathcal{S}_Y(\omega)}(\Omega)\right] \ . \tag{6.63}$$

The characteristic function $\phi_{\mathcal{S}_Y(\omega)}(\Omega)$ of the received PSD $\mathcal{S}_Y(\omega)$ is defined as the expected value of the function $e^{j\Omega s}$ of the PSD value s:

$$\phi_{\mathcal{S}_Y(\omega)}(\Omega) = E_{\mathcal{S}_Y(\omega)}\left[e^{j\Omega s}\right] = \int P_{\mathcal{S}_Y(\omega)}(s) e^{j\Omega s}\, ds \ , \tag{6.64}$$

The PDF $P_{\mathcal{S}_Y(\omega)}(s)$ of the PSD $\mathcal{S}_Y(\omega)$ is computed through the Fourier transform [30] of the exponential with the log-characteristic function $\psi_{\mathcal{S}_Y(\omega)}(\Omega)$ as argument. This is expressed as follows:

$$P_{\mathcal{S}_Y(\omega)}(s) = \int e^{\psi_{\mathcal{S}_Y(\omega)}(\Omega)} e^{-j\Omega y}\, d\Omega \ , \tag{6.65}$$

As mentioned above, the formula in (6.65) does not in general result in a closed-form expression, and it is computed through numerical methods.

In the following, we derive the log-characteristic function $\psi_{\mathcal{S}_Y(\omega)}(\Omega)$, which admits an analytical expression as a function $\Psi(.)$ of the the transmitter density λ, the diffusion coefficient D and the average power σ^2 of the molecular signals emitted by the transmitters, PSD frequency variable ω, the characteristic function frequency variable Ω, expressed as follows:

$$\psi_{\mathcal{S}_Y(\omega)}(\Omega) = \Psi(\lambda, D, \sigma^2, \omega, \Omega) \; . \tag{6.66}$$

6.3.3 Log-Characteristic Function and PDF of the Received Power Spectral Density

In this section, we analytically derive the log-characteristic function $\psi_{\mathcal{S}_Y(\omega)}(\Omega)$ of the received PSD $\mathcal{S}_Y(\omega)$. Through the derivation detailed in Section 6.3.3, we obtain the following analytical expression:

$$\psi_{\mathcal{S}_Y(\omega)}(\Omega) = j\frac{16\sqrt{2}\lambda\sigma^2\Omega}{3\pi\sqrt{D^3\omega}} \int_0^\infty (x+1)e^{-2x}e^{-j\frac{e^{-2x}}{x^2}\frac{\sigma^2\omega\Omega}{2\pi^2D^3}}dx \; , \tag{6.67}$$

where λ is the transmitter density (number of transmitters per unit volume), D is the diffusion coefficient, σ^2 is the average power of the molecular signals emitted by the transmitters, ω is the PSD frequency variable, and Ω is the frequency variable of the characteristic function. Subsequently, we derive the PDF $P_{\mathcal{S}_Y(\omega)}(s)$ of the received PSD $\mathcal{S}_Y(\omega)$ by numerically computing the expression in (6.65).

Derivation of the Log-characteristic Function $\psi_{\mathcal{S}_Y(\omega)}(\Omega)$

In the following, we adapt the analytical computation of the log-characteristic function of the received signal in case of radio communication networks [51] to derive the log-characteristic function $\psi_{\mathcal{S}_Y(\omega)}(\Omega)$ of the received PSD $\mathcal{S}_Y(\omega)$ in diffusion-based molecular nanonetworks. By applying the rule of the iterated expectations [74], we can perform the expectation in (6.64) with respect to the transmitter locations $R = \{r_k\}_{k=1,2,...,\infty}$, where r_k are the random distances between each transmitter $k = 1, 2, ..., \infty$ and the receiver, and substitute the PSD value s with the PSD $\mathcal{S}_{Y|R}(\omega)$ of the received signal given a realization of the transmitter locations. As a consequence, we obtain the following

expression:

$$\phi_{\mathcal{S}_Y(\omega)}(\Omega) = E_R\left[e^{j\Omega\mathcal{S}_{Y|R}(\omega)}\right] , \tag{6.68}$$

where the PSD $\mathcal{S}_{Y|R}(\omega)$ is computed through (6.60) and (6.61).

Since the transmitter locations are resulting from a spatial homogeneous Poisson process, as described in Sec. 6.3.1, the distances r_k are i.i.d. random variables, and the distribution in the number k of molecular transmitters in a space region V is given by (6.46). As a consequence, for an infinite space region, represented by a sphere centered at the receiver with infinite radius, namely, $V = \lim_{\rho\to\infty}(4/3)\pi\rho^3$, we derive the following expression from (6.60) applied to (6.68):

$$\begin{aligned}\phi_{\mathcal{S}_Y(\omega)}(\Omega) = \quad & \lim_{\rho\to\infty}\sum_{k=0}^{\infty}\left(E_{r_k}\left[e^{j\Omega\sigma^2|G_d(r_k,\omega)|^2}\right]\right)^k \cdot \\ & \cdot\frac{[\lambda(4/3)\pi\rho^3]^k e^{-\lambda(4/3)\pi\rho^3}}{k!} ,\end{aligned} \tag{6.69}$$

where the summation from (6.60) is substituted with the power k operator $(.)^k$, and the average operator $E_R[.]$ is written in terms of summation in k of the average operator $E_{r_k}[.]$ of the k-th transmitter distance, weighted by the probability density from (6.46).

By applying the following Taylor series expansion [1] substitution to (6.69):

$$\sum_{k=0}^{\infty}\frac{x^k}{k!} = e^x , \tag{6.70}$$

and by applying the definition of log-characteristic function $\psi_{\mathcal{S}_Y(\omega)}(\Omega)$ from (6.63), we obtain the following expression:

$$\psi_{\mathcal{S}_Y(\omega)}(\Omega) = \lim_{\rho\to\infty}\frac{4}{3}\pi\rho^3\lambda\left(E_{r_k}\left[e^{j\Omega\sigma^2|G_d(r_k,\omega)|^2}\right] - 1\right) . \tag{6.71}$$

Since the transmitters are distributed according to a Poisson process (6.46), the distribution of the distance between the transmitter and the receiver, given a space region $V = (4/3)\pi\rho^3$, has the following expression:

$$P_{r_k}(r) = \frac{3r^2}{\rho^3} , \;\; 0 \le r \le \rho . \tag{6.72}$$

If we express in (6.71) the average operator $E_{r_k}[.]$ of the distance r_k between the transmitter and the receiver by using the distribution of

this distance in (6.72), we obtain the following:

$$\psi_{\mathcal{S}_Y(\omega)}(\Omega) = \lim_{\rho\to\infty} \frac{4}{3}\pi\rho^3\lambda \left(\int_0^\rho e^{j\Omega\sigma^2|G_d(r,\omega)|^2} \frac{3r^2}{\rho^3} dr - 1 \right) . \qquad (6.73)$$

By using the formula of the integration by parts [1] for the integral in (6.73), we obtain the following expression:

$$\begin{aligned} \psi_{\mathcal{S}_Y(\omega)}(\Omega) = \lim_{\rho\to\infty} \frac{4}{3}\pi\rho^3\lambda \Bigg(& e^{j\Omega\sigma^2 \frac{e^{-2\sqrt{\frac{\omega}{2D}}\rho}}{(\pi D\rho)^2}} + \\ & - \frac{4j\Omega\sigma^2}{\rho^3(\pi D)^2} \int_0^\rho \left(\sqrt{\frac{\omega}{2D}} r + 1 \right) \cdot \\ & \cdot e^{-2\sqrt{\frac{\omega}{2D}}r} e^{j\Omega\sigma^2 \frac{e^{-2\sqrt{\frac{\omega}{2D}}r}}{(\pi Dr)^2}} dr - 1 \Bigg) . \end{aligned} \qquad (6.74)$$

We note the following result:

$$\lim_{\rho\to\infty} \rho^3 \left(e^{j\Omega\sigma^2 \frac{e^{-2\sqrt{\frac{\omega}{2D}}\rho}}{(\pi D\rho)^2}} - 1 \right) = 0 , \qquad (6.75)$$

which is demonstrated by considering the following inequality:

$$\frac{e^{-2\sqrt{\frac{\omega}{2D}}\rho}}{(\pi D\rho)^2} < \frac{1}{\rho} , \quad \text{for}\, \rho \to \infty , \qquad (6.76)$$

and by repeatedly applying L'Hôpital's rule [1] to the following limit:

$$\lim_{\rho\to\infty} \rho^3 (e^{1/\rho} - 1) = 0 . \qquad (6.77)$$

By applying (6.75) to (6.74), we obtain the following expression:

$$\begin{aligned} \psi_{\mathcal{S}_Y(\omega)}(\Omega) = j\frac{16}{3}\frac{\lambda\sigma^2\Omega}{\pi D^2} \int_0^\infty \left(\sqrt{\frac{\omega}{2D}} r + 1 \right) \cdot \\ \cdot e^{-2\sqrt{\frac{\omega}{2D}}r} e^{j\Omega\sigma^2 \frac{e^{-2\sqrt{\frac{\omega}{2D}}r}}{(\pi Dr)^2}} \frac{r^3}{R^3} dr . \end{aligned} \qquad (6.78)$$

By operating in the integral of (6.78) the following variable substitution:

$$x = \sqrt{\frac{\omega}{2D}} r , \qquad (6.79)$$

we obtain the final expression of the log-characteristic function $\psi_{\mathcal{S}_Y(\omega)}(\Omega)$ of the received PSD $\mathcal{S}_Y(\omega)$, which is as follows:

$$\psi_{\mathcal{S}_Y(\omega)}(\Omega) = j\frac{16\sqrt{2}\lambda\sigma^2\Omega}{3\pi\sqrt{D^3\omega}}\int_0^\infty (x+1)e^{-2x}e^{-j\frac{e^{-2x}}{x^2}\frac{\sigma^2\omega\Omega}{2\pi^2D^3}}dx\ , \quad (6.80)$$

where λ is the transmitter density (number of transmitters per unit volume), D is the diffusion coefficient, σ^2 is the average power of the molecular signals emitted by the transmitters, ω is the PSD frequency variable, and Ω is the frequency variable of the characteristic function.

Derivation of the PDF $P_{\mathcal{S}_Y(\omega)}(s)$

In this section, we derive the PDF $P_{\mathcal{S}_Y(\omega)}(s)$ of the received PSD $\mathcal{S}_Y(\omega)$. In general, the log-characteristic function expressed in (6.80) does not have an expression which can be recognized as from a known probability distribution. For this, we numerically compute the formula in (6.65) by using the MATLAB © fft function applied to the values of the expression in (6.80). We also numerically compute the infinite integral in (6.80) by using the MATLAB © numerical integration.

The numerical results in terms of PDF $P_{\mathcal{S}_Y(\omega)}(s)$ of the received PSD $\mathcal{S}_Y(\omega)$ are shown in Fig. 6.6 and Fig 6.7. The values of the PDF $P_{\mathcal{S}_Y(\omega)}(s)$ are computed for a transmitter density λ equal to 10^9 [transmitters m^{-3}], an average power σ^2 of the molecular signals equal to 10^6 [molecules^2 m^{-6} sec^{-3}], and for values of the PSD value s ranging from 0 to $5 \cdot 10^4$ [molecules^3 m^{-6} sec Hz^{-1}]. The diffusion coefficient $D \sim 10^9$ [m^{2}sec^{-1}] is set to the diffusion coefficient of molecules diffusing in a biological environment (cellular cytoplasm, [31]). Different curves in Fig. 6.6 refer to different values of the frequency ω, from 0.09Hz to 1.89Hz, while Fig. 6.7 shows the PDF $P_{\mathcal{S}_Y(\omega)}(s)$ values for a range of frequencies ω from 0 to 2 Hz.

As apparent from Fig. 6.6 and Fig 6.7, the curves of the PDF $P_{\mathcal{S}_Y(\omega)}(s)$ as function of the PSD value s tend to horizontal lines for low values of the frequency ω, while they tend to concentrate the higher values around $s = 0$ as the frequency ω increases. This is an expected behavior since, according to the absolute value of the expression of the Fourier transform of the propagation function $G_d(r_k, \omega)$ in (6.61), which

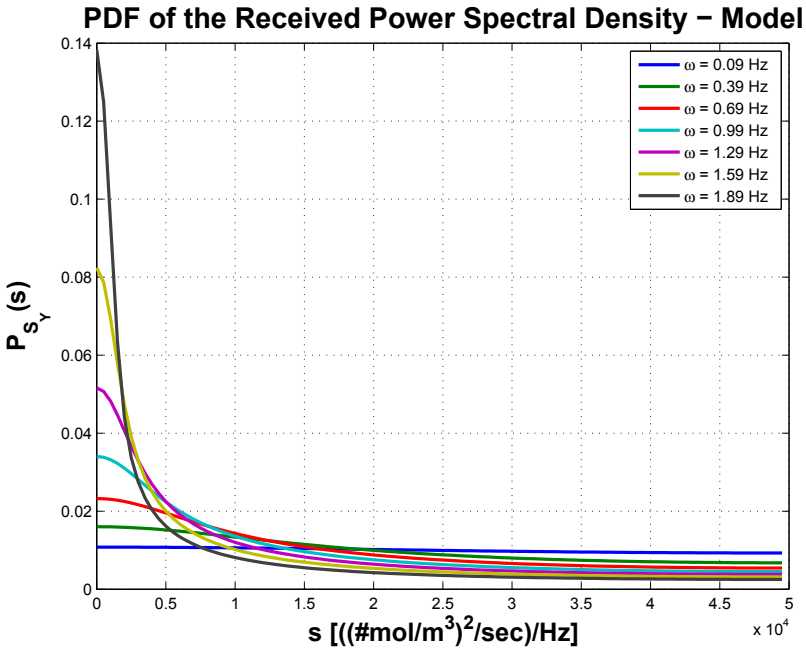

Figure 6.6: PDF $P_{\mathcal{S}_Y(\omega)}(s)$ of the received PSD $\mathcal{S}_Y(\omega)$. Different curves refer to different values of the frequency ω.

is a negative exponential function of the square root of the frequency ω, lower frequencies are subject to lower attenuation than higher frequencies in the diffusion propagation. As a consequence, for lower frequencies the received PSD tends to have a shape similar to the PSD of the white transmitted signals $s_k(t)$ in (6.47), equally distributed among all the possible PSD values s with a probability value around 0.01. On the contrary, since higher frequencies are more attenuated, for a high ω lower values of the received PSD are more probable, which is more likely distributed around $s = 0$, with the highest value around 0.16 for ω close to 2 Hz.

6.3.4 Numerical Results

In this section, we provide a simulation environment to evaluate the statistical-physical interference model presented in this paper

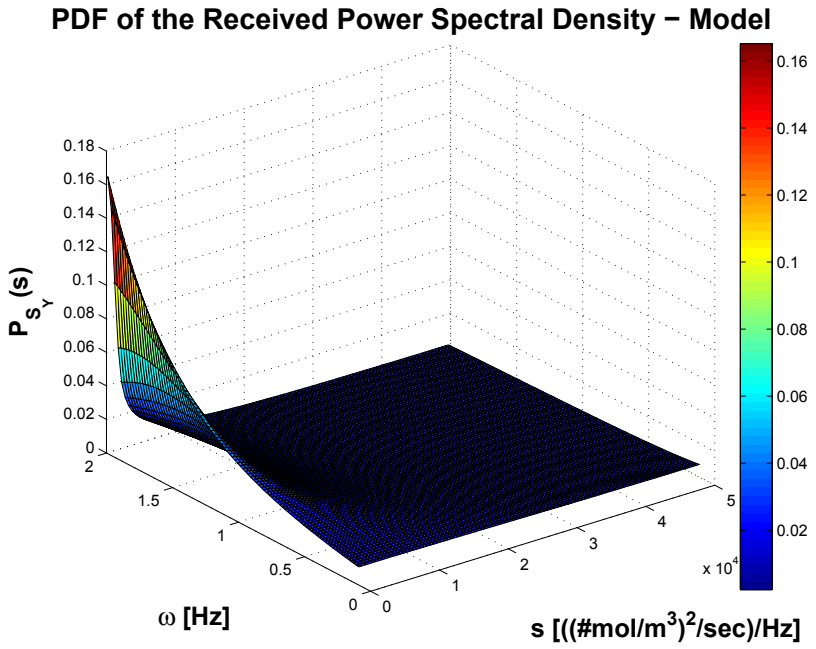

Figure 6.7: PDF $P_{\mathcal{S}_Y(\omega)}(s)$ of the received PSD $\mathcal{S}_Y(\omega)$ for a range of frequencies ω from 0 to 2 Hz.

(Sec. 6.3.4). In addition, we study the probability of interference, defined as the probability for a single molecular signal sent by a transmitter to suffer interference at the receiver, by using both the statistical-physical interference model and the simulation environment (Sec. 6.3.4).

Simulation-based Evaluation

The simulation environment is based on the following additional assumptions:

- The space where the transmitters are distributed is confined within a sphere with radius ρ around the receiver location. This is motivated by the need to have in the simulation environment a finite number of transmitters, which is equal to $K = \lfloor \lambda(4/3)\pi\rho^3 \rfloor$,

where $\lfloor . \rfloor$ denotes the rounding to the nearest lower integer.

- The transmitted signal $s_k(n/f_s)$ from each transmitter is discrete, sampled with a frequency f_s, and composed by N_s samples.
- The simulation is repeated for a number of iterations $Iter$, where each iteration is based on i) a different realization of the spatial Poisson process with density λ of the molecular transmitter distribution expressed in (6.46), ii) a different realization of the Gaussian process in (6.47) with variance equal to σ^2 for each transmitter k and for each sample $s_k(n/f_s)$.

The PDF $P_{\mathcal{S}_Y(\omega)}(s)$ of the received PSD $\mathcal{S}_Y(\omega)$, where $\omega = qf_s/N_s$, and $q = 1, ..., N_s$, is computed though the following expression:

$$P_{\mathcal{S}_Y(\omega)}(s)|_{\omega=qf_s/N_s} = \frac{1}{Iter} \sum_{l=1}^{Iter} \mathbf{1}_{\mathcal{S}_{Y_l}(qf_s/N_s)=s} \ , \tag{6.81}$$

where $\mathbf{1}_{S_{Y_l}(qf_s/N_s)=s}$ is non-zero and equal to 1 only when the PSD $S_{Y_l}(qf_s/N_s)$ from the l-th iteration is equal to the value s at frequency qf_s/N_s, and f_s and N_s are the sampling frequency and the number of samples for the transmitted molecular signals, respectively. The PSD $\mathcal{S}_{Y_l}(qf_s/N_s)$ results from the following formula:

$$\mathcal{S}_{Y_l}(qf_s/N_s) = \left(\sum_{k=1}^{K} S_k(qf_s/N_s) G_d(r_k, qf_s/N_s) \right)^2 \ , \tag{6.82}$$

where $S_k(qf_s/N_s)$ is the discrete Fourier transform of $s_k(n/f_s)$, computed through the MATLAB © fft function, and $G_d(r_k, qf_s/N_s)$ is the Fourier transform of the propagation function in (6.61) computed at the frequency value qf_s/N_s.

In Fig. 6.8 we show the values of $P_{\mathcal{S}_Y(\omega)}(s)$ computed for the same parameters as for the results in Fig. 6.7, namely, a transmitter density λ equal to 10^9 [transmitters m^{-3}], an average power σ^2 of the molecular signals equal to 10^6 [molecules^2 m^{-6} sec^{-3}] a diffusion coefficient $D \sim 10^9$ [m^{2}sec^{-1}], and for PSD values s ranging from 0 to $5 \cdot 10^4$ [molecules^3 m^{-6} sec Hz^{-1}]. Moreover, the simulation is run with the following parameters: a spherical space radius $\rho = 19\mu$m, a sampling frequency

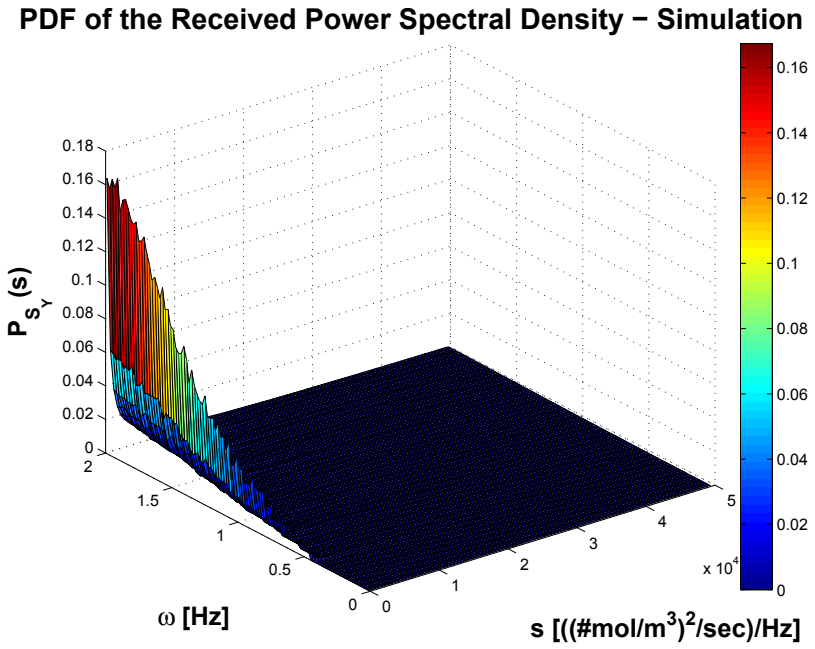

Figure 6.8: Simulation-based PDF $P_{\mathcal{S}_Y(\omega)}(s)$ of the received PSD $\mathcal{S}_Y(\omega)$ for a range of frequencies ω from 0 to 2 Hz.

$f_s = 100$Hz, a number of samples $N_s = 10^4$, and a number of iterations $Iter = 50$. The curves in Fig. 6.8 have been also post-processed through the use of a moving average filter [91] along the dimension of the PSD value s to reduce the noise given by the limited dataset.

The simulation-based results in terms of $P_{\mathcal{S}_Y(\omega)}(s)$ in Fig. 6.8 show a high degree of similarity with the values computed through the statistical-physical model in Fig 6.7. Also in the simulation-based results, the curves of $P_{\mathcal{S}_Y(\omega)}(s)$ as function of the PSD value s tend to horizontal lines for low values of the frequency $\omega = qf_s/N_s$, while they tend to concentrate the higher values around $s = 0$ as the frequency ω increases. While for high frequencies ω around 2 Hz the simulation-based PDF has a value around $s = 0$ of 0.16, very close to the results of the statistical-physical model, for lower frequencies the values of the model-based PDF are overall lower than the values from the statistical-

physical model. We believe that these differences between the values in Fig. 6.7 and Fig. 6.8 are due to the limited number of transmitters and the sampling of the molecular signals s_k considered for the simulation environment.

Probability of Interference

We define here the probability of interference $P_{Interf}(\omega)$ as the probability of having at the receiver a contribution from the interference whose PSD at frequency ω exceeds the PSD of a contribution coming from a single transmitter. This single transmitter is placed at a distance r_{Tx} from the receiver, and it transmits a signal $s_{Tx}(t)$ with power equal to σ_{tx}^2, expressed as

$$s_{Tx}(t) = \sigma_{tx} \frac{\sin[t(\omega_b - \omega_a)]}{t} e^{j\omega_a t} \ , \tag{6.83}$$

The PSD of the signal $s_{Tx}(t)$ is then constant over the frequency range defined by ω_a and ω_b, and it is expressed as follows:

$$\mathcal{S}_{Tx}(\omega) = \sigma_{tx}^2 \text{rect}\left(\frac{\omega - \omega_a}{\omega_b - \omega_a}\right) \ , \tag{6.84}$$

where rect(.) is the rectangular function, and σ_{tx}^2 is the constant PSD value. The contribution $\mathcal{S}_{Rx}(\omega)$ to the PSD of the received signal coming from the transmitted signal $s_{Tx}(t)$ is given as

$$\mathcal{S}_{Rx}(\omega) = \mathcal{S}_{Tx}(\omega) \left|G_d(r_{Tx}, \omega)\right|^2 \ , \tag{6.85}$$

where $G_d(r_{Tx}, \omega)$ is the Fourier transform [30] of the Green's function of the diffusion equation expressed in (6.61). The probability of interference $P_{Interf}(\omega)$ is expressed as follows:

$$P_{Interf}(\omega) = \int_{\mathcal{S}_{Rx}(\omega)}^{\infty} P_{\mathcal{S}_Y(\omega)}(s) ds \ , \tag{6.86}$$

where $\mathcal{S}_{Rx}(\omega)$ is the PSD of the signal $s_{Tx}(t)$ emitted by the single transmitter, given in (6.84), and $P_{\mathcal{S}_Y(\omega)}(s)$ is the PSD of the received PSD $\mathcal{S}_Y(\omega)$ computed above with either the statistical-physical model, given by (6.80), or the simulation environment, given by the numerical results of (6.81).

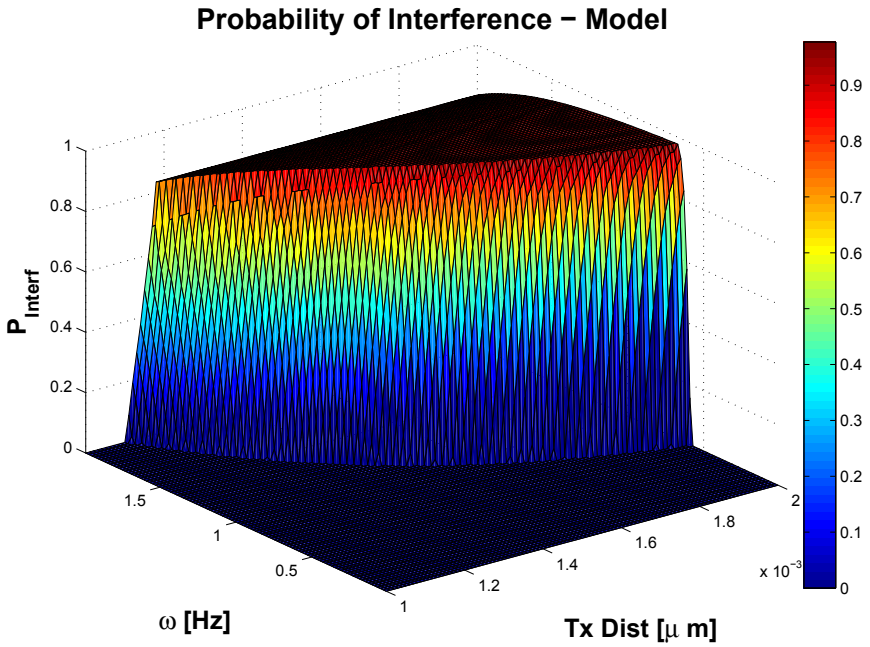

Figure 6.9: Probability of interference according to the statistical-physical model.

In Fig. 6.9 and Fig. 6.10 we show the probability of interference $P_{Interf}(\omega)$ according to the statistical-physical model and the simulation environment, respectively, for a range of frequencies ω from $\omega_a = 0$ Hz to $\omega_b = 2$ Hz and for a distance r_{Tx} between the single transmitter and the receiver ranging from 1 μm to 2 μm. The values in Fig. 6.9 are derived from the expression in (6.86) by using the PDF $P_{\mathcal{S}_Y(\omega)}(\omega)$ computed in Sec. 6.3.3, while for Fig. 6.10 we applied the values of the PDF $P_{\mathcal{S}_Y(qf_s/N_s)}(s)$ computed through the simulation detailed in Sec. 6.3.4. The constant PSD of the signal $s_{Tx}(t)$ is here set to two orders of magnitude higher than the average power of the molecular signals emitted by the interfering transmitters, namely, $\sigma_{tx}^2 = 10^2\sigma^2$.

In both Fig. 6.9 and Fig. 6.10 we observe an almost zero probability of interference $P_{Interf}(\omega)$ for low values of the frequency ω and low values for the transmitter distance r_{Tx} from the receiver. As the frequency ω and the distance r_{Tx} increase, also the probability of interference

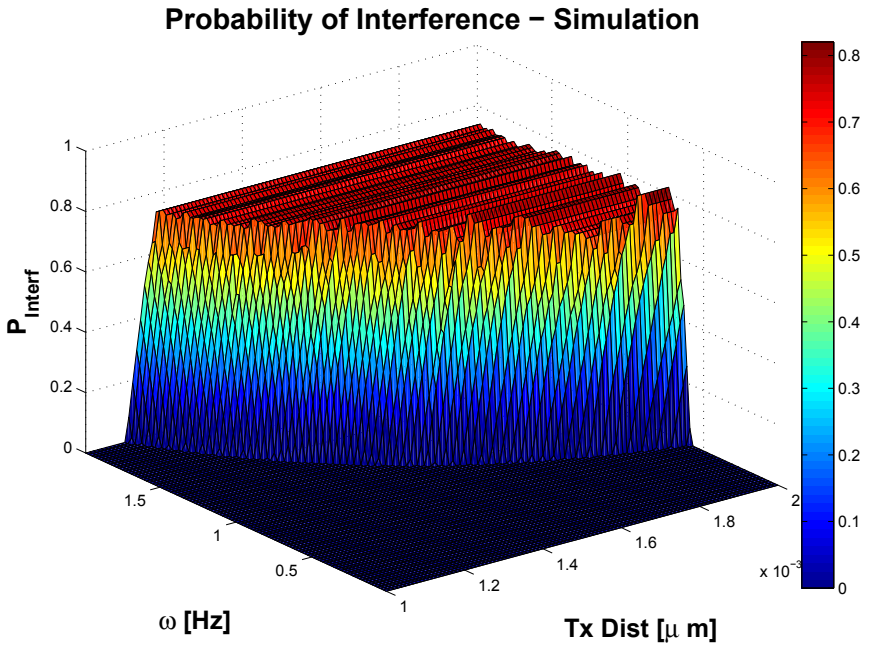

Figure 6.10: Probability of interference according to the simulation environment.

$P_{Interf}(\omega)$ increases from zero to a maximum value. In both Fig. 6.9 and Fig. 6.10, values of the probability of interference higher than zero occur only for a frequency ω higher than 0.59 Hz and a distance r_{Tx} higher than 1.1 μm. In Fig. 6.9 the maximum value of the probability of interference $P_{Interf}(\omega)$ is 0.98 and it occurs for the range frequencies ω between 0.67 Hz and 0.89 Hz and for a distance r_{Tx} higher than 1.4 μm. The maximum value of the probability of interference $P_{Interf}(\omega)$ in Fig. 6.10 is around 0.82 and it occurs for a frequency ω around 0.73 Hz and a distance r_{Tx} higher than 1.9 μm. The overall lower values of the simulation-based probability of interference $P_{Interf}(\omega)$ in Fig. 6.10 compared to the values in Fig. 6.9 from the statistical-physical model are likely due to the limited number of interfering transmitters and iterations of the transmitter distribution realizations considered in the simulation environment, as explained in Sec. 6.3.4, while the statistical-physical model considers an infinite number of transmitters and it is

based on their distribution PDF.

Different behaviors of the probability of interference $P_{Interf}(\omega)$ for high frequencies ω and high distances r_{Tx} are shown in Fig. 6.9 and Fig. 6.10. In the former, the $P_{Interf}(\omega)$ reaches a plateau, corresponding to the aforementioned maximum value of 0.98, and then decreases as the frequency value increases from 0.89 Hz to 2 Hz, where it has a PDF value of 0.83. In the latter, after a maximum value at 0.82, and as the frequency increases from 0.73 Hz to 2 Hz, the $P_{Interf}(\omega)$ oscillates between 0.74 and 0.72. Again, this oscillatory behavior is likely due to the limited data used in the simulation environment to compute the PDF $P_{\mathcal{S}_Y(\omega)}(s)$, where we considered a limited number of interferers, within a spherical space of radius $\rho = 19\mu$m, and a limited number of iterations for the realization of their location distribution.

6.4 Conclusions

In this chapter of the article, the interference in a diffusion-based MC nanonetwork is analyzed when MC links from multiple transmitter to a single receiver are simultaneously active. First, the characterization of the diffusion channel in terms of signal propagation is provided by studying two main parameters, namely, the attenuation and the dispersion, and simple closed-form formulas for the evaluation of the ISI and the CCI are derived for the baseband modulation and the diffusion wave modulation schemes. Second, a statistical-physical modeling of the interference is developed by deriving an analytical expression to estimate of the received Power Spectral Density (PSD) probability distribution.

According to the ISI and CCI formulas, the diffusion wave modulation scheme shows lower values of interference with respect to the baseband modulation scheme. This is also confirmed by numerical results obtained through the simulation of the MC nanonetwork, which also assess the validity of the derived formulas. Through the statistical-physical model, it was possible to compute the probability of having at the receiver a contribution from the interference whose PSD exceeds the PSD of a contribution coming from a single transmitter. For a dif-

fusion coefficient value that can be found in a biological environment, this probability shows very low values for frequencies lower than 0.59 Hz and a distance range lower than 1.1 μm, while it assumes very high values otherwise.

The interference analysis presented in this section of the article will contribute to the general understanding of molecular communication systems based on diffusion and it will support the design of nanonetwork architectures based on this paradigm, in particular towards the realization of interference mitigation techniques in the molecular domain.

7

Conclusions and Future Work

Molecular communication (MC) is a promising bio-inspired paradigm for the exchange of information among autonomous intelligent nanotechnology-enabled devices, or nanomachines. MC realizes the exchange of information through the transmission, propagation, and reception of molecules, and it is proposed as a feasible solution for nanonetworks. This idea is motivated by the observation of nature, where MC is successfully adopted by cells for intracellular and intercellular communication. Thanks to the feasibility of MC in biological environments, MC-based nanonetworks have the potential to be the enabling technology for a wide range of applications, mostly in the biomedical, but also in the industrial and surveillance fields.

The focus of this article is on diffusion-based MC, where the propagation of information-bearing molecules between a transmitter and a receiver is realized through free diffusion in a fluid. This choice is motivated by a preliminary analysis, which identifies the diffusion-based as the most fundamental type of MC among different options suggested in the literature. Since there are profound differences between the diffusion-based MC paradigm and classical electromagnetic communication paradigms, the classical communication engineering models

and techniques are not directly applicable for the study and the design of diffusion-based MC systems. As a consequence, there is a need of to build a complete understanding of the diffusion-based MC paradigm from the ground up.

The objectives of the research presented in this article are to analyze a diffusion-based MC link from the point of view of communication engineering and information theory, and to provide solutions to the modeling and design of MC-based nanonetworks. First, through a deterministic model of a diffusion-based MC link we learn that the gains of the molecule emission, molecule propagation, and molecule reception in a diffusion-based MC have non-linear curves as function of the frequency components of the information signal exchanged through the system, and as function of the distance range. Non-linear curves as function of the frequency components are also shown for the delays of the molecule reception and propagation processes. Moreover, the delay of the propagation process shows non-linear curves also as function of the distance range, but only for low-frequency components.

Second, through the study of the noise sources affecting the communication of information through diffusion-based MC we learn that the noise arises from the discrete nature of the signaling molecules used for the transmission of the information signals, from the randomness of their Brownian motion propagation, and from the stochasticity of the chemical reactions in which they are involved. As a result of the peculiarities of these noise-generating processes, the statistical parameters of the noises in a diffusion-based MC link are functions of the amplitude of the information signal exchanged between the transmitter and the receiver.

Third, though the analysis of upper and lower bounds to the capacity of diffusion-based MC we learn how the performance of a diffusion-based MC link depend on the system bandwidth, the distance range, and the average transmitted power. In particular, capacity values of a few [Kbit/sec] can be reached within a distance of tenth of μm between the transmitter and the receiver, and for an average transmitted power around 1 pW (Note that this power value should not be compared to the transmitted power values used for electrical devices, since the

transmitted power in a MC system is a thermodynamic quantity).

Finally, through the analysis of the interference, we learn that the ISI and CCI of a Gaussian-pulse-encoded information signal have lower values when this signal is modulated by a carrier oscillation. Moreover, the higher is the frequency of the carrier oscillation, the lower are the values of the ISI and CCI. Through the statistical-physical modeling of the interference, we derive the PSD probability distribution of a received signal in a diffusion-based MC system as function of physical parameters, such as the diffusion coefficient, the transmitter density, and the average power of molecule emissions. As apparent from the PDF of the received PSD, the power of low frequency components of the received signal tends to a uniform distribution over the range of considered values, while the power of higher frequencies tends with more probability to lower values.

In the future, we plan to extend our work on molecular communication in several directions, including a bio-inspired analysis of the energy consumptions for transmitting, receiving, and processing information in diffusion-based MC systems, the study of addressing mechanisms and routing processes in diffusion-based MC systems, the study of other molecular communication architectures, e.g., advection-based and walkway-based, and the study of more specific designs for molecular communication, stemming from the engineering of synthetic biological circuits for the realization of biological nanomachines.

Acknowledgements

This work was supported by the U.S. National Science Foundation under Grant CNS-1110947.

References

[1] M. Abramowitz and I. A. Stegun. *Handbook of Mathematical Functions with Formulas, Graphs, and Mathematical Tables*. New York: Dover Publications, 1972.

[2] I. F. Akyildiz, F. Brunetti, and C. Blazquez. Nanonetworks: a new communication paradigm at molecular level. *Computer Networks (Elsevier) Journal*, 52(12):2260–2279, August 2008.

[3] I. F. Akyildiz and J. M. Jornet. Electromagnetic wireless nanosensor networks. *Nano Communication Networks (Elsevier) Journal*, 1(1):3–19, June 2010.

[4] I. F. Akyildiz and J. M. Jornet. The internet of nano-things. *IEEE Wireless Communication Magazine*, 17(6):58–63, December 2010.

[5] I. F. Akyildiz, J. M. Jornet, and M. Pierobon. Nanonetworks: a new frontier in communications. *Communications of the ACMs*, 54(11):84–89, November 2011.

[6] R. Aleixo and E. Capelas de Oliveira. GreenŠs function for the lossy wave equation. *Revista Brasileira de Ensino de Fisica*, 30(1):1302, 2008.

[7] G. Alfano and D. Miorandi. On information transmission among nanomachines. In *Proc. of First Intl. Conf. on Nano-Networks and Workshops*, pages 1–5, September 2006.

[8] Y.M. Ali and L.C. Zhang. Relativistic heat conduction. *International Journal of Heat and Mass Transfer*, 48:2397–2406, March 2005.

[9] G Arfken. Green's functions–two and three dimensions. *Mathematical Methods for Physicists*, pages 480–491, 1985.

[10] D. Arifler. Capacity analysis of a diffusion-based short-range molecular nano-communication channel. *Computer Networks Journal (Elsevier)*, 55(6):1426–1434, April 2011.

[11] B. Atakan and O. B. Akan. An information theoretical approach for molecular communication. In *Proc. of Second Intl. Conf. on Bio-Inspired Models of Network, Information and Computing Systems (Bionetics)*, pages 33–40, December 2007.

[12] B. Atakan, S. Galmes, and O. B. Akan. Nanoscale communication with molecular arrays in nanonetworks. *IEEE Transactions on NanoBioscience*, 11(2):164–168, June 2012.

[13] Baris Atakan and Ozgur B. Akan. On molecular multiple-access, broadcast, and relay channels in nanonetworks. In *Proc. of Third Intl. Conf. on Bio-Inspired Models of Network, Information and Computing Systems (Bionetics)*, pages 16:1–16:8, November 2008.

[14] Baris Atakan and Ozgur B. Akan. On channel capacity and error compensation in molecular communication. *Springer Transaction on Computational System Biology*, 10:59–80, December 2009.

[15] Baris Atakan and Ozgur B. Akan. Deterministic capacity of information flow in molecular nanonetworks. *Nano Communication Networks Journal (Elsevier)*, 1(1):31–42, March 2010.

[16] David Baker, George Church, Jim Collins, Drew Endy, Joseph Jacobson, Jay Keasling, Paul Modrich, Christina Smolke, and Ron Weiss. Engineering life: building a fab for biology. *Scientific American*, 294(6):44–51, June 2006.

[17] M. S. Bartlett. *An introduction to stochastic processes, with special reference to methods and applications*. Press Syndicate of the University of Cambridge, 1978.

[18] Bahareh Behkam and Metin Sitti. Bacterial flagella-based propulsion and on/off motion control of microscale objects. *Appl. Phys. Lett.*, 90(2):023902, January 2007.

[19] A. Ben-Naim. *A Farewell to Entropy: Statistical Thermodynamics Based on Information*. World Scientific Publishing Company, 2008.

[20] H.C. Berg and E.M. Purcell. Physics of chemoreception. *Biophysical Journal*, 20(2):193–219, November 1977.

[21] J. M. Bernardo. Psi (digamma) function. *Journal of the Royal Statistical Society. Series C (Applied Statistics)*, 25(3):315–317, 1976.

[22] Michael J. Berridge. The AM and FM of calcium signalling. *Nature*, 386(6627):759–780, April 1997.

[23] William Bialek and Sima Setayeshgar. Physical limits to biochemical signaling. *Proceedings of the National Academy of Sciences (PNAS) of the USA*, 102(29):10040–10045, July 2005.

[24] William H. Bossert and Edward 0. Wilson. The analysis of olfactory communication among animals. *Journal of Theoretical Biology*, 5(3):443–469, November 1963.

[25] C. Bustamante, D. Keller, and G. Oster. The physics of molecular motors. *Accounts of Chemical Research*, 34(6):412–420, 2001.

[26] L.J Clancy. *Aerodynamics*. Pitman Publishing Limited, 1975.

[27] J. W. Costerton, P. S. Stewart, and E. P. Greenberg. Bacterial biofilms: a common cause of persistent infections. *Science*, 67(5418):1318–1322, May 1999.

[28] Thomas M. Cover and Joy A. Thomas. *Elements of Information Theory, 2nd Edition*. Wiley, 2006.

[29] E. L. Cussler. *Diffusion. Mass Transfer in Fluid Systems*. 2nd edition, Cambridge University Press, 1997.

[30] Brian Davies. *Integral transforms and their applications*. Springer, New York, 2002.

[31] B. S. Donahue and R. F. Abercrombie. Free diffusion coefficient of ionic calcium in cytoplasm. *Cell Calcium*, 8(6):437–48, December 1987.

[32] E. Drexler. Molecular engineering: Assemblers and future space hardware. American Astronautical Society: AAS-86-415, 1986.

[33] E. Drexler. *Nanosystems: Molecular Machinery, Manufacturing, and Computation*. John Wiley and Sons, Inc, 1992.

[34] J. Matthew Dubach, Daniel I. Harjes, and Heather A. Clark. Fluorescent ion-selective nanosensors for intracellular analysis with improved lifetime and size. *Nano Letters*, 7(6):1827–2831, 2007.

[35] E.R.G. Eckert and R.M. Drake. *Analysis of Heat and Mass Transfer*. McGraw-Hill, 1972.

[36] Arash Einolghozati, Mohsen Sardari, Ahmad Beirami, and Faramarz Fekri. Capacity of discrete molecular diffusion channels. In *Proc. of 2011 IEEE International Symposium on Information Theory (ISIT)*, pages 603–607, July 2011.

[37] Arash Einolghozati, Mohsen Sardari, and Faramarz Fekri. Capacity of diffusion-based molecular communication with ligand receptors. In *Proc. of 2011 IEEE Information Theory Workshop (ITW)*, pages 85–89, October 2011.

[38] Arash Einolghozati, Mohsen Sardari, and Faramarz Fekri. Collective sensing-capacity of bacteria populations. In *Proc. of 2011 IEEE International Symposium on Information Theory (ISIT)*, pages 2959–2963, July 2012.

[39] Arash Einolghozati, Mohsen Sardari, and Faramarz Fekri. Molecular communication between two populations of bacteria. In *Proc. of 2012 IEEE Information Theory Workshop (ITW)*, pages 437–441, September 2012.

[40] Albert Einstein. On the electrodynamics of moving bodies. *Annalen der Physik*, 17:891–921, 1905.

[41] Drew Endy. Foundations for engineering biology. *Nature*, 438(24):449–453, November 2005.

[42] E. Fermi. *Thermodynamics*. Prentice-Hall Company, 1936.

[43] R. A. Freitas. *Nanomedicine, Volume I: Basic Capabilities*. Landes Bioscience, Georgetown, TX, 1999.

[44] Robert A. Freitas. Pharmacytes: An ideal vehicle for targeted drug delivery. *Journal of Nanoscience and Nanotechnology*, 6:2769–2775, 2006.

[45] A. Gelman, J. B. Carlin, H. S. Stern, and D. B. Rubin. *Bayesian Data Analysis, Second Edition*. Chapman and Hall/CRC, 2003.

[46] J. W. Gibbs, H. A. Bumstead, and R. G. Van Name. *Scientific Papers of J. Willard Gibbs, Vol. 1: Thermodynamics*. Longmans, Green and Company, 1961.

[47] Daniel T. Gillespie. The chemical langevin equation. *Journal of Chemical Physics*, 113(1):297–306, July 2000.

[48] Daniel T. Gillespie. Stochastic simulation of chemical kinetics. *Annual Review of Physical Chemistry*, 58:35–55, May 2007.

[49] Maria Gregori and Ian F. Akyildiz. A new nanonetwork architecture using flagellated bacteria and catalytic nanomotors. *IEEE Journal on Selected Areas in Communications (JSAC)*, 28(4):602–611, May 2010.

[50] Maria Gregori, Ignacio Llatser, Albert Cabellos-Aparicio, and Eduard Alarcón. Physical channel characterization for medium-range nanonetworks using flagellated bacteria. *Computer Networks*, 55(3):779–791, 2011.

[51] Kapil Gulati, Brian L. Evans, Jeffrey G. Andrews, and Keith R. Tinsley. Statistics of co-channel interference in a field of poisson and poisson-poisson clustered interferers. *IEEE Transactions on Signal Processing*, 58(12):6207–6222, December 2010.

[52] Yu-Chueh Hung, Wei-Ting Hsu, Ting-Yu Lin, and Ljiljana Fruk. Photoinduced write-once read-many-times memory device based on dna biopolymer nanocomposite. *Appl. Phys. Lett.*, 99:253301, October 2011.

[53] J. Ilow and D. Hatzinakos. Analytic alpha-stable noise modeling in a poisson field of interferers or scatterers. *IEEE Transactions On Signal Processing*, 46(6):1601–1611, June 1998.

[54] E. T. Jaynes. Information theory and statistical mechanics. *The Physical Review*, 106(4):620–630, May 1957.

[55] S. Kadloor and R. Adve. A framework to study the molecular communication system. In *Proc. of 18th Intl. Conf. on Computer Communications and Networks*, pages 1–6, August 2009.

[56] C.J. Kerr, K.S. Osborn, G.D. Robson, and P.S. Handley. The relationship between pipe material and biofilm formation in a laboratory model system. *Journal of Applied Microbiology*, 85:295–385, 1999.

[57] M. S. Kuran, H. B. Yilmaz, T. Tugcu, and I. F. Akyildiz. Interference effects on modulation techniques in diffusion based nanonetworks. *Nano Communication Networks (Elsevier) Journal*, 3(1):65–73, March 2012.

[58] M. S. Kuran, H. B. Yilmaz, T. Tugcu, and I. F. Akyildiz. Interference effects on modulation techniques in diffusion based nanonetworks. *Nano Communication Networks (Elsevier) Journal*, 3:65–73, March 2012.

[59] M. P. Langevin. Paul langevinÕs 1908 paper ÔÔon the theory of brownian motionÕÕ. *American Journal of Physics*, 65(11):1079–1081, November 1997.

[60] Jianping Li, Tuzhi Peng, and Yuqiang Peng. A cholesterol biosensor based on entrapment of cholesterol oxidase in a silicic sol-gel matrix at a prussian blue modified electrode. *Electroanalysis*, 15(12):1031–1037, 2003.

[61] Jian-Qin Liu and Tadashi Nakano. An information theoretic model of molecular communication based on cellular signaling. In *Proc. of Second Intl. Conf. on Bio-Inspired Models of Network, Information and Computing Systems (Bionetics)*, pages 316–321, December 2007.

[62] M.U. Mahfuz, D. Makrakis, and H.T. Mouftah. Characterization of intersymbol interference in concentration-encoded unicast molecular communication. In *Proc. of 24th Canadian Conference on Electrical and Computer Engineering (CCECE)*, pages 139–146, May 2011.

[63] Andreas Mandelis. Diffusion waves and their uses. *Physics Today*, 53(29):29–34, August 2000.

[64] Andreas Mandelis. *Diffusion-wave fields: mathematical methods and Green functions*. Springer-Verlag, 2001.

[65] M. L. McGlashan. *Physico-Chemical Quantities and Units*. London: Royal Institute of Chemistry, 1968.

[66] Donald A. McQuarrie. Kinetics of small systems. I. *The Journal of Chemical Physics*, 38(2):433–436, January 1963.

[67] Milan Merkle. Convexity in the theory of the gamma function. *International Journal of Applied Mathematics & Statistics*, 11(V07):103–117, November 2007.

[68] M A Model and G M Omann. Ligand-receptor interaction rates in the presence of convective mass transport. *Biophysical Journal*, 69(5):1712–1720, 1995.

[69] M. Moore, A. Enomoto, T. Nakano, R. Egashira, T. Suda, A. Kayasuga, H. Kojima, H. Sakakibara, and K. Oiwa. A design of a molecular communication system for nanomachines using molecular motors. In *Proc. of Fourth Annual IEEE Intl. Conf. on Pervasive Computing and Communications Workshops*, pages 6–12, March 2006.

[70] M.-J. Moore, T. Suda, and K. Oiwa. Molecular communication: modeling noise effects on information rate. *IEEE Transactions on NanoBioscience*, 85:295–385, June 2009.

[71] T. Nakano, T. Suda, T. Koujin, T. Haraguchi, and Y. Hiraoka. Molecular communication through gap junction channels: system design, experiments and modeling. In *Proc. of 2nd Intl. Conf. on Bio-Inspired Models of Network, Information and Computing Systems (Bionetics)*, pages 139–146, December 2007.

[72] T. Nakano, T. Suda, M. Moore, R. Egashira, A. Enomoto, and K. Arima. Molecular communication for nanomachines using intercellular calcium signaling. In *Proc. of Fifth IEEE Intl. Conf. on Nanotechnology*, volume 2, pages 478–481, July 2005.

[73] D. L. Nelson and M. M. Cox. *Lehninger Principles of Biochemistry*, chapter 12.2, pages 425–429. W. H. Freeman, 2005.

[74] A. Papoulis and S. U. Pillai. *Probability, Random Variables and Stochastic Processes, 4th ed.* McGraw-Hill, 2002.

[75] Lluís Parcerisa and Ian F. Akyildiz. Molecular communication options for long range nanonetworks. *Computer Networks (Elsevier) Journal*, 53(16):2753–2766, August 2009.

[76] Jean Philibert. One and a half century of diffusion: Fick, Einstein, before and beyond. *Diffusion Fundamentals*, 4:6.1–6.19, 2006.

[77] M Pierobon and I. F. Akyildiz. A physical end-to-end model for molecular communication in nanonetworks. *IEEE Journal on Selected Areas in Communications (JSAC)*, 28(4):602–611, May 2010.

[78] M Pierobon and I. F. Akyildiz. Diffusion-based noise analysis for molecular communication in nanonetworks. *IEEE Transactions on Signal Processing*, 59(6):2532–2547, June 2011.

[79] M. Pierobon and I. F. Akyildiz. Information capacity of diffusion-based molecular communication in nanonetworks. In *in Proc. of IEEE Intl. Conf. on Computer Communication, INFOCOM, Miniconference*, April 2011.

[80] M Pierobon and I. F. Akyildiz. Noise analysis in ligand-binding reception for molecular communication in nanonetworks. *IEEE Transactions on Signal Processing*, 59(9):4168–4182, September 2011.

[81] M. Pierobon and I. F. Akyildiz. Intersymbol and co-channel interference in diffusion-based molecular communication. In *in Proc. of the 2nd IEEE Intl. Workshop on Molecular and Nano Scale Communication (MoNaCom), ICC*, June 2012.

[82] M Pierobon and I. F. Akyildiz. Capacity of a diffusion-based molecular communication system with channel memory and molecular noise. *IEEE Transactions on Information Theory*, 59(2):942–954, June 2013.

[83] Klaus Prank, Fabrizio Gabbiani, and Georg Brabant. Coding efficiency and information rates in transmembrane signaling. *Biosystems*, 55(1-3):15–22, February 2000.

[84] Michael Reed and Ron Rohrer. *Applied introductory circuit analysis for electrical and computer engineers*. Prentice-Hall, Inc. Upper Saddle River, NJ, USA, 1999.

[85] Jordi Riu, Alicia Maroto, and F. Xavier Rius. Nanosensors in environmental analysis. *Talanta*, 69(2):288–301, 2006.

[86] Jean-Pierre Rospars, Vlastimil Křivan, and Ptr Lánský. Perireceptor and receptor events in olfaction. Comparison of concentration and flux detectors: a modeling study. *Chemical Senses*, 25(3):293–311, June 2000.

[87] Howard Salis, Alvin Tamsir, and Christopher Voigt. Engineering bacterial signals and sensors. *Contrib. Microbiol.*, 16:194–225, June 2009.

[88] E. Schrödinger. *Statistical thermodynamics*. Dover Publications New York, 1989.

[89] A. Sezginer and Weng Cho Chew. Closed form expression of the greenŠs function for the time-domain wave equation for a lossy two-dimensional medium. *IEEE Transactions on Antennas and Propagation*, 32(5):527–528, 1984.

[90] C. E. Shannon. A mathematical theory of communication. *The Bell System Technical Journal*, 27:379–423, July 1948.

[91] Jeffrey S. Simonoff. *Smoothing Methods in Statistics*. Springer Series in Statistics. Springer-Verlag New York, 1998.

[92] D. J. Spencer, S. K. Hampton, P. Park, J. P. Zurkus, and P. J. Thomas. The diffusion-limited biochemical signal-relay channel. *Advances in Neural Information Processing Systems*, 16, 2004.

[93] P. Tallury, A. Malhotra, L. M. Byrne, and S. Santra. Nanobioimaging and sensing of infectious diseases. *Advanced Drug Delivery Reviews*, 62(4-5):424–437, March 2010.

[94] Gabriel Vasilescu. *Electronic Noise and Interfering Signals: Principles and Applications*. Springer Series in Signals and Communication Technology. Springer, 2005.

[95] C. R. Yonzon, D. A. Stuart, X. Zhang, A. D. McFarland, C. L. Haynes, and R. P. V. Duyne. Towards advanced chemical and biological nanosensors - an overview. *Talanta*, 67(3):438–448, 2005.

[96] Steven S. Zumdahl. *Thermochemistry*. Chemistry. Cengage Learning., 2008.